NASA CR-165746

IN-SERVICE INSPECTION METHODS FOR GRAPHITE-EPOXY STRUCTURES ON COMMERCIAL TRANSPORT AIRCRAFT

M. L. Phelps

Boeing Commercial Airplane Company
Seattle, Washington

Prepared for
Langley Research Center
under contract NAS1-15304

NASA
National Aeronautics and
Space Administration

November 1981

(ADVANCE)

CONTENTS

IN-SERVICE INSPECTION METHODS FOR GRAPHITE-EPOXY STRUCTURES ON COMMERCIAL TRANSPORT AIRCRAFT.

M. L. PHELPS
BOEING COMMERCIAL AIRPLANE COMPANY
SEATTLE, WASHINGTON

CONTRACT NAS1-15304
OCTOBER, 1981

NATIONAL AERONAUTICS AND
SPACE ADMINISTRATION

LANGLEY RESEARCH CENTER
Hampton Virginia 23665

1.0 SUMMARY

A program was conducted to determine in-service inspection methods for graphite epoxy composite structures on commercial transport aircraft. The types of service incurred defects, current inspection practices and concerns of the airlines and manufacturers, and other related information were determined by survey. Based on this information applicable inspection/NDI methods were evaluated and inspection techniques determined. New technology was developed primarily in eddy current inspection.

The most significant conclusion is that standard inspection methods with some variations for specific requirements have proven adequate for current in-service inspection of Gr/Ep structures. Recommended inspection guidelines are provided.

2.0 INTRODUCTION

The significant weight advantage of graphite epoxy and other advanced composites over aluminum aircraft structure has prompted a vigorous industry wide effort to develop and implement advanced composite components on commercial transport aircraft. This effort has been strongly supported by NASA as one of the projects within its Aircraft Energy Efficiency (ACEE) program – the goal being to reduce fuel consumption in the air transportation industry. Advanced composite structures have the potential to reduce fuel consumption by 10 to 15 percent.

Implementation of these structures on new airplanes requires a substantial development effort to acquire the necessary technology and confidence required not only by the manufacturers but also by FAA and the airlines. While the structures development/validation programs are the essential confidence builders, peripheral programs addressing durability, repair, and in-service inspection are also required.

This program concerns the inspection methods required for graphite epoxy structures on in-service aircraft. It was conducted in two phases. Phase I[1] consisted of literature surveys, questionnaires, and on-site visits to determine standard in-service inspection practices on commercial transport airplanes, and experience to date on in-service advanced composite structures. A significant conclusion was that state-of-the-art inspection methods (those currently in use on aluminum structure) were used to satisfactorily perform the required inspections on in-service Gr/Ep components. Thus the Phase II objective was to define the details and capabilities of existing inspection methods when applied to Gr/Ep structures in the flight service environment. A secondary goal was to develop new methods or techniques, if feasible, to provide improved inspection capability. In this regard an eddy current development task was conducted as part of Phase II. It is reported in detail in Appendix A. Appendix B was added to provide recommended inspection guidelines and data for commercial airlines' use in developing inspection programs for their specific needs. The program was funded by NASA-Langley Research Center and performed by the Quality Control Research and Development organization of the Boeing Commercial Airplane Company from April, 1978 through September, 1980.

Use of commercial products or names of manufacturers in this report does not constitute official endorsement of such products or manufacturers, either expressed or implied, by the National Aeronautics and Space Administration.

3.0 MATERIALS, STRUCTURES, DEFECTS

3.1 MATERIALS

The predominant material in the make-up of Gr/Ep structures is a Gr/Ep woven fabric impregnated with an uncured epoxy resin in a tacky but nonliquid state. Nonwoven tape with unidirectional graphite fibers is also used but in less quantities. A glass/epoxy and an aramid/epoxy fabric called Kevlar is also used in combination with the Gr/Ep materials in some structures.

Many structures contain honeycomb core, either Nomex, HRP, or syntactic core – a *microballoon filled epoxy material.*

Fasteners and adhesives are used to join Gr/Ep parts or details together or to other materials such as nonmetallic core, metal plate and fittings, or aluminum honeycomb.

Figure 1 illustrates a typical fabrication process of manual lay-up, vacuum bagging for compaction, autoclave cure, and assembly by mechanical fastening.

Other techniques employ automated filament winding and pultrusion layup; thermal rubber expansion, press, die, and bladder compaction; and die, oven, and microwave heating for cure.

3.2 STRUCTURES

Technology development and commitment to new airplanes has been accomplished for a variety of secondary structures and nonstructural components as shown in figures 2 through 5. Also, the NASA ACEE composite secondary and primary components are listed with weight and size data in figure 6.

Representative detailed structural configurations are presented in figure 7.

3.3 DEFECTS

Service incurred defects in Gr/Ep structures were identified in Phase I[(1)] as impact damage, delamination between plies, disbond at bondlines, fractures, fastener hole damage, fraying, water-in-honeycomb, lightning damage, and burn damage. These are described as follows.

3.3.1 IMPACT DAMAGE

This is simple damage to any exterior surface caused by impact from ground equipment, runway debris, dropped tools, hailstones, birds, and others. The damage is localized with possible damage to substructure such as honeycomb core, ribs, spar caps, etc. The damage may result in tears, fractures, scratches, painted surface blemishes, dents, local delamination, frayed and broken fibers, crushed honeycomb core, and water ingression into damaged laminates and honeycomb. See figure 8.

3.3.2 PLY DELAMINATION

Separation between plies may result from impact damage, fastener hole damage, lightning or heat damage, or a weak initial interply bond due to improper processing during manufacture. Small voids not detectable in the fabricated part may grow into a detectable defect in the service environment.

3.3.3 DISBOND

This defect is similar in all respects to ply delamination except it is a separation between two adhesively bonded members, such as laminate/laminate, laminate/honeycomb, and laminate/metal bonded joints. In addition to the causes for defects listed in Section 3.3.2, water-in-honeycomb structure may cause a laminate/honeycomb disbond and a laminate/metal joint may disbond due to corrosion at the interface.

3.3.4 FRACTURES

Fractures are caused by impact, lightning strike, overstressing, etc., and can occur with entrapped water (due to freeze expansion) and fastener hole damage. Experience to date indicates little probability of slow growth fatigue cracks. See figure 8.

3.3.5 FRAYING

Fraying is the freeing-up of fibers at fracture faces, fastener hole damage, impact damage, lightning strike, and burns. It can occur at contact points where wear may occur. The best example of fraying is the lightning damage defect shown in figure 9.

3.3.6 FASTENER HOLE DAMAGE

Fastener hole damage can occur due to overstressing, vibration, improper fastener installation and others. It is typified by fastener pull-through, hole elongation, fraying, fractures, delamination, and spalled and chipped paint. See figure 10.

3.3.7 ENTRAPPED WATER-IN-HONEYCOMB

Any surface defect that provides an opening to the honeycomb cell structure is a potential site for this defect. It most likely will occur as a result of impact damage but can result from a pin hole size opening or edge delamination. Potential damage would be delamination or disbond and possible core damage.

3.3.8 LIGHTNING DAMAGE

Associated with the surface burn and puncture, lightning strike can cause ply delamination, splintered and frayed fibers, and interior damage. In honeycomb structure, there can be core damage beneath the skin along a path up to several feet long. See figure 9.

3.3.9 BURN DAMAGE

Surface blemishes from burns are easily seen, particularly on a painted surface. Depending on severity, burnt area will cause surface blisters, charring, fiber fraying, bulging types of ply delamination, and interior damage. See figure 11.

4.0 Gr/Ep INSPECTION TECHNOLOGY DEVELOPMENT

One of the objectives of this program was the development of new Gr/Ep inspection capability. Accordingly, a substantial development effort was devoted to a general investigation of the eddy current method for application to Gr/Ep structures inspection. Specific problem areas for X-ray and ultrasonics were addressed in a limited investigation. Also, several potentially applicable methods were given a brief examination.

4.1 EDDY CURRENT

The Phase I survey[1] turned up very little evidence of work with eddy current inspection for Gr/Ep structures. This was possibly due to the extremely low (less than 0.1% IACS) conductivity of Gr/Ep and a probable expectation that crack detection sensitivity would be poor to nonexistent. One investigator, however, reported some success[2] using very high frequencies up to 80 MHz. On this basis and because the eddy current method is preferred for field inspection due to portability, ease of use, etc., it was selected as the major technical development task within the program.

The investigation included frequency, probe design, instrument, instrument adjustment, and read-out variables. Defects of concern that were used for the detection criteria were surface fractures, subsurface fractures, impact damage, and delaminations.

This effort culminated in an eddy current capability to detect surface, subsurface, and substructure (2nd layer) fractures as well as impact damage and hole damage. Especially encouraging is the fact that these inspections can be done with commercially available instruments although special design probes are required.

An immediate benefit of this work has been realized at Boeing. An eddy current inspection technique has been developed for use, as needed, on the Boeing 757 elevator and rudder. The method detects hole-to-hole fractures in the rib and spar flanges hidden beneath the skin. This is illustrated in figures 12 and 13. Saw notches were used to simulate a fracture.

Appendix A is the detailed report on this project.

4.2 X-RAY

The use of low K.V. radiography and a radiographically opaque penetrant is a well reported technique for flaw enhancement and detection in Gr/Ep structures. Since access is required to apply the penetrant, other inspections can be done in lieu of radiography. However, this technique has some field application possibilities. While evaluating detection capability, a problem was encountered with the radiographically opaque penetrant materials. This problem investigation is reported as follows.

4.2.1 PROBLEM AND INVESTIGATION

The X-ray opaque liquids that have been used are tetrabromoethane (TBE) and diiodobutane (DIB). While working with TBE initially it was noted that after application and completion of the radiographic task, self-removal did not occur by evaporation as was expected. Following this experience it was decided to switch to DIB due to the reported toxicity of TBE. A sample of DIB from within Boeing was then used on several impact damage and fracture test parts. A radiograph made three weeks after application revealed DIB still in the defects. See figures 14a and 14b. It was also noted that considerable staining had occurred on the part surface.

As others had reported good evaporation and self-removal, it was suspected that the DIB sample that had been used was deficient. A phone call and discussion with a representative of a chemical supply house revealed that DIB has a shelf life of 3 to 6 months after which breakdown into free iodide occurs. Fresh DIB is clear with a slight tint so that deterioration is recognizable as the free iodide colors the liquid brown and the degree is indicated by the darkness of the liquid. It was also recommended that the liquid be stored away from light.

Additional testing was done with fresh material. The results are seen in figures 15a and 15b.

4.2.2 CONCLUSION

Self-removal of DIB after application to defects is dependent on the degree of deterioration. This can be judged by the darkness of the liquid which will have optimum self-removal capability when fresh and is a clear liquid.

4.3 ULTRASONIC

4.3.1 INVESTIGATION

The ultrasonic pulse-echo method was investigated to determine longitudinal and possibly shear wave propagation characteristics in thicker Gr/Ep structures. The purpose was to determine if the common uses of ultrasonics in aluminum structure could be duplicated in Gr/Ep structure. Two specific applications were of interest: detection of cracks in lugs or clevis fittings as shown in figure 16a and detection of fastener hole cracks in laminates near the edge of overlying structure as shown in figure 16b.

Figure 17 shows the thick laminate specimens used. These were fabricated by lay-up of Gr/Ep fabric and tape plies in alternating orientations as shown in the sketch of figure 18. A plate about .53 cm (.210 in.) thick, fabricated of Gr/Ep fabric, was also used.

4.3.2 SOUND BEAM PROPAGATION THROUGH THICK SECTION

This test was done to establish propagation characteristics for ultrasound in thick laminated Gr/Ep sections. The test is illustrated as shown in figure 18. A 1.0 MHz, 19MM (0.75 in.) diameter transmit transducer, and a 1.59MM, (.062 in.) 15.0 MHz transducer was used as the detector for thru-transmission work. The results are as follows:

Beam Direction	Maximum Observed Dispersion Angle Measured From 90° to Part Surface	Calculated Velocity	
		Thru-Transmission Method	Pulse-Echo Method
Through 2.54 cm (1 in.) Thickness (90° to Laminate Plys and Fiber Orientation).	15°	3010 m/sec	2950 m/sec
Through 7.62 cm (3 in.) Thickness (0° to Laminate Plys and 45° to Fiber Orientation).	45° – 48°	4600 m/sec	4600 m/sec

It should be noted that the sound propagating through the 7.62 cm (3 in.) direction encountered the fibers at 45° to the sound path. It appears that this causes a redirection of the sound along the fiber orientation paths. Also the sound velocity is considerably higher in this direction indicating an influence of the graphite fibers on the velocity.

It was also observed that as the detector transducer was moved toward a position beneath the transmit transducer and away from the 45° position the signal amplitude and the velocity gradually decreased to reach a minimum directly beneath the transmit transducer.

4.3.3 CRACK DETECTION IN LUG SPECIMEN

Lug specimens and a block with a simulated fracture 0.64 cm (0.25 in.) deep at the hole were evaluated. These specimens also were made of Gr/Ep fabric oriented as shown in figure 19. The simulated crack was detected using a 10° incident angle for optimum signal. Smaller cracks were marginally detectable to nondetectable. Good reflected signals were obtained from the surface of the deeper holes but detection of cracks similar in size to that in figure 19 would be doubtful at the deeper holes.

It is concluded that any ultrasonic inspection of Gr/Ep lug hardware for cracks emanating from the lug hole will require a duplicate part with simulated cracks to establish ultrasonic technique and sensitivity. With more study it may be possible to define ultrasound propagation properties to the extent that capability may be approximated by knowing the construction details of the Gr/Ep part.

4.3.4 CRACK DETECTION IN LAMINATED Gr/Ep PLATE

A 0.53 cm (0.210 in.) thick specimen made of laminated Gr/Ep fabric was used to evaluate crack detection in a laminated plate. The specimen and test is illustrated in figure 20. The incident angle of the sound beam to the plate surface was varied as was the scanning motion toward and away from the notch defect. Notch depth was 0.127 cm (0.050 in.). The notch was easily detected through a range of angles with the optimum signal occurring at 46°. See figure 21.

Though only a single plate thickness was evaluated it is concluded that ultrasonic angle beam testing may be used to detect fracture like flaws in areas hidden from view but accessible for ultrasonic propagation to the area of concern.

4.4 OTHER METHODS

The following methods were briefly investigated for in-service inspection of Gr/Ep structures.

4.4.1 INFRARED

Two infrared cameras (different manufacturers) were evaluated on delamination type defect panels. The advantage of infrared is rapid inspection of a large area as compared to a probe-scan method. Sensitivity was limited in the thick and very thin laminates bonded to honeycomb core and the inspection process was considered not as adaptable to field inspection use as several other methods.

4.4.2 THERMAL-ACOUSTIC EMISSION

A heat gun was used to heat impact and delamination defect areas in laminates and honeycomb structure. An acoustic emission (AE) transducer was applied to the surface and, with a commercial AE instrument, an attempt was made to detect noise emitted from the defective areas during the cool down cycle. The results were negative.

4.4.3 HARDNESS TESTER

A rebound portable hardness testing instrument was briefly evaluated for nonvisible impact damage detection and was determined to be unsatisfactory on Gr/Ep surfaces.

5.0 EVALUATION AND TECHNIQUE DEVELOPMENT

Visual, tap test, and the commonly used NDI methods, with the exception of magnetic particle inspection, were evaluated on fabricated defect test panels, engineering test specimens, and assembled parts. Technique details and application data were identified concurrently with the evaluation work.

5.1 TEST PARTS

Test parts used in the evaluation are shown collectively in figure 22. They are also listed with construction and defect data. The test panels with built in delaminations or impact damage are described in detail in figures 23 and 24.

The type of defects and the method of inducing them into the parts are as follows.

5.1.1 DELAMINATION—DISBOND DEFECTS

These were placed between Gr/Ep plys or between the honeycomb core and the interfacing plys by (1) making cut-outs of the appropriate shape in the Gr/Ep fabric (single ply) using a prepared pattern and (2) placing 3 plys of 2 mil Teflon in the cut-outs. The 6 mil thickness of the Teflon inserts was approximately equal to the one ply Gr/Ep fabric thickness.

Teflon inserts placed at the edge of the panels was purposely made large enough to leave tabs at the panel edge. This was used to pull the inserts out of the cured panel leaving a void defect.

Figure 25 is a radiograph and an ultrasonic thru-transmission recording of a typical delamination/disbond defect panel showing the actual defects in place within the panel. Note the evidence on the radiograph that the edge defects are voids as compared to the interior defects with embedded Teflon. The delamination/disbond defect panels were designed to include a representation of several variables in as few panels as possible. Consequently the panel construction as explained in figure 23 requires some study to identify all details and defect locations. Variables include laminate vs honeycomb vs transition area, laminate thickness, painted surface vs unpainted surface, defect size, defect shape, edge defects vs interior defects, void defects vs nonvoid defects, defect depth below the surface in one ply increments, and ply-to-honeycomb defects vs ply-to-ply defects. A total of 309 defects were built into 14 test panels.

5.1.2 IMPACT DAMAGE DEFECTS

These defects were put in the impact damage test panels using the device shown in figure 26. The test panels with impact defects described in terms of cm-kg (in-lb) of force are listed in figure 27. Other impact defects were induced by dropping a 224g (8 oz) adjustable wrench from various heights up to 2.7 m (9 ft) on selected test parts. All impact defects were placed in painted parts to simulate the exterior surface of an airplane.

5.1.3 WATER-IN-HONEYCOMB DEFECTS

Water was injected into honeycomb cells using a hypodermic syringe and inserting the needle through small drilled holes. While each cell was completely filled, the number of cells with water was varied. Some migration of water to nearby cells was noted.

5.1.4 LIGHTNING DAMAGE DEFECTS

Lightning damage defects were produced in the Boeing lightning test laboratory using low energy discharges to produce defects as seen in figure 28.

5.1.5 BURN DAMAGE

Burn damage as seen in figure 29 was produced with a torch on a painted Gr/Ep skin-to-Nomex honeycomb panel. The lighter damage is characterized by blistered paint and bulging and delaminated skin. The severe damage had a delaminated and charred skin, a portion of which fell off with subsequent handling.

5.2 VISUAL

5.2.1 EVALUATION

All surface defects in the test parts were visually inspected. Defects included impact damage, fractures, hole damage, lightning damage, and burn damage.

Visual aids included a light and 10X magnifier but, without specimens typifying internal damage, other optical devices such as mirrors and borescopes were not used. As is commonly done during visual inspection, tactile methods, such as pushing on soft or buckled areas, scraping, prying, and tapping, were also used. The tap test is reported separately in Section 5.3.

5.2.2 RESULTS

Inspection at 6.4-7.8 m (20-25 ft) to simulate a walk-around visual inspection detected major surface defects and many minor surface indications. Though photos do not represent true visual capability, figure 22 is indicative of defect visibility and shows impact damage and burn damage. Visibility is enhanced due to the white painted surface against which the exposed black Gr/Ep is quite visible. Since impact defects occur almost entirely on exterior surfaces, they will always have a painted background.

An enhancement effect is also obtained on surface dents or bulges by varying the incident light. Figure 30 shows this effect and is an example of impact defect visibility using close visual inspection.

Some of the low energy impact damage defects were not visible except for slight surface depressions. These were small (0.64 cm -.25 in. diameter) and there was no paint cracking or chipping visible. Far visual would never detect these defects while near visual would only find them if the surface was marred or dented.

Impact damage visibility results are presented in figure 31 for defects made with a wrench dropped from various heights and at various incident angles to the part surface.

Fastener hole damage was detectable by close visual inspection. Only severe damage such as fasteners pulling into the hole with paint chipping is detectable by remote visual inspection.

Lightning strike damage on an exterior surface is easily detected by remote visual inspection. Close visual and radiographic inspection may be required to determine if internal damage has occurred along a current path in the structure.

Heat damage of any consequence results in visible damage such as scorched or burnt and blistered paint. Severe damage is indicated by charred resin, loose fibers, and flaked off skin. Figure 29 shows two levels of heat damage.

Visual detectability of defects on interior surfaces is reduced due to restricted accessibility (which often prevents direct viewing) accompanied by poor lighting. Defect detection is especially difficult on unpainted, fabric textured surfaces typical of the interiors of some Gr/Ep structures.

5.2.3 CONCLUSIONS

Visual inspection will detect serious surface defects by a "walk around" far visual inspection. Though a surface anomaly may be small, it would indicate a need for a close visual inspection and possibly the use of other inspection methods. The following defects can be detected visually (with tactile and optical aids): impact damage, fractures, hole damage, lightning strike, heat damage, scratches, and delamination that results in surface bulges or uneven appearance.

5.3 TAP TEST

5.3.1 EVALUATION

Tapping on the surface of an adhesive bonded or composite part as an adjunct to visual inspection is common practice. Tap test using a small pocket knife was evaluated on delamination/disbond defects, impact damage, lightning damage, and burn damage. The presence of a defect is indicated by a tone change compared to adjacent areas.

5.3.2 RESULTS

All heat damage and lightning damage defects were easily detectable and indicated delaminated areas well beyond the center of the defect area.

5.3.3 CONCLUSIONS

Tap test can detect badly delaminated or disbonded thin laminates and can detect delamination defects near the surface of thicker laminates. Impact damage is also detectable but usually the detectable level is also visible. Severe forms of lightning and burn damage are easily detectable.

For general inspection use wherein all types of structures and laminate thicknesses (and stiffness) must be considered, the tap test method is the least reliable in comparison with the commonly used inspection methods employing ultrasonic or bond test instruments.

5.4 PENETRANT INSPECTION

5.4.1 INVESTIGATION

Penetrant materials representing groups I through V, MIL-I-25135, were evaluated for processing characteristics and sensitivity on representative Gr/Ep specimens. These included both bare and Tedlar coated (moisture barrier) specimens with surface scratches to simulate small cracks, a part with damaged fastener holes, and a section typical of a trailing edge component with edge delaminations.

Standard procedures were used including precleaning, application and removal of the penetrant, and enhancement with developers. Experimental variations in the basic procedure were included to determine the best technique. Precleaning was done with a solvent wipe using acetone.

5.4.2 RESULTS

The data in figure 32 summarizes the results of the process/sensitivity evaluation using simulated crack specimens.

A group VI penetrant was not evaluated as the results did not indicate the need for a higher sensitivity penetrant. Figure 33 illustrates penetrant inspection capability and affords a comparison between visible dye and a group IV fluorescent penetrant.

For hole damage evaluation, a group IV penetrant was applied to two holes having different levels of damage. Figure 34 clearly shows the difference in the severity of hole damage in the two specimens. As expected, the penetrant method easily detected edge delaminations which would not have been detected by visual inspection.

No compatibility problems with Gr/Ep were observed for the cleaning solvents and penetrant process materials used in the evaluation.

5.4.3 CONCLUSIONS

The penetrant inspection method is a usable in-service inspection method for Gr/Ep components. The optimum technique for bare Gr/Ep surfaces is a group IV penetrant, removal by wiping with a damp sponge or cloth, and use of a developer. On Tedlar coated surfaces, the developer is not required. While removal of background penetrant was good, excessive washing did not remove the defect indications. Complete removal required a solvent rinse.

Sensitivity to small defects was good. Small fluorescent indications on the Tedlar coated surface were viewed under a wide field microscope and found to be minute tears in the Tedlar coating.

Dye penetrants did not prove to be satisfactory due to poor sensitivity on the Gr/Ep material surfaces.

5.5 RADIOGRAPHY

5.5.1 INVESTIGATION

Low KV radiography (10-50 KV) was evaluated for detection of fractures, hole damage, entrapped water-in-honeycomb, and assessment of impact, heat, and lightning damage. Exposure curves for low KV ranges on various Gr/Ep thicknesses were developed experimentally. They are included in Appendix B, "Recommended Inspection Guidelines."

5.5.1.1 FRACTURE DAMAGE

Fractured fatigue specimens shown in figure 35 were examined visually, radiographed without DIB, and then radiographed with DIB. The large fractures were easily detectable either visually or by unenhanced radiography. Consequently, the small tight cracks were used for sensitivity comparisons. Figure 36 shows the improvement in crack visibility after DIB enhancement.

A fatigue specimen with large fractures was used to evaluate capability of low KV radiography to detect fractured internal structure. Specimen No. 1 in figure 22, the 727 elevator section, was used and was X-rayed as shown in the sketches of figures 37 and 38. DIB enhancement was not used since the test represented radiography of inaccessible areas. Figures 37 and 38 show the results.

The lug specimen, figure 39, was also radiographed to determine crack detectability. It was X-rayed both before and after DIB treatment. The fractures were not adequately detected due to the thickness through the vertical plane of the lug.

5.5.1.2 Hole Damage

Specimen No. 7 in figure 22 was used to evaluate radiographic assessment of hole damage without fastener removal. This specimen is typical of a fastened joint such as a rib fastened to a skin. A 0.475 cm (3/16 in.) diameter CSK titanium fastener with a CRES collar was used. Two holes were evaluated– one being severely damaged with the fastener partially pulled through the skin and the other only slightly damaged. DIB was applied around the periphery of the holes with the assumption that the DIB would penetrate into the damaged areas. The results (figure 40) confirmed that the DIB did penetrate the damaged areas and clearly showed the considerable difference in the extent of the damage. Later disassembly and inspection determined that the DIB had not accumulated at the interfaces which would have given a false indication of hole damage.

5.5.1.3 Entrapped Water-in-Honeycomb

The 727 elevator section, Specimen 1 in figure 22, was used for this evaluation. Water was injected into a cluster of cells in the honeycomb rib using a hypodermic syringe. The radiographs were taken at the optimum angle to the rib and, using an additional test panel, the test set-up simulated an actual radiograph through the upper and lower skin panels and the rib – each being a Gr/Ep laminate-honeycomb construction. See figure 41. Defects as small as 5 water filled cells were detectable. The radiographic method was further validated on a Gr/Ep elevator installed on the Boeing experimental 727 airplane and then incorporated in the inspection details for the Gr/Ep 727 elevator flight service evaluation program.

5.5.1.4 Impact Damage

Impact damage will ordinarily be detected by visual inspection. The potential application for radiography on these defects is evaluation of severity after visual detection. By using DIB enhancement, the existence of skin ply fractures and/or delaminations as well as substructure damage should be detectable by radiography when not evident by visual means. Impact damage in Specimen Nos. 2, 3, and 8, figure 22, were evaluated by X-ray before and after DIB application. The results confirmed that this method considerably enhances damage area extent and detail. Figure 42 shows the capability.

5.5.2 CONCLUSIONS

Low KV radiography with DIB enhancement can detect small fractures, pinholes, and other defects open to an accessible surface. With DIB, radiography can also be used to evaluate extent of impact damage and hole damage.

Without DIB, radiography can detect large fractures in internal structure, entrapped water-in-honeycomb down to 4-5 cells in size, and can be used to evaluate extent of damage in lightning strike and burn defects.

5.6 ULTRASONIC AND BOND TESTER METHODS

5.6.1 EVALUATION

Four ultrasonic techniques and six bond test instruments were evaluated for detection of delamination disbond and impact damage defects. See figures 23 and 24. One of the instruments was used both ways – as a thru-transmission ultrasonic technique and as a "single side" bond test instrument. The ultrasonic pulse-echo technique, included in this evaluation, was also investigated for fracture detection in thick sections and lugs as reported in Section 3.4.

5.6.1.1 Ultrasonic Techniques

The following ultrasonic techniques were evaluated.

1) The thru-transmission ultrasonic (TTU) technique requires general purpose ultrasonic inspection instruments and either contact transducers or special water-jet search units to couple the ultrasound to the part. Water-jet search units and automatic or manual scanning with a yoke were used to inspect the delamination/disbond and impact damage test panels. See figure 43. Defects in the part are detectable due to their attenuation of the sound beam as compared to the surrounding nondefect areas.

   The other TTU evaluation involved a Sonatest/Shadow instrument (figure 44) which has recently appeared on the market. This instrument uses rubber-tipped or rubber tire search units which contact the surface with no couplant required.

2) The pulse echo technique uses the same general purpose instruments as the TTU technique. The inspection is performed on one side of the part with the search unit contacting the surface. A liquid or paste couplant is required. Defects reflect sound back to the transducer resulting in detectable signal pattern changes as seen on the instrument oscilloscope.

3) The ultrasonic angle beam technique is a variation of the pulse echo technique. The search unit includes a wedge shaped (usually plexiglass) shoe on which the transducer is mounted to direct the sound beam at an angle to the surface.

4) Ultrasonic thickness gage instruments (figure 45) also uses the pulse-echo technique. The read-out, usually digital, is in terms of the thickness of the laminates on which the search unit is placed. An indication of a thinner area, denotes a delamination/disbond defect.

5.6.1.2 Bond Testers

Each of the bond test instruments evaluated use a form of ultra sonic energy to sense the presence of defects in Gr/Ep structures. They are identified as bond testers rather than ultrasonic techniques as they are specialized instruments limited to bond testing. Operating characteristics include low frequency operation and continuous wave or long pulse length transmission. Some instruments sense mechanical resonance changes caused by defects. Four of the instruments evaluated do not require a couplant.

The Sonatest/Shadow instrument, used with the dual probe search unit for inspecting from one side, was evaluated as a bond tester. See figure 46.

A recent model Sondicator (S-1A), figure 47, and the 210 Bondtester, figure 48, were included in the evaluation. Other bond testers evaluated are not identified.

5.6.2 RESULTS

The results of all methods for impact damage detection including visual and tap test are summarized in figure 49. Figure 50 presents a similar summary for the delamination/disbond detection methods. Because of the large number of individual readings taken, over 500 each for most methods, it was necessary to present the data in a summary. The graphical presentation facilitated interpretation of results and permitted a "percentage detectable" comparison in each category.

5.6.3 SEPTUM HONEYCOMB DISBONDS

Another somewhat different inspection problem was also evaluated though not included in the data in figures 49 and 50. The structure is the septumized honeycomb shown in figure 22, No. 10. Sections of a typical part – a landing gear door – are shown in figure 51. The problem was detection of disbonds at the skin-to-core and core-to-core (septum) bondlines. All methods including several bond testers were evaluated on test parts having built-in defects in multiple core-to-core bondlines.

The only technique capable of detecting the disbond defects in the core-to-core bonds was pulse-echo using special 0.5 and 1.0 mHz contact transducers and a Model UJ Reflectoscope. The Sondicator bond tester detected the skin-to-core disbonds.

5.6.4 CONCLUSIONS

The following conclusions are based on the data presented in figures 49 and 50.

1) The best technique for both types of defects is thru-transmission ultrasonic with water-jet coupling.

2) Each of the following methods are satisfactory for both types of defects: 210 Bondtester, S-1A Sondicator, and both of the Sonatest/Shadow techniques.

3) The tap test method is unreliable for detecting either type of defect.

4) Several methods are very poor for honeycomb structure inspection.

5) Visual detectability of impact damage defects was poor, showing that a significant number had no visible surface damage.

6) Individual capabilities for several instruments varied considerably dependent on the type of structure, defect depth, or location. Consequently, the data in figures 49 and 50 should be reviewed to determine capability for specific applications.

5.7 EDDY CURRENT

5.7.1 EVALUATION

The evaluation of the eddy current method for defect detection was conducted concurrently with the development project reported in Section 4.1 and Appendix A. This was accomplished by an experimental process as described in detail in Appendix A. Capability was determined for detection of surface and subsurface fractures, impact damage, and delaminations.

5.7.2 RESULTS

The eddy current method detected simulated surface cracks in Gr/Ep down to 0.64 cm (0.25 in.) long by 0.03 cm (0.01 in.) deep. The following simulated substructure cracks were detected in Gr/Ep laminates:

Crack Size (In Substructure)	Top Layer Thickness
1.14 cm (0.45 in.) long x 0.15 cm (0.06 in.) deep	0.46 cm (0.18 in.)
0.79 cm (0.31 in.) long x 0.10 cm (0.04 in.) deep	0.23 cm (0.09 in.)

Actual substructure fractures were also detected. Figure 52 is a typical stiffener structure failed at the fastener. This was readily detectable from the opposite surface in comparison to the surrounding fasteners.

Simulated cracks in the rib flange of the 727 elevator seen in figures 12 and 13 were easily detectable.

The simulated crack in a unidirectional tape lay-up panel was not detectable. Conductivity in this material was very low apparently due to fiber orientation in one direction not being conducive to the circular current flow normally induced by eddy current probes.

5.7.3 CONCLUSIONS

The eddy current method can detect surface and subsurface fractures and small, sometimes nonvisible impact damage in fabric or cross ply tape lay-up. Its optimum application identified to date is fracture detection in substructure beneath an overlying member such as a laminated skin. As this can be performed with currently available instruments, it would be preferred over other inspection methods.

Since Kevlar and fiberglass materials are nonconductive, eddy current inspection capability on Gr/Ep and Kevlar or fiberglass laminate combinations is questionable and has yet to be determined.

6.0 COST ANALYSIS

A cost comparison of the in-service inspection methods reported herein has been made for two different requirements. One estimate was based on inspection of Gr/Ep composite structures in a specific localized area – for example a hinge fitting to spar attachment. The second estimate was for a large area inspection such as all rib-to-spar attachments and rib/spar-to-skin attachments in a rudder. See figure 53.

The estimates are based on labor and material costs. Cost of equipment is omitted. Also two indirect costs are omitted that are often the largest cost item. These are the cost of aircraft nonoperational down time for inspection purposes and the requirement of removing all personnel from the area during radiography causing suspension of maintenance operations.

Assumptions are: the inspection technique has been documented sufficiently so it can be used as-is with no preliminary investigation; reference standards as required have not been furnished; and two men are required due to accessibility-to-rudder problem.

Method	*	On-Aircraft Inspection Time (hrs)	Suspension of Maintenance	Reference Standards Required	Labor (hrs)	Materials Including Ref. Stds.
Radiography	S	1.5	Yes	No	6.0	$18
	L	13.0	Yes	No	28.5	$300
Ultrasonic TTU (With Yoke)	S	1.5	No	Yes	1.5	$130
	L	6.0	No	Yes	12.0	$130
Ultrasonic or Bondtester w/Couplant	S	1.0	No	Yes	2.0	$130
	L	5.0	No	Yes	10.0	$130
Ultrasonic or Bondtester w/o/Couplant	S	0.75	No	Yes	1.5	$130
	L	4.0	No	Yes	8.0	$130
Eddy Current	S	0.5	No	Yes	1.0	$130
	L	3.5	No	Yes	7.0	$130
Fluorescent	S	0.5	No	No	1.0	–
	L	Not Applicable to Large Areas				
Far Visual (1 Person)	S	0	No	No	0.25	–
	L	0	No	No	0.25	–
Close Visual and Tap Test	S	0.25	No	No	0.50	–
	L	1.0	No	No	2.0	–

* S = Small localized area

* L = Large area – assume 18.5 lineal meters (50 ft) along rib and spar areas

7.0 CONCLUSIONS

Standard inspection methods with some variations for specific requirements have proven adequate for current in-service inspection of graphite/epoxy structures. Service incurred defects and structural configurations were defined and NDI capability has been determined. Appendix B "Recommended Guidelines for In-Service Inspection of Graphite/Epoxy Composite Structures" reflects individual method capability as determined in the evaluation/development effort.

New "graphite/epoxy applicable" inspection technology resulted from the eddy current development project providing an economical alternative to other methods for certain defects. Technique guideline data was also obtained regarding the use of angle beam ultrasonics and radio-opaque liquids for radiographic image enhancement.

During the program, considerable development in advanced composites structures technology and advances in NDI methods has occurred. While current inspection capability for graphite/epoxy structures has been defined and is reflected in Appendix B, new technology and resultant change is inevitable. Consequently, Appendix B is intended as a current baseline to be updated as new in-service inspection problems and capability is defined.

REFERENCES

(1) NASA Contract Report 158969, Assessment of State-of-the-Art of In-Service Inspection Methods for Graphite/Epoxy Composite Structures on Commercial Transport Aircraft, M. L. Phelps, January 1979.

(2) Eddy Current Methods for the Examination of Carbon Fiber Reinforced Epoxy Resins, C. N. Owston, Materials Evaluation, Nov. 1976 pp 237-250.

APPENDIX A

INVESTIGATION AND DEVELOPMENT OF EDDY CURRENT INSPECTION FOR GRAPHITE EPOXY COMPOSITES

1.0 INTRODUCTION

Investigation of the eddy current method for inspection of graphite/epoxy (Gr/Ep) structures was conducted by Boeing Quality Control Research and Development as part of the NASA contract NAS1-15304. The objective was to develop capability and determine applications and guidelines for eddy current inspection of Gr/Ep composite structures on in-service airplanes. Three in-service defect types were selected as potentially detectable with eddy current and were used in the development and evaluation work. These were: surface and subsurface (substructure) fractures, impact damage, and delamination defects. The equipment used is commercially available except for the experimental probes designed for the Gr/Ep applications. Two of the instruments used are in common use by commercial airlines.

2.0 INSTRUMENTATION

Three commercially available eddy current instruments were used in this project: the EM 4300 and the MIZ-10, manufactured by Zetec, Inc., and the ED 520 manufactured by Magnaflux Corporation. The EM 4300 is basically the same as the MIZ-10, except that it has an automatic null and maximum frequency of 6 mHz instead of 1 mHz. The ED 520 is basically a fixed frequency instrument which operates around 200 kHz and uses a tuned circuit principal to create parallel resonance with the test probe. Most of the available commercial probes were not suitable and the manufacture of specialized probes was required for this project. These probes are shown in figure A-1 with the EM 4300 instrument.

3.0 SURFACE FRACTURES

3.1 TEST PANELS

Surface fractures were simulated in test panel I-27, which was 0.53 cm (0.21 in.) thick with 27 plies of the fabric type weave. The defects were created using a 0.013 cm (0.005 in.) wide x 2.3 cm (0.9 in.) diameter circular saw. The depth and length of the saw cuts are shown in figure A-2. Similar saw cuts were also made in a unidirectional Gr/Ep panel. Actual fatigue specimens were also available and fractures are shown in figure A-3. Radiographic opaque penetrant (DIB) was used to enhance the fractures. The fatigue specimens were 0.23 cm (0.09 in.) thick with fabric (cross ply) type weave.

3.2 INVESTIGATION

In the initial look at Gr/Ep panels, a comparison was made of the apparent conductivity of conventional metals with the Gr/Ep fabric and unidirectional plies. The impedance plane type presentation was viewed on a storage scope and is shown in figure A-4.

Figure A-4a displays the relative impedance values of various metals with conductivity being measured according to percent International Annealed Copper Standard (IACS). These measurements are usually made at 60 kHz. However, to obtain sensitivity to low conductivity materials, a higher test frequency is required. A presentation at 2 mHz is shown in figure A-4b and shows the sensitivity to lower conductivity is expanded relative to the total range of 0 to 100% IACS. By amplifying the signal (increased instrument gain) one may start to sense the Gr/Ep with unidirectional fibers. Figure A-4c compares unidirectional and cross ply conductivity using 12X amplification.

Similar impedance plane analysis was conducted on saw cut No. 1 shown in figure A-2 and on the fractured specimen shown in figure A-3. In each test the EM 4300 was used with phase rotation control adjusted such that variations in lift-off (probe to part spacing) cause impedance changes along the horizontal axis of the scope. The tests were conducted with frequencies from 50 kHz to several mHz. Only the fabric laminate yielded encouraging results. They are presented in figure A-5 for frequencies of 1, 2 and 3 mHz. Although frequencies up to 6 mHz were available on the EM 4300, the results were not as satisfactory as at 3 mHz. By comparing the responses between frequencies in figure A-5 one can see that the higher frequency offers better separation angle between the defect vector and the lift-off vector. However, the tip of the vector still tends to intersect with the locus of points forming the lift-off vector. This can be rather confusing when monitoring vertical voltage changes via a meter (as is commonly done).

Since the defect signals tend to parallel lift-off changes and since current commercial equipment is generally limited to less than 4 mHz, it became apparent that the conventional meter monitoring would have to be done with the lift-off rotated and maximized on the vertical axis. This would provide sensitivity to defects and to the unwanted lift-off variable. In a scope presentation the rotation of the impedance plane for lift-off is not necessary since all of the information is displayed all of the time.

As was mentioned previously, the unidirectional laminate did not give sufficient signal amplitude on these defects. An instrument with much higher frequency capabilities would be required. Consequently, the remainder of this report deals only with fabric laminates.

3.3 PROBE DEVELOPMENT

In developing probes for Gr/Ep a number of design parameters had to be considered. In some cases the parameters were interrelated and required simultaneous solution. Some of the more important parameters are:

- Match probe inductance for test frequency for best sensitivity.
- Select frequency to obtain necessary penetration.
- Select frequency for improved separation angle on impedance plane for suppression of unwanted variable (generally lift-off).
- Use large probe diameter to increase signal amplitude but limit probe diameter so that detectable crack length is a significant portion of probe diameter.
- Adjust probe geometry (height versus diameter) for best coupling of electromagnetic field with test part.

The solution was accomplished by an iterative process where several frequencies were initially chosen and probes built to match the frequency. Each probe was tested over various size defects for noise and detection capability. From the results, a rough idea of detectable defect length was obtained and new values were selected for probe diameter and frequency. Another probe was then made incorporating the new design values and also evaluated. As one test parameter approached optimization, a new parameter was evaluated. Some of the probes manufactured and evaluated are shown in figure A-6, which describes the electrical and physical characteristics of each probe. There are two common types of cores used in eddy current testing which are shown at the top of figure A-6. One is a ferrite rod and the other a ferrite pot core commonly used in transformers. Both types of cores were evaluated.

From the probe evaluation, it was determined that probe diameter was a key parameter. Conventional probes intended for use above 200 kHz, range in diameter from 0.31 cm (0.12 in.) to 0.13 cm (0.05 in.). These probes provided weak signals from the low conductivity Gr/Ep beneath the small surface area of the coil. Increasing the coil diameter proportionally increased the signal from the Gr/Ep. The limiting factor is that as coil diameter increases a relatively smaller percentage of the total eddy currents become disrupted by small defects. In general, the optimal probe diameter was equal to, or up to 1-½ times the defect length. Still further improvement was obtained using a ferrite pot core shown in figure A-6. The ferrite pot core encloses the coil on three sides and provides further concentration of the electromagnetic field directly beneath the pot core and coil, thereby increasing eddy current density and sensitivity. The pot cores were manufactured by Ferroxcube Corporation and are their 3B7 type material.

3.4 TESTING WITH TUNED CIRCUITS

A probe was evaluated by putting the probe in parallel with a variable capacitor and then connecting to the EM 4300. The capacitor was adjusted to obtain the maximum voltage across the coil. At this point, the current in the coil was maximum which maximized the magnetic field. The result was an increase in both the sensitivity of the probe to the defect and to undesired noise, such that the defect signal to noise ratio (S/N) did not change.

Since the tuned circuit approach improved defect sensitivity, the ED 520 instrument, which uses a similar principle, was evaluated. Normally, one would not expect successful results from an instrument operating in the 100-200 kHz frequency range. Such was the case when the ED 520 was calibrated in the conventional manner. This is reasonable if one considers the impedance plane approach shown in figure A-5, which indicates that at frequencies below 1 mHz defect indications tend to superimpose themselves on lift-off indications. However, if instead of calibrating the ED 520 to suppress meter indications caused by lift-off, one adjusts it to give a maximum response for lift-off, then sensitivity to Gr/Ep surface defects is obtained. This setup point is easily attainable by monitoring the voltage across the test coil and adjusting the LIFT-OFF/FREQ control to obtain the maximum voltage. Probes for the ED 520 were designed in the manner previously described. One probe, the FLEX ECII manufactured by USEC, Inc. is commercially available and provided satisfactory results.

3.5 RESULTS

Tests were performed to evaluate the performance of the EM 4300, ED520 and various probes. These tests were conducted on the test panel shown in figure A-2. The signals

from the defects were obtained using a meter presentation. Comparison between the most promising systems is shown in figure A-7.

In figure A-7, the signal from each defect is divided by the nonrelevant indications (noise). This noise is the change in response experienced from noncracked sections of the panel. Noise results from rough surfaces, coarseness of the weave, wrinkles, geometry changes or thickness changes. Generally a 2.0 to 3.0 S/N ratio is suitable for field use.

From figure A-7 one can see that the ED 520 with the Boeing ED-3 probe provided the best signal to noise ratio and, therefore, the most desired for detection of surface fractures. The FLEX ECII probe was also suitable. Both systems could detect defect No. 6 a 0.64 cm (0.25 in.) long x 0.03 cm (0.01 in.) deep saw cut. Paint bubbles and dirt, which cause significant changes in lift-off, can be detected by feel.

Also of interest is the fact that the maximum signal (90%) from defect No. 6 occurred when the center of the probe was over one end of the defect. Had the defect initiated from a hole containing a titanium or aluminum fastener, it would have been equally easy to detect. Conventional methods of scanning the probe around the periphery of the fastener head while maintaining equal distance from probe to fastener are applicable to Gr/Ep.

Sensitivity to the edge of the test panel is shown in figure A-8 using the ED520 and FLEX ECII probe. From the figure one can see that the magnetic field extends approximately 0.8 cm (0.3 in.) beyond the coil (probe.)

Figure A-9 is an enlarged picture of a 0.476 cm (0.188 in.) diameter countersunk hole containing two small fractures less than 0.3 cm (0.1 in.) long with fraying and delaminations. The two fractures were just detectable under laboratory conditions and could not be expected to be detected under field conditions. Should the detection of small fractures be required, one might try optimizing a probe design which would sit directly on top of the fastener. Figure A-10 shows the ED 520 being used with the FLEX ECII probe in a typical inspection for fractures initiating from a fastener hole. The ED-3 probe is laying beside the instrument.

Inspection was attempted on open holes. Here the probe is inserted into the hole and rotated so that the wall of the hole is inspected for cracks. Both the conventional hand scan technique with the ED 520 and an automated technique were tried, but without success. This was expected since most of the fibers were cut by the drilled hole destroying the eddy current paths.

4.0 SUBSURFACE FRACTURES

4.1 TEST PANELS

Panel I 27, shown in figure A-2 was also used for subsurface fracture tests. Tests were run with a single 0.23 cm (0.09 in.) thick Gr/Ep panel or two 0.23 cm (0.09 in.) thick Gr/Ep panels laid on top of the I 27 panel. Figure A-11 shows the three layer combination setup with the EM 4300 and Boeing-built probe No. 8.

4.2 INVESTIGATION

The impedance plane analysis was once again used to determine optimum frequency and defect signature characterization. Tests were conducted with a 0.23 cm (0.090 in.) thick layer on top of Panel I 27. The EM 4300 with built-in scope was used with probe No. 6 at various frequencies. At each frequency the instrument was adjusted so that changes in probe impedance due to lift-off variations gave signals along the horizontal axis of the storage scope. The probe was then scanned directly over defect 1 in the I 27 panel and the maximum response from the defect noted. The presentations for frequencies 1 to 4 mHz are shown in figure A-12. The maximum response from the defect is indicated by the small circle and is connected to the origin by a straight line forming a vector with magnitude (length of line) and direction. The origin is the response obtained when no defect is present.

One can see from figure A-12 that the separation angle formed by the second layer defect vector and the lift-off vector increases as frequency is increased. This is desirable for a better S/N ratio as long as penetration is sufficient. In the 4 mHz case the vector is becoming shorter due to the shallower penetration of the higher frequency. Conversely, too low a frequency causes the weaker subsurface defect vector to approach the lift-off vector and become obscured by surface roughness. From figure A-12, it can be seen that for a 0.23 cm (0.09 in.) thick top layer, frequencies of 2 to 3 mHz with their 60° to 90° lift-off/crack separation angle, provide stronger defect signals.

The ED 520 was also evaluated on subsurface defects but did not provide adequate signals when calibrated in the conventional manner or with the lift-off maximized.

4.3 PROBE DEVELOPMENT

The same probe design parameters previously mentioned in this report apply to subsurface defect detection. Of these parameters, probe diameter plays an even more important role. Large probe diameter was not only required for increased signal size, but the larger diameter was required for satisfactory penetration and hence, subsurface defect detection. This may be seen in figure A-13. In this figure, two probes having similar electrical properties and optimized for 3 mHz, but differing in coil diameter, were compared. The 0.69 cm (0.27 in.) diameter probe was probe No. 6 and the 0.46 cm (0.18 in.) diameter probe was probe No. 5. Both probes were tested at the same instrument sensitivity setting and with the S/N ratio determined on the six defects in Panel I 27 covered by a 0.23 cm (0.09 in.) thick top layer. The 0.69 cm (0.27 in.) diameter probe showed improved signal strength and better S/N ratio. This lead to still larger probe diameter development, probes No. 7 and No. 8, the characteristics of which are listed in figure A-6. Once again the limiting factor on size of the probe was that the detectable crack length be a significant portion of the probe diameter (approximately ½ the probe diameter or more).

4.3.1 RESULTS

Of the probes listed in figure A-6, probe No. 8 was the most sensitive to defects in Panel I 27 for both the 0.23 cm (0.09 in.) thick and 0.46 cm (0.18 in.) thick upper layers. The results for probe No. 8 are shown in figure A-14. From the figure one can see that defect No. 2, 1.14 cm (0.45 in.) long x 0.15 cm (0.06 in.) deep, is detectable beneath the .46 cm (.18 in.) top layer and defect No. 4, 0.79 cm (0.31 in.) long x 0.10 cm (0.04 in.) deep, is detectable beneath a 0.23 cm (0.09 in.) top layer.

In both cases the S/N ratio exceeds 2.5. Probe No. 8 was designed for penetrating through 0.46 cm (0.18 in.) top layer at 400-500 kHz. Although this frequency is really lower than required for the 0.23 cm (0.09 in.) thick top layer, the extra sensitivity from the increase in diameter more than makes up for the less optimum frequency. Future probe designs should take this into consideration.

The maximum response from a second layer defect with either a 0.23 cm (0.09 in.) or 0.46 cm (0.18 in.) thick top layer occurred when the center of the probe was over one end of the notch.

Penetration as a function of frequency and probe diameter is shown in figure A-15. From the figure one sees that probe No. 6 ceases to sense the increase in panel thickness beyond 0.38 cm (0.15 in.), regardless of how low the frequency goes. This demonstrates that probe diameter along with frequency determine penetration. Similar phenomena occur in aluminum structures.

The size of the magnetic field created by probe No. 8 is illustrated in figure A-16. One can see that the edge of the part was sensed when the edge of the probe was 0.17 cm (0.46 in.) from the edge of the test part. Similarly, the edge of the structure beneath a 0.23 cm (.09 in.) thick top layer was sensed when the edge of the probe was 0.84 cm (0.33 in.) from the edge of the second layer structure is shown in figure A-17. From this information it is apparent that the deeper the electromagnetic field penetrates, the more confined it is to the area directly beneath the probe.

Tests were made on actual structure containing subsurface fractures as shown in figure A-18. In this case, both the upper and lower layers were .25 cm (.10 in.) thick and fastened together with a 0.478 cm (0.188 in.) diameter titanium fastener. The fracture was easily detected with a 50% of full meter scale change in response using probe No. 8 with the EM 4300 or MIZ-10 at 400 kHz, as shown in figure A-19. In this case, the probe was placed adjacent to the fastener over the area where the fracture is expected to occur.

A similar test was conducted on model 727 Gr/Ep elevator. A saw cut was made in the second layer structure and extended from one fastener hole to the adjacent fastener hole. The saw cut was easily detected by placing the probe between the fasteners and is shown in figure A-20.

5.0 IMPACT DAMAGE

5.1 TEST PANELS

Figure A-21 describes the three test panels and the defects they contain. In all cases the impact damage was created by dropping an anvil 0.317 cm (0.125 in.) in diameter onto the part.

5.2 INVESTIGATION

The probes of figure A-6 were used in these tests. The evaluation was conducted with the EM 4300 to determine optimum frequency and instrument calibration. Since the impact damage was basically a surface defect, it came as no surprise that the optimum instrument calibration, frequency and probe requirements closely followed the surface

fracture requirements. Similarly, the defect response, as viewed on a storage scope, was very close to the response for liftoff changes. This again lead to calibrating the EM 4300 so that lift-off changes appeared along the vertical axis of the storage scope, thereby allowing the largest possible signal change from the defect to be seen on the meter.

5.3 RESULTS

All three panels in figure A-21 were tested. The result of these tests is typified in the results from Panel I-11. This is shown in figure A-22 where four different instrument/probe/frequency combinations are compared. These combinations are designated by symbol and described as follows:

EM 4300 with probe No. 8 at 400 kHz with phase rotation adjusted so that lift-off changes are presented along the vertical axis of scope.

EM 4300 with probe No. 6 at 3 mHz with phase rotation adjusted so that lift-off changes are presented along the vertical axis of the scope.

EM 520 with FLEX ECII probe calibrated for maximum sensitivity to lift-off changes.

ED 520 with probe ED-3 calibrated for maximum sensitivity to lift-off changes.

The straight lines through the data points were determined using a linear regression and produced a correlation coefficient of 0.97 or better. The best sensitivity (S/N) was obtained with ED 520 and probe ED-3, which detected defect No. 1 with 2.5 S/N ratio. Although both the FLEX ECII and the ED-3 probe exhibit much the same S/N ratio, the ED-3 probe was able to detect the defects with approximately 50% higher signal than the FLEX ECII Probe. The ED 520, ED-3 probe and impact damage panel are shown in figure A-23. This same setup was used to inspect 100 Gr/Ep specimens 0.25 cm (0.10 in.) thick and containing impact damage from a 1.27 cm (0.50 in.) diameter steel sphere at 56.4 cm-kg (10.0 in.-lb) impact. All defects were detected by eddy current and could not be seen visually.

6.0 DELAMINATION

A brief investigation was conducted on Gr/Ep panels containing delamination of plies. The inspection method was the same as we used for subsurface fractures. Delamination in which the plies were physically separated creating a void could be detected. Panels where the plies were delaminated but in close contact could not be detected.

The eddy currents also sense any change in the graphite fiber density relative to the nonconductive epoxy matrix. This fact was demonstrated in a 0.64 cm (0.25 in.) thick Gr/Ep panel where a comparison was made between ultrasonics and eddy current. Results of the through transmission ultrasonic tests detected approximately a 15.2 cm (6 in.) diameter delaminated area, whereas eddy current detected approximately a 30.4 cm (12 in.) diameter area. The discrepancy was due to the eddy currents sensing additional areas where the graphite fibers had not been compressed as tightly. The panel was 0.064 cm (0.025 in.) thicker in these areas. Because of the inability of eddy current to detect delaminations where plies are in close proximity and because of their

sensitivity to the density of the graphite fibers, this method was not as suitable for delamination detection. It may, however, be useful should one need to compare the fiber to resin ratio.

7.0 CONCLUSIONS

As a result of this project, it is concluded that the commercially available ED 520 manufactured by the Magnaflux Corporation with the FLEX ECII eddy current probe manufactured by USEC, Inc. are suitable for detection of surface fractures in Gr/Ep panels with fabric (cross ply) weave. It is also determined that the ED 520 should be calibrated for maximum sensitivity to lift-off variations. This same set up when used with the Boeing-built ED-3 probe is suitable for detection of impact damage. Since the ED 520 is calibrated for maximum sensitivity to lift-off variations, the detection of the smaller defects would be limited by the amount of noise from lift-off variations.

It is further concluded that the MIZ-10 manufactured by Zetec, Inc. with the Boeing-built probe No. 8 is suitable for detection of subsurface fractures in Gr/Ep fabric panels beneath top layers as thick as 0.46 cm (0.18 in.). Instrument calibration is identical to conventional calibration. Although an optimum frequency and probe diameter exists for each top layer thickness, it is felt that probe No. 8 at 400 kHz would provide suitable results. Structure beneath top layers thicker than 0.46 cm (0.18 in.) can be inspected but would require lower frequencies and larger probe diameters.

Further probe design could enhance the detection capability of both surface and subsurface defects but probably is not warranted until more specific applications are defined. It also is important to note that the circumstances surrounding a particular application will dictate the detectable defect size.

APPENDIX B
RECOMMENDED GUIDELINES FOR IN-SERVICE INSPECTION 0F Gr/Ep COMPOSITE STRUCTURES

1.0 INTR0DUCTION

This report is based on the results of the program and is intended as an aid to the airlines in the preparation of their inspection procedures for Gr/Ep structures. Many of the techniques are very familiar to inspection personnel, but new techniques are also included which are specifically applicable to Gr/Ep composite structures. It is recommended that this document be considered a current baseline that will be expanded considerably in the next few years as advanced composite structures come on-line at the airline operations level. The current activity level and recognized challenges for NDI of advanced composites will assure rapid changes.

2.0 SCOPE

The Gr/Ep structures inspection guidelines are presented in the normal sequence of addressing an inspection problem, i.e., details of the inspection problem, selection of the inspection method, procedure to be used, and a section describing reference standards. The guidelines concern general structure/defect combinations. Specific problems must be defined as they occur on in-service aircraft.

3.0 INSPECTION PROBLEM

The problem should be defined as to structure to be inspected, area(s), access, materials, and defect type and location.

3.1 STRUCTURE

Details of the structure to be inspected should be determined. The following are suggested:

1) Materials Used
   - Gr/Ep fabric
   - Gr/Ep unidirectional tape
   - Other ply materials
   - Honeycomb core
   - Metals
   - Fasteners
   - Coatings

2) Joints
   - Cocure (no adhesive bonds)
   - Adhesive bond
   - Fastened
   - Sealant

3) Structures
   - Configuration - figure B-1 contains basic structural details - more should be added as identified.
   - Thicknesses: laminates, honeycomb, and metals
   - Ply layup details for direction - tape and fabric

3.2 DEFECTS

Defects are described as follows:

1) Delamination - separation between plies in a laminated epoxy/fiber composite part or at the bondline of two separately identified parts.

2) Disbond - separation at the bondline of parts joined by an adhesive bond.

3) Impact Damage - shattering of matrix, small cracks, broken fibers, etc. resulting from impact of an object on part surface.

4) Fracture - material separation in the resin matrix or across plies rather than between plies.

5) Fastener Hole Damage - cracks, small delaminations, matrix shattering, hole elongation, and fastener head pulled beneath part surface.

6) Lightning Damage - burns, matrix shattering, fiber fraying, etc. resulting from lightning strike.

7) Heat Damage - overheating, burns causing blistering, discoloration, delamination, and charring.

8) Water-in-Honeycomb - entrapped water in honeycomb cells.

9) Surface Blemishes - scratches, dents, etc. indicating possible impact damage.

4.0 METHOD SELECTION

The method should be selected relative to the structural details per Section 3.1 and defect type per Section 3.2. The data table in figure B-2 provides a method selection reference. Two tasks are included: (1) the detection task which indicates the presence of a defect and (2) the evaluation task which confirms the defect exists and evaluates its extent or severity.

The first letter after the task (number 1 or 2) is the preferred method or technique, the next letter indicates second preference, and so on.

5.0 INSPECTION PROCEDURE

5.1 VISUAL, OPTICAL, TAP TEST
5.1.1 Far Visual (walk-around)
Requirements: Proper lighting.

Procedure:
1) Inspect for abnormal surface conditions (bulges, dents, scratches, blemishes).

2) If above conditions are observed proceed to near visual inspection.

5.1.2 Near Visual, Optical, Tap Test

Requirements: Portable light, 10X magnifier, borescope, mirror, and pocket knife.

Procedure:
1) Inspect at arm's length or less on exterior surface or inside access holes.

2) Look for cracks, dents, bulges, blemishes – push, pry, and tap on surface for soundness of material. Definite defect indication requires no further investigation. If in doubt or if evaluation for size is desired, proceed to NDI methods per figure B-2. NOTE: Lack of defect indication by tap test is not sufficient to confirm absence of defect. Tap test can be used with good confidence only if a reference defect part is used which duplicates the structure and defect and the defect is clearly detectable by tap test.

5.2 ULTRASONIC PULSE-ECHO TECHNIQUES

5.2.1 Pulse-Echo, Straight Beam

Ultrasonic pulses are generated by a single transducer in contact, through a couplant, with the part surface. The pulses travel internally in the part and reflect or echo from each material change, for example, the interface of skin bonded to substructure. The reflected pulses are detected by the transducer and resultant signals on a cathode ray tube (CRT) display are monitored for changes caused by defects within the part.

Requirements: Standard pulse-echo U/T instrument with good pulse power and sensitivity at low frequencies, transducers in the low frequency ranges of 0.5-2.25 MHz, couplant, and delamination reference standard (Sec. 6.0)

Procedure:
1) Adjust instrument per manufacturer's instructions and calibrate to the reference standard.

2) Inspect area noting instrument signal pattern on area away from inspection location and compare pattern at inspection location.

3) A pattern similar to the reference standard pattern indicates a defect.

4) Report the defect or proceed to further evaluation per NDI methods of figure B-2.

5.2.2 Pulse-Echo, Angle Beam

This technique is similar to Section 5.2.1 except the search unit is a transducer mounted on a plexiglass wedge to cause the sound to enter the part at an angle. This angle can range widely for Gr/Ep material, dependent on the type of defect, the lay-up of the Gr/Ep laminates, and the structure. This method is not recommended for delamination/disbond defects but is recommended for fracture detection in plates and lugs.

Requirements: Same as Section 5.2.1 except for the wedge search unit – the reference standard is critical. A simple notch representing a fracture is satisfactory. However the lay-up of the laminates must duplicate the part to be inspected. Fabric and tape orientation must be duplicated. See Section 6.0.

Procedure: Same as Section 5.2.1 except the transducer is moved toward and away from the reference standard defect and compared to an identical area with no defect. The defect signal must be identified when setting up on the reference standard. A similar indication in the part is the basis for reporting a defect.

5.2.3 PULSE-ECHO – ULTRASONIC THICKNESS GAGE

This method, also a pulse-echo method as described in Section 5.2.1, is identified separately due to the specific application, i.e., thickness gaging. Most of these instruments read thickness on a digital readout. The optimum Gr/Ep inspection application is detection of delaminations in skin or skin to substructure disbonds.

Requirements: Ultrasonic thickness gage, appropriate transducers, couplant, and step thickness standard of Gr/Ep laminates per Section 6.

Procedure: Same as Section 5.2.1 except readout is in thickness readings. A defect appears as a reduced thickness in a localized area.

5.3 ULTRASONIC THRU-TRANSMISSION (TTU)

TTU inspection is primarily used for manufactured parts but has been used for some field inspection work. As sound is transmitted from a search unit through the part to a receiver search unit, these search units must be held in steady alignment while scanning over a part. Also; a couplant is required except for a recent instrument – the Sonatest/Shadow device. The couplant may be an oil or grease spread on the part surface. With water-jet search units, the water jets provide the couplant medium. The water-jet systems in use are generally fabricated for a particular application, not commercially available equipment.

Defects are detected by attenuation of the sound passing through the part.

Requirements: Standard ultrasonic instrument equipped for send-receive mode and operable in the 0.5-2.25 MHz range, transducers to match the frequency range, couplant, or water-jet search unit system, yoke for mounting the send-receiver search units. See figure B-3.

No couplant or water-jet system is required for the Sonatest/Shadow instrument.

A reference standard simulating the structure and defect to be detected is required for optimum reliability. An alternative is to establish a strong signal on the part to be inspected and, if consistent over a general area, a localized signal loss will indicate a defect.

Procedure:

1) Adjust instrument to manufacturer's instructions and check sensitivity on the reference standard per Section 6.0. With no reference standard, establish a reliable signal on a good area of the part.

2) Scan the area to be inspected. A significant or total signal loss indicates a defect.

3) Other methods per Section 4.0 can be used for further evaluation if desired.

5.4 BOND TESTERS

There are a variety of bond test instruments, each a little different in operating principle. Most use piezoelectric transducers for generation and detection of the sound energy. Some instruments use fixed frequencies, some a variable frequency as selected by the operator, and some a repetitive sweep of frequencies through a given range. Frequencies used may range from a few kHz to as high as 80-100 kHz. All instruments require transducer contact with the surface, but some do not require a couplant. Detection of the sonic energy, as modified by the structure and possible defects, is accomplished by piezoelectric transducers or microphone devices. Readout methods include cathode ray tube, meter, and audible or visible alarms.

Requirements: A bond test instrument that will detect the reference standard defect, transducers as needed, couplant, if needed, and a reference standard which duplicates the strucure and type of defect to be detected.

Procedure:

1) Adjust the instrument to manufacturer's instructions and adjust sensitivity on the reference standard.

2) An instrument reading similar to that from the reference standard indicates a defect.

3) Report the defect or proceed to further evaluation per the NDI methods, figure B-2.

5.5 LOW KV RADIOGRAPHY

The principle of defect detection with radiography is well known. Low KV (10-50 KV) radiography is specified due to the low density of the Gr/Ep materials. Some advantage can be gained by use of a radiographically opaque penetrant which is used to penetrate defects prior to X-ray. This greatly enhances defect images and detectability by radiography. However the materials are expensive, have a limited shelf life, and one of these – tetrabomoethane – is toxic.

Requirements: X-ray equipment operable in the 10-50 KV, 5 ma range, X-ray processing and film reading facility, film, accessories, radiographically opaque penetrant-diiodobutane (DIB) is recommended, and reference radio graphs may be required if there is no prior information on the structure/defect combination to be radiographed. A set of exposure

curves were developed for this procedure as shown in figure B-4. A cleaning solvent and wiping rags are also required. The area to be X-rayed must be cleaned, as low KV radiography is sensitive to debris, grease, hydraulic fluid, etc.

Procedure:

1) Clean area with solvent.

2) Position film and source and expose film per established procedure.

3) Without an established procedure determine film and source position as dictated by structure and defect information.

4) With structure thicknesses known, consult the exposure curves, pages 17 through 44, and determine initial test technique. Adjust technique as necessary and re-X-ray.

5) Develop and interpret film.

6) With DIB enhancement, apply DIB to area after cleaning, wait one hour or more, X-ray per 2 through 5 above. Self removal of DIB by evaporation should occur within 5 days.

5.6 EDDY CURRENT

The eddy current method is only usable on material that is at least slightly electrically conductive. This is necessary so that eddy currents can be induced into and flow in the material to be inspected. Crack type defects are detectable due to the interruption or distortion of the normal eddy current flow pattern. Electrical conductivity in Gr/Ep composite materials is less than 0.1% IACS, consequently its use on Gr/Ep structures is somewhat different than the usual aluminum applications.

Requirements: Eddy current instrument and probe capable of detecting the reference standard defect, and reference standard duplicating the structure and defect type, size, and location expected in the structure. The two instruments that were used in the development of the following procedure were the ZETEC MIZ-10 and the Magnaflux ED-520.

Procedure: Detailed procedures for Gr/Ep inspection were developed during the eddy current research effort of the contract which can be used to detect surface or substructure fractures in Gr/Ep fabirc materials. Because of the high sensitivity of eddy current inspection to metallic materials during Gr/Ep inspections, an evaluation of defect indications may be desirable to determine if metal structure or debris is present. The recommended method is radiography.

Calibration of ED 520 for Surface Defect
Detection in Graphite/Epoxy Fabric Weave Structure

(1) Turn Mode Switch to Low Sensitivity Position.

(2) Set the LIFT-OFF/FREQ control and BALANCE control dials to their zero positions (fully counterclockwise).

(3) Place the probe on the surface of the reference standard duplicating structure to be inspected and adjust the BALANCE control so that the meter needle is placed on "scale."

NOTE: If after fully turning the BALANCE control in clockwise direction, the meter needle is not on scale, return the BALANCE control to zero setting and advance the LIFT-OFF/FREQ control to higher setting, e.g., 020 on the dial. Then repeat Step 3.

(4) Lift the probe from the reference standard. Note the difference in meter reading.

(5) Readjust the LIFT-OFF/FREQ control (and BALANCE control if necessary to keep the meter needle on scale) until the change in meter reading between probe on the part and lifted off the part is at a maximum or greater than 500. Adjust instrument such that a higher meter reading is obtained when the probe is in air than on the reference standard.

NOTE: If the meter needle cannot be brought on scale with the BALANCE control, continue advancing the LIFT-OFF/FREQ control until the needle comes on scale.

(6) Pass the probe over the simulated defect and adjust the sensitivity so that the desired response is obtained.

Calibration of MIZ-10 for Substructure Defect Detection in Graphite/Epoxy Fabric Weave Structure

(1) Determine test frequency to be used, dial in the first two significant digits on the rotary thumbwheel switches. Then select the range switch multiplier located below the thumb wheel switch. Connect the probe(s) to the connectors on the front panel; the probe connection depends upon the specific test being used. Note that the most significant digit will not rotate below 1 or greater than 9.

(2) Turn function selector switch to Battery Check Position, observe that the meter needle is in the "Battery OK" area of the meter face.

(3) Place function selector switch in the balance position (BAL). Place probe upon the material under test, or standard, increase sensitivity from zero until meter indicates approximately half scale deflection. Rotate X and R balance controls for a minimum meter reading. Increase sensitivity again until meter indicates half scale deflection and again rotate balance controls until meter deflection is minimum. Repeat until sensitivity is maximum and meter is at minimum deflection after balancing.

(4) To set lift-off with a pancake-type probe, turn function selector switch to operate; place probe on standard under test. Rotate meter position control until meter is on scale. Rock the probe to provide a lift-off signal. It may be necessary to reduce sensitivity to prevent meter overrange. While rocking probe, rotate the lift-off (sometimes called phase rotation) control until meter movement is minimum. Now hold probe firmly on material or standard and pass over a known defective area.

Observe that meter indication deflects upscale. If meter deflects down scale, lift-off is 180° out of phase. Rotate lift-off control 180° and readjust for minimum meter movement when rocking probe. Check for upscale deflection when passing over a known defect.

To set up the instrument using a storage oscilloscope, connect the MIZ-10 vertical (V) and horizontal (H) signal components located on the front panel to the oscilloscope inputs. Obtain a display on the oscilloscope screen. As before, rock or move probe to obtain a lift-off signal and rotate lift-off control until the probe motion signal is set in a horizontal plane. Pass probe over defective area and observe the defect signals, adjust MIZ-10 and oscilloscope for best display of signal pattern. Connections may also be made to recorders and/or other monitors.

5.7 FLUORESCENT PENETRANT

Equipment: Fluorescent penetrant and developer, emulsifier, water solvent, wiping rags, and black light.

Procedure:

1) Clean area to be inspected thoroughly.

2) Apply penetrant, remover, and developer if needed per standard procedures.

3) Inspect with black light.
   NOTE: A group IV penetrant with water-wash removal and no developer is recommended on bare Gr/Ep structure.

6.0 REFERENCE STANDARDS

Reference standards are required for in-service inspection of advanced composite structures with ultrasonic and bond tester methods and recommended for tap test. The best reference standard would be a duplicate part or section of structure to be inspected, including the actual defects of concern. However, obtaining parts with defects of the desired sizes and locations is very seldom possible, and the alternative is to fabricate reference standards that duplicate the parts to be inspected with built in simulated defects of the required sizes and locations.

Figure B-5 indicates the recommended reference standard configuration. The reference standard material, layup, dimensions, and structure details should simulate the part to be inspected.

a) PANEL LAYUP

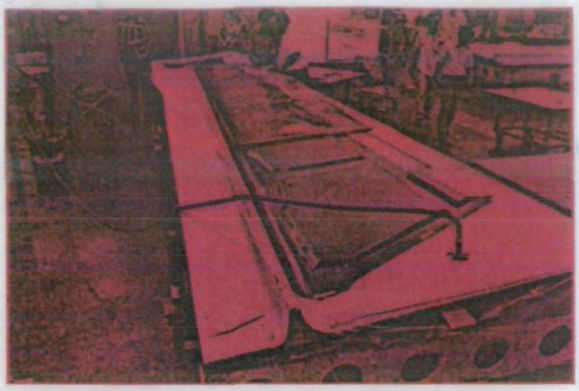

b) BAGGED FOR AUTOCLAVE CURE

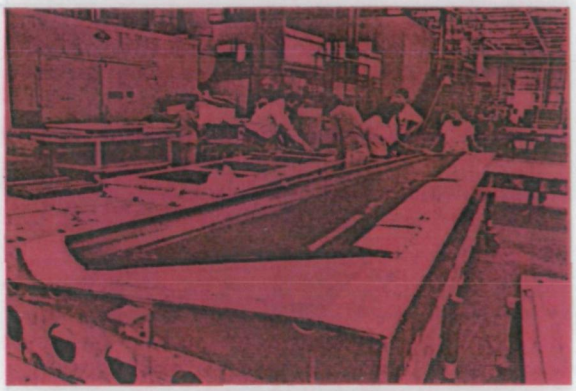

c) AFTER CURE

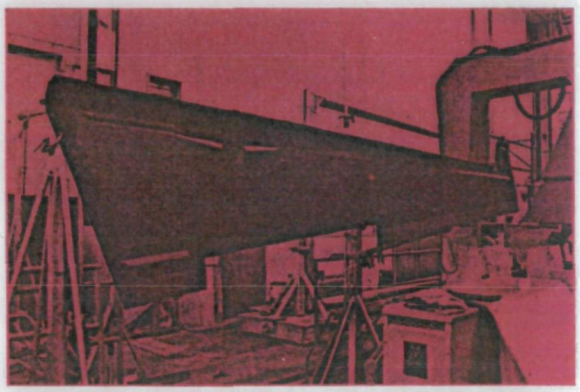

d) TTU INSPECTION OF COMPLETED PANEL

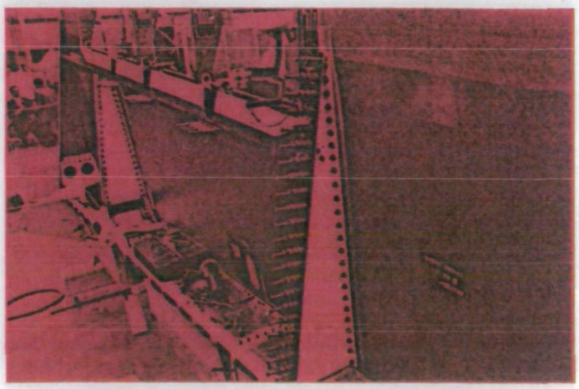

e) RIB, SPAR, AND PANEL ASSEMBLY

Figure 1. — Boeing 727 Elevator Fabrication Sequence

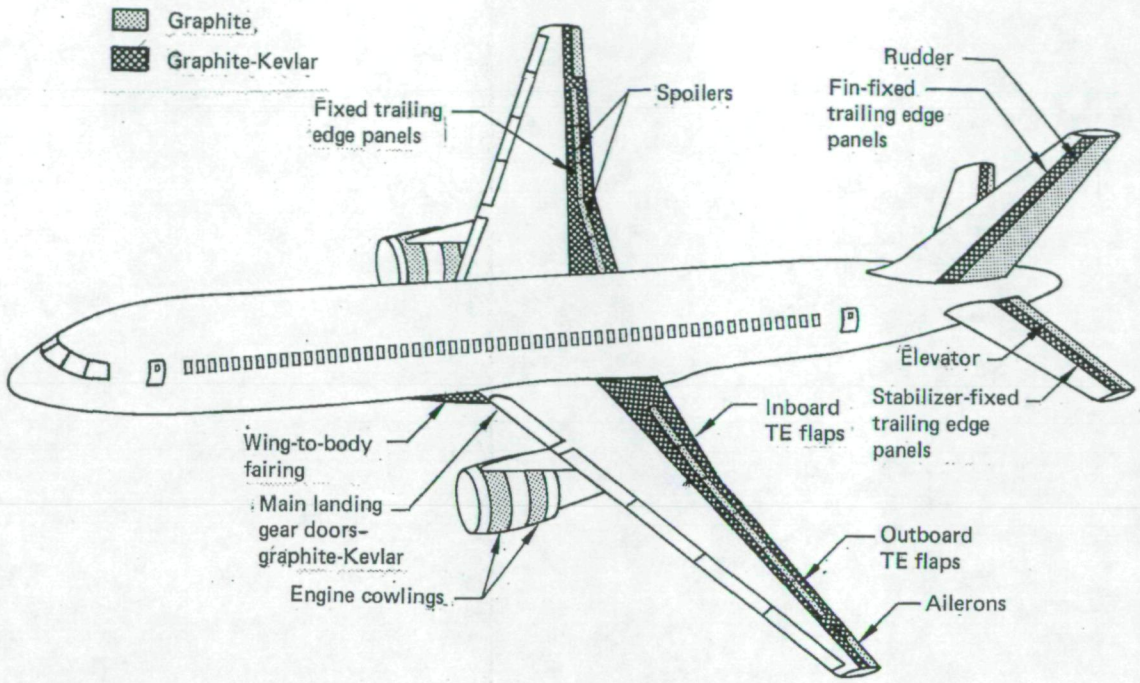

Figure 2. —Boeing 757 Composite Components

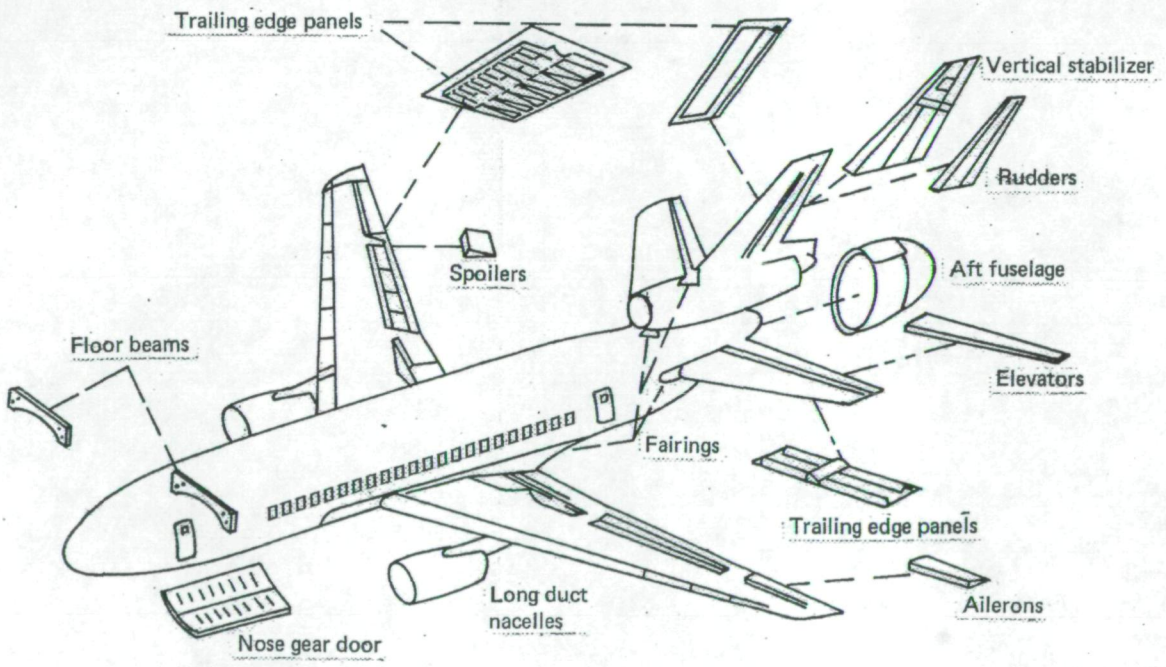

Figure 3. —Douglas DC-10 Potential Composite Components

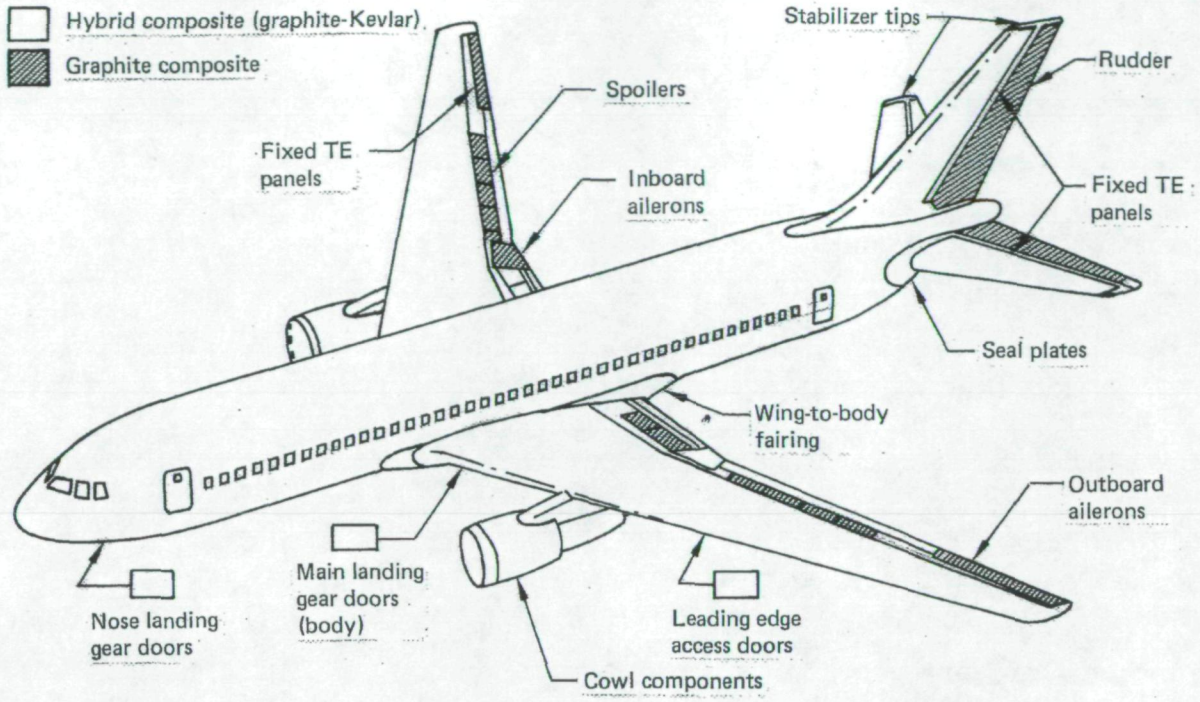

Figure 4. — Boeing 767 Composite Components

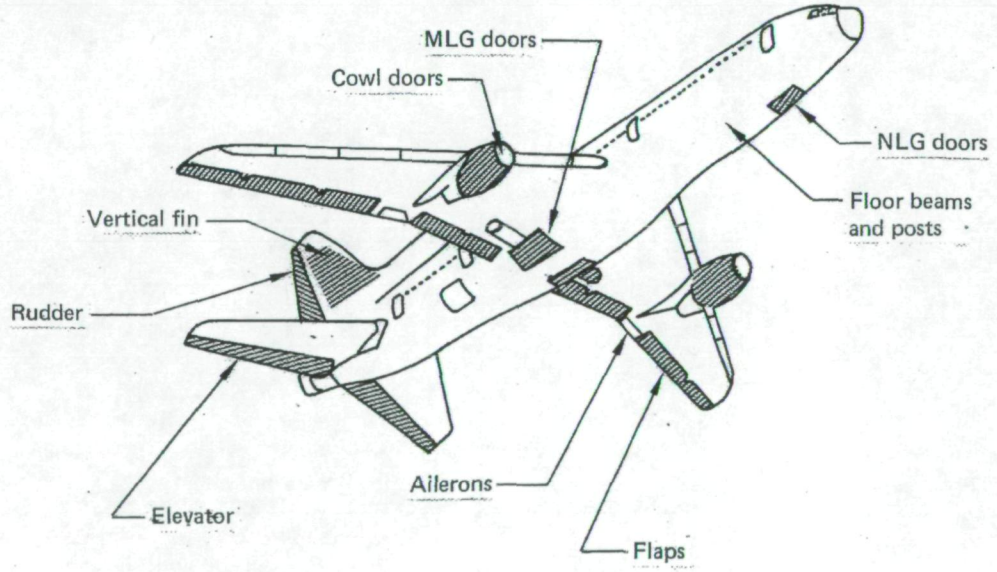

Figure 5. — Lockheed L-1011 Potential Composite Components

Component	Primary structure			Secondary structure		
	L-1011 Vertical fin	DC-10 Vertical stabilizer	B-737 Horizontal stabilizer	L-1011 Aileron	DC-10 Rudder	B-727 Elevator
Size, m	2.7 by 7.6	2.4 by 7.6	1.2 by 5.2	1.2 by 2.4	0.8 by 4.0	0.9 by 5.8
Baseline metal mass, kg	389.2	453.6	118.9	63.5	41.4	117.0
Composite mass, kg	272.2	350.3	91.6	45.4	30.3	89.4
Projected mass savings, %	30.1	22.8	22.9	28.5	26.8	23.6

Figure 6. — NASA ACEE Composite Structures

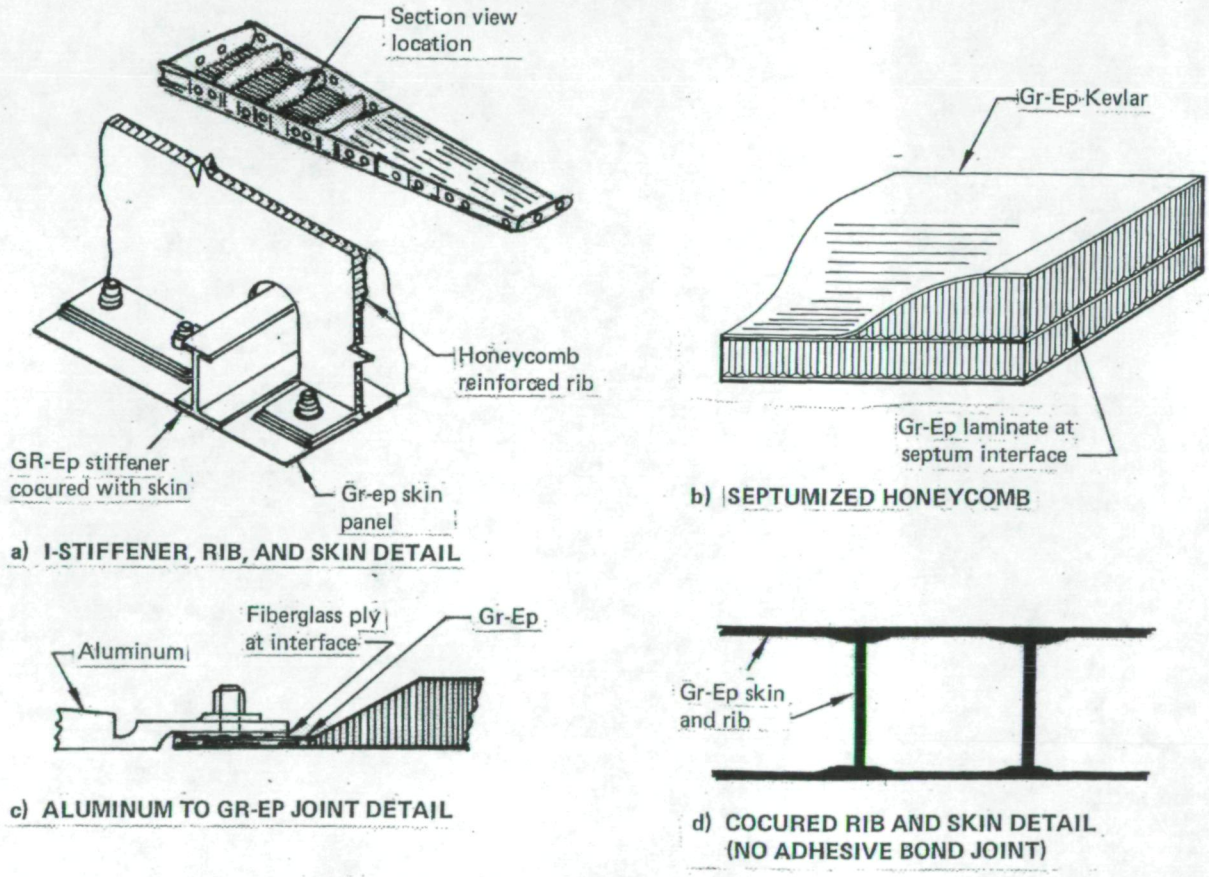

Figure 7. — Typical Gr-Ep Detailed Structural Configurations

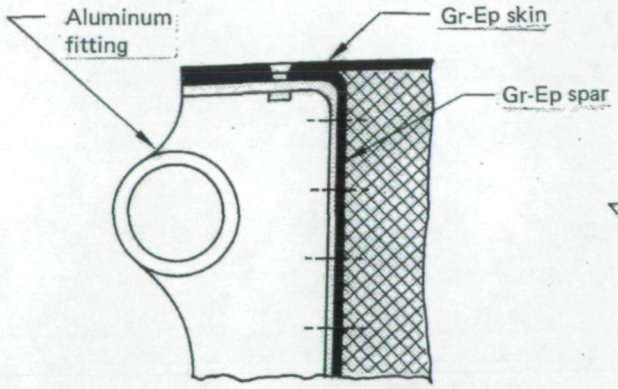

e) HINGE FITTING TO GR-EP STRUCTURE DETAIL

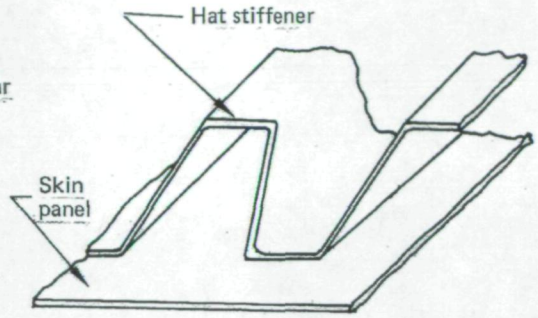

f) ALL GR-EP HAT-STIFFENED SKIN (COCURED—NO ADHESIVE BOND)

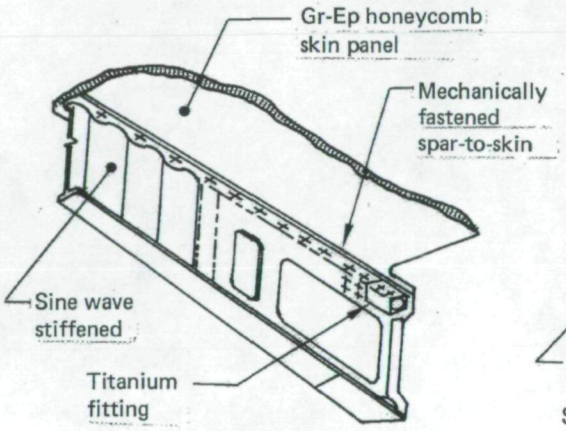

g) SINE WAVE-STIFFENED SPAR/SKIN ATTACH FITTING DETAIL

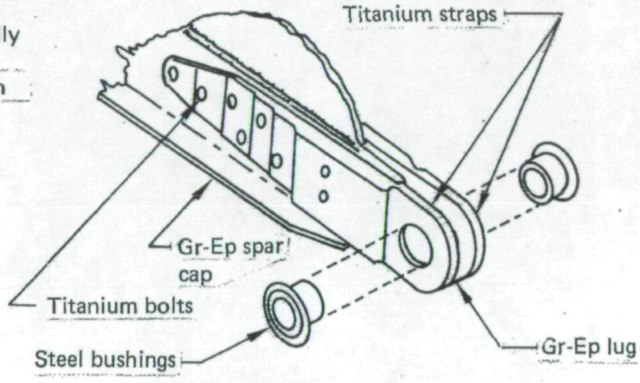

h) LUG FITTING

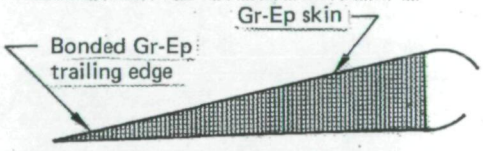

i) FULL DEPTH HONEYCOMB (NOMEX OR HRP CORE)

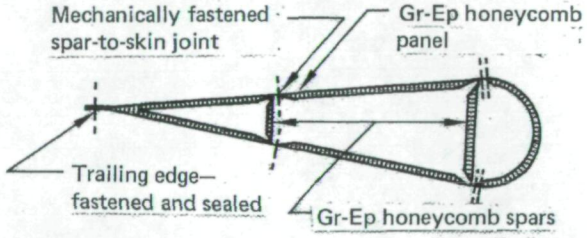

j) MECHANICALLY FASTENED GR-EP HONEYCOMB SKIN AND SPARS

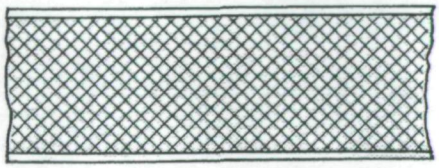

k) GR-EP SKINS AND SYNTACTIC CORE

Figure 7. — (Concluded)

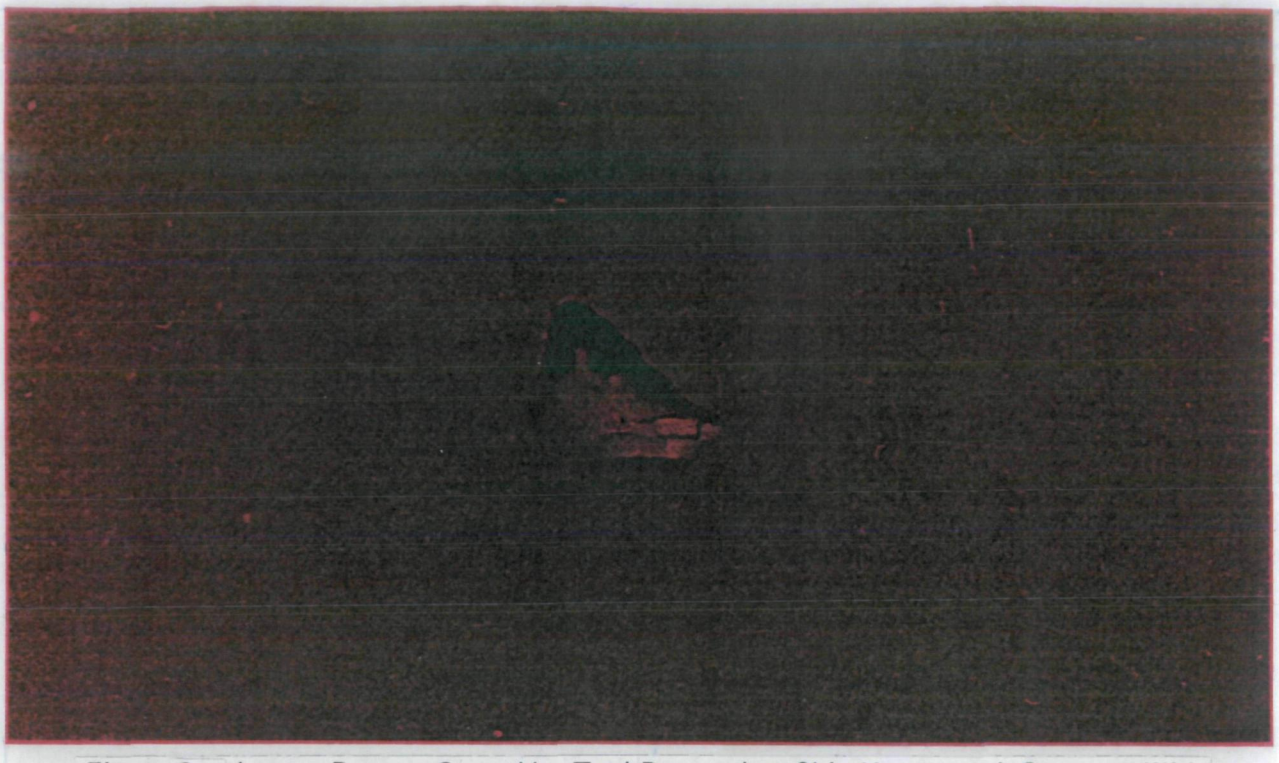

Figure 8. – Impact Damage Caused by Tool Dropped on Skin-Honeycomb Structure With Dent and Fractures Visible

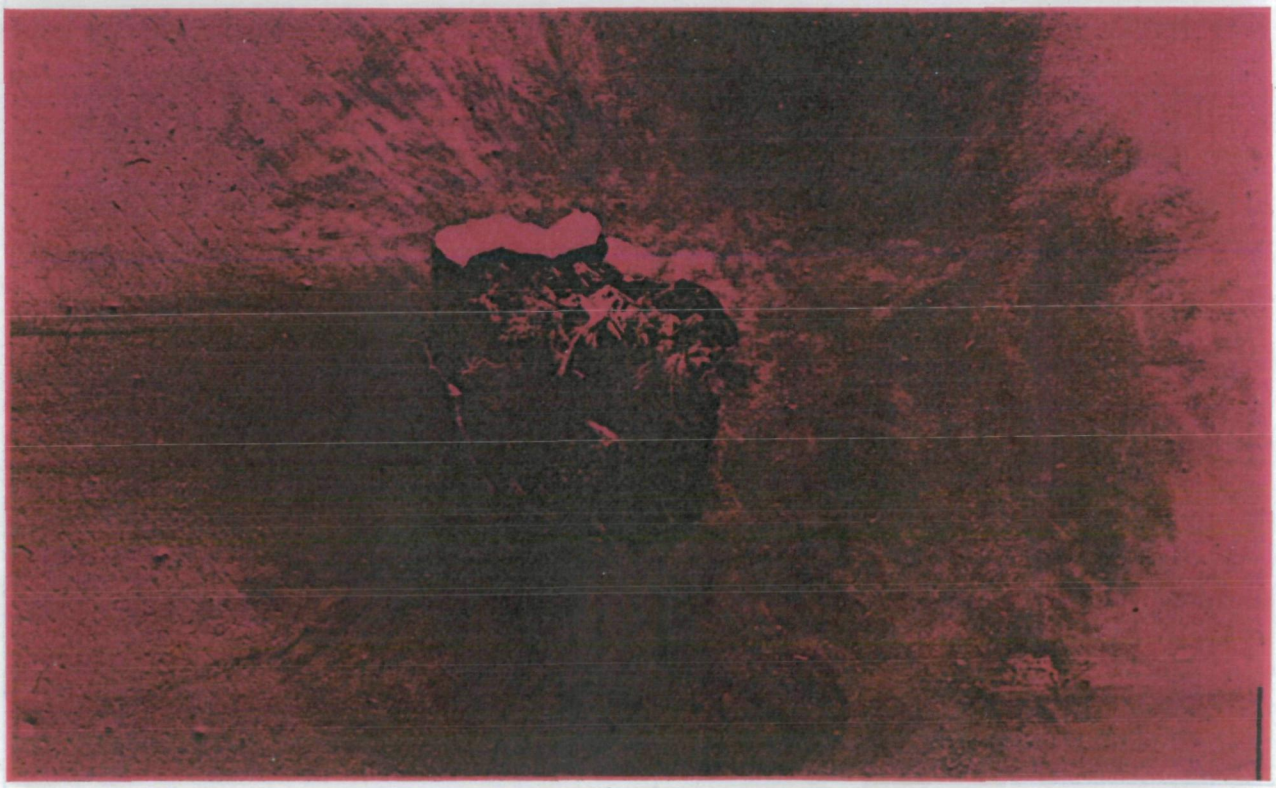

Figure 9.– Lightning Damage With Delamination and Internal Damage

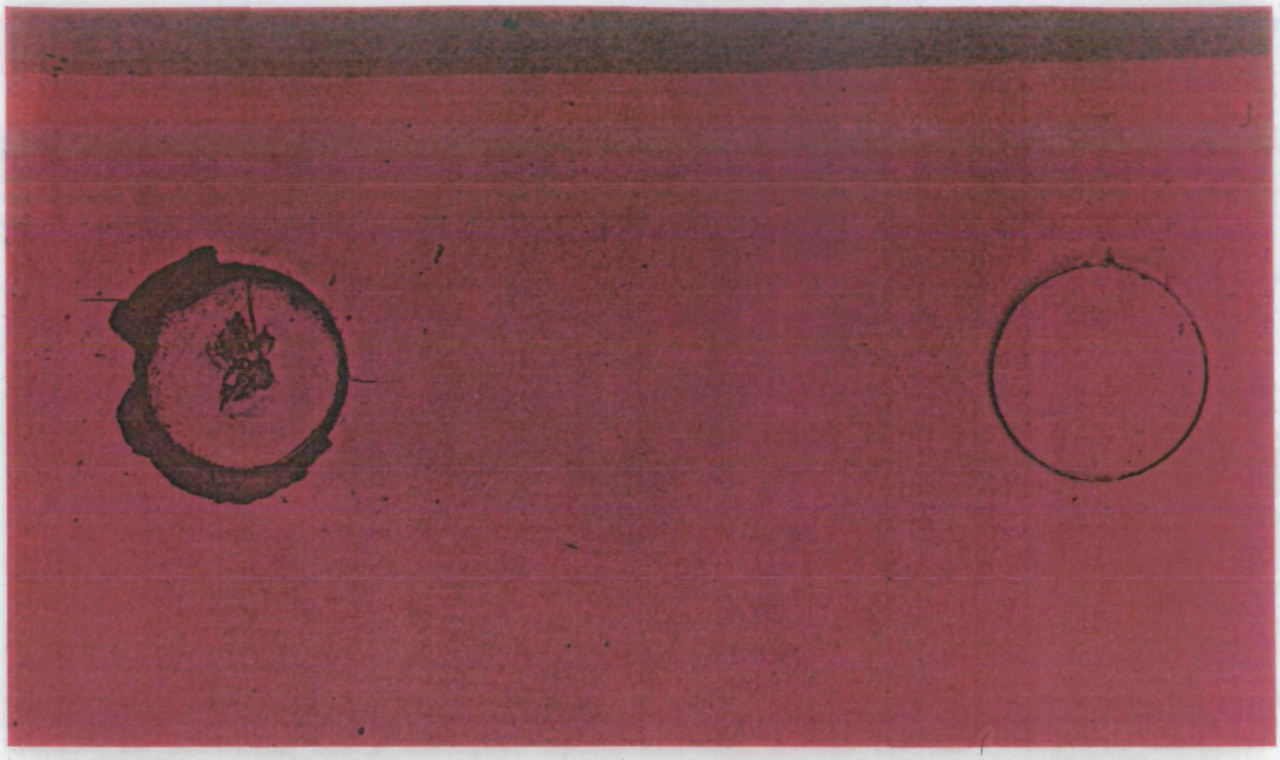

Figure 10. – Hole Damage Showing Fastener Pullthrough

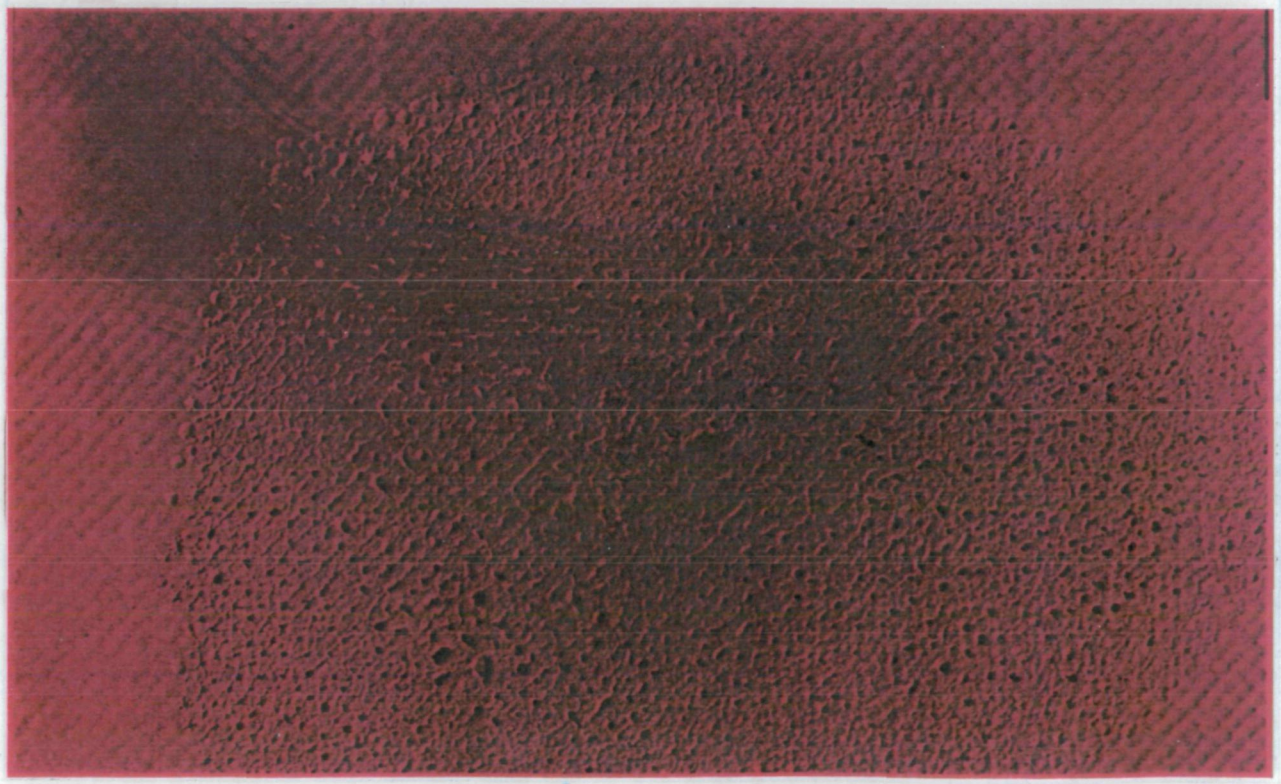

Figure 11. – Burn Damage

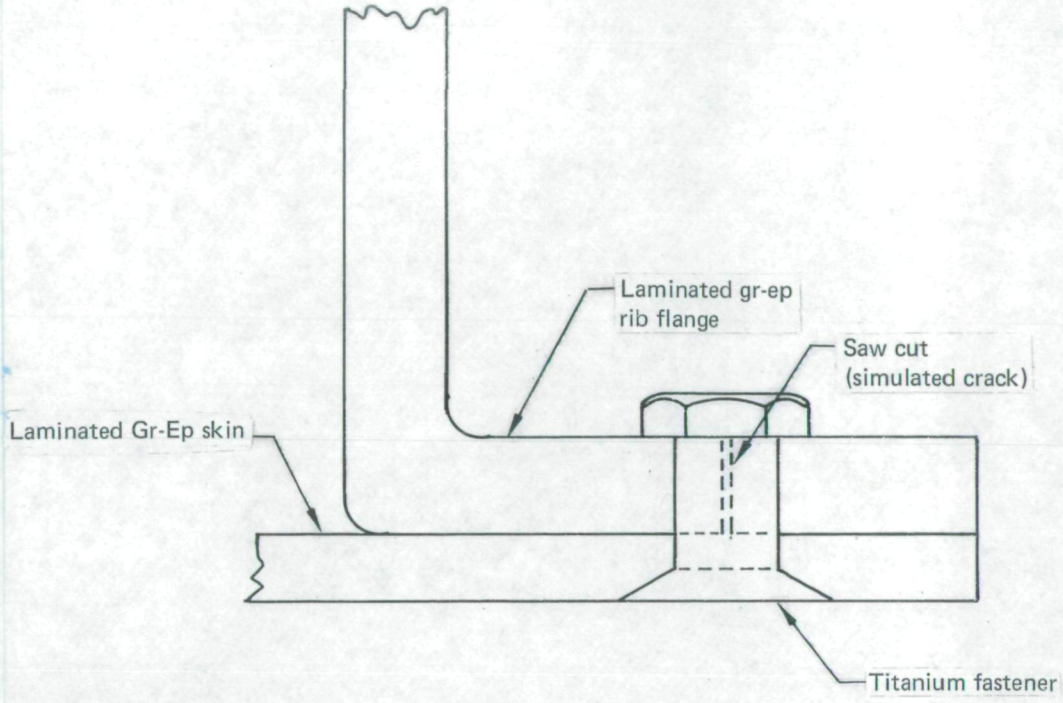

Figure 12. —Simulated Crack in Elevator Rib

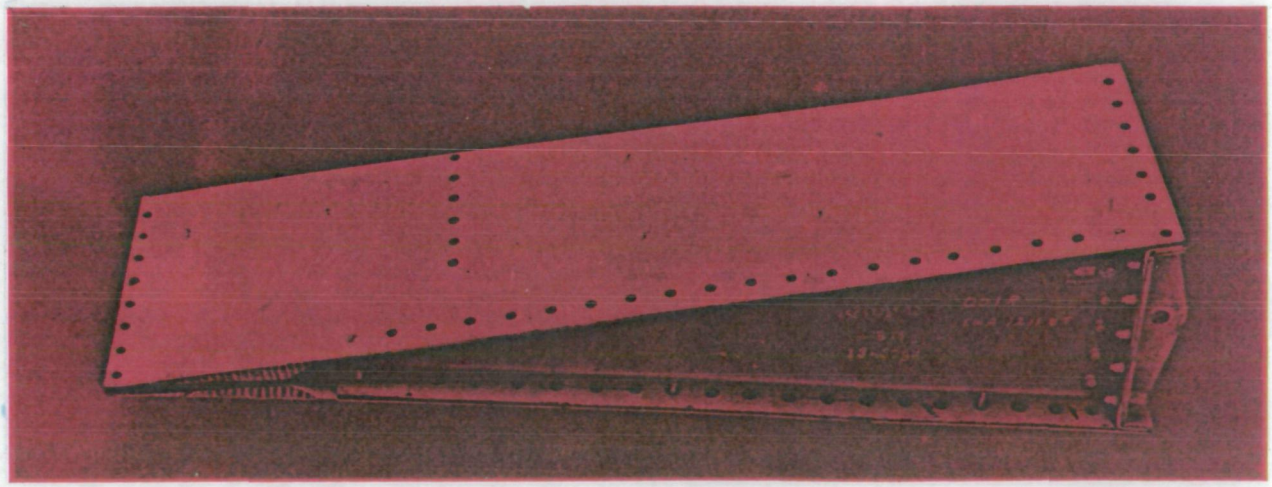

Figure 13. — Boeing 727 Elevator Section

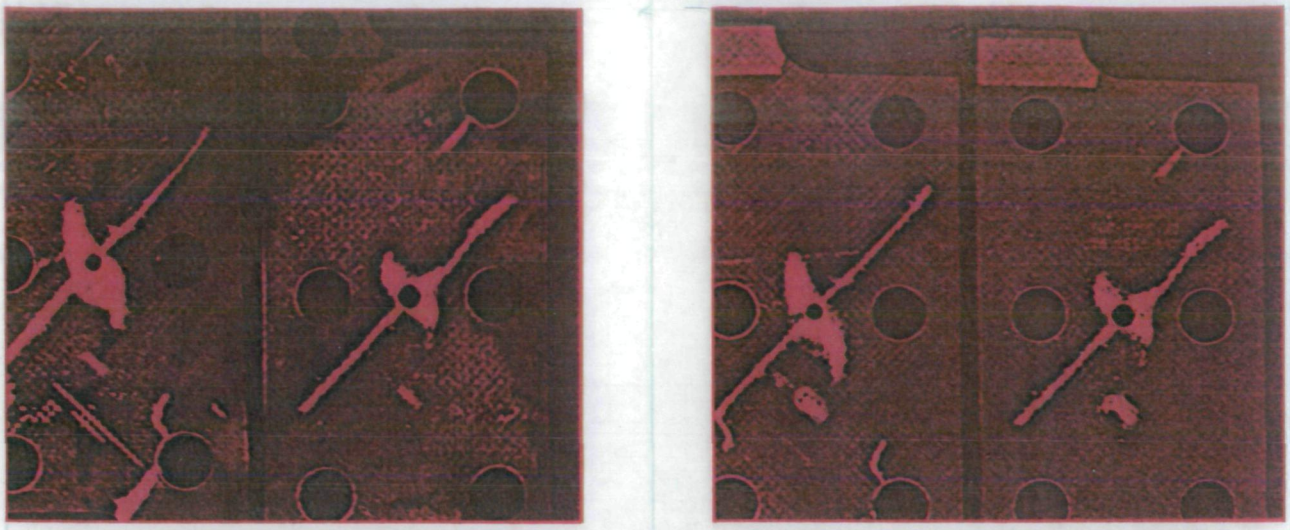

a) A FEW MINUTES AFTER APPLICATION

b) THREE WEEKS AFTER APPLICATION

Figure 14. — Radiograph of DIB Indication (DIB over 6 Months Old)

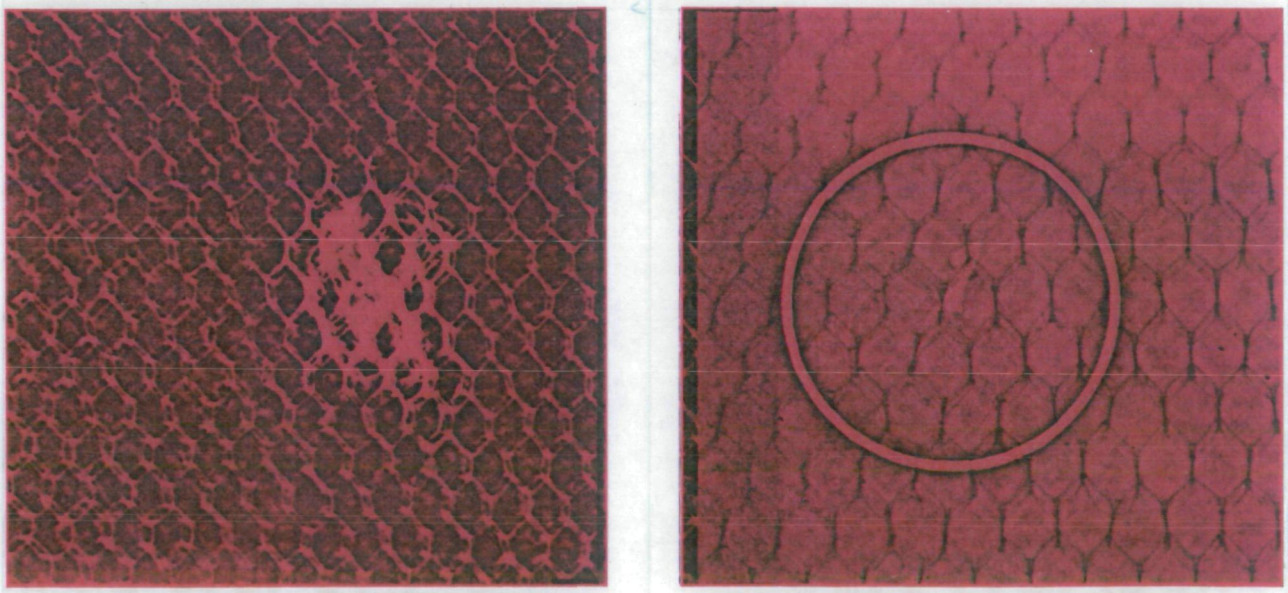

a) A FEW MINUTES AFTER APPLICATION

b) THREE WEEKS AFTER APPLICATION

Figure 15. — Radiograph of Fresh DIB

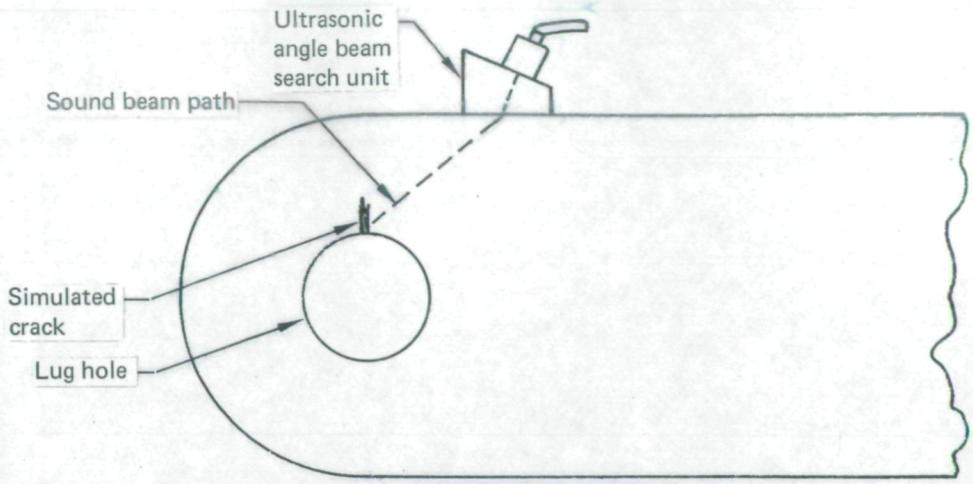

a) CRACKS IN LUGS

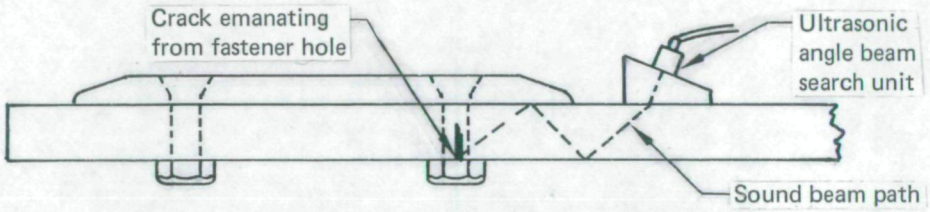

b) HOLE CRACKS IN LAMINATED PLATE

Figure 16. — Angle Beam Ultrasonic Inspection

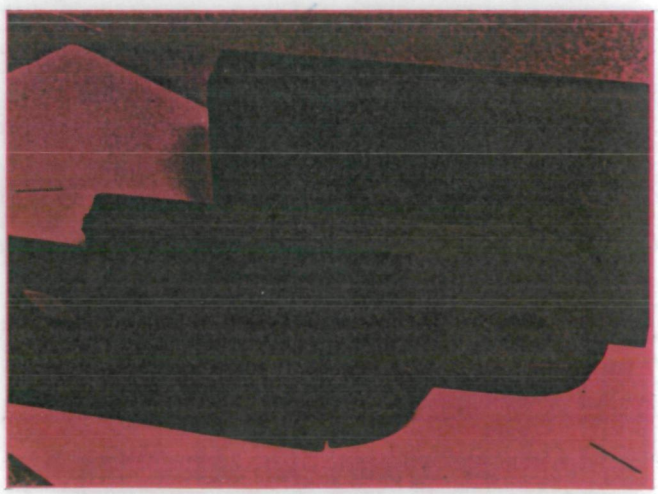

Figure 17. — Ultrasonic Test Specimens of Laminated Gr-Ep Fabric

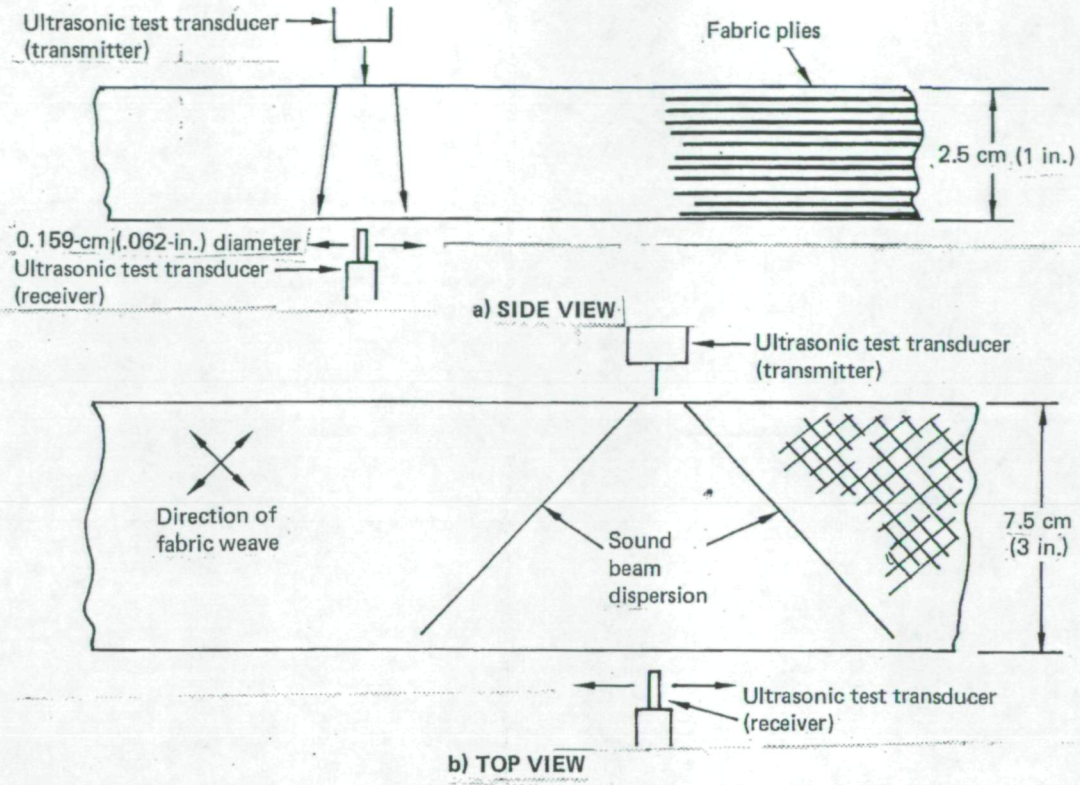

Figure 18. — Beam Dispersion Evaluation

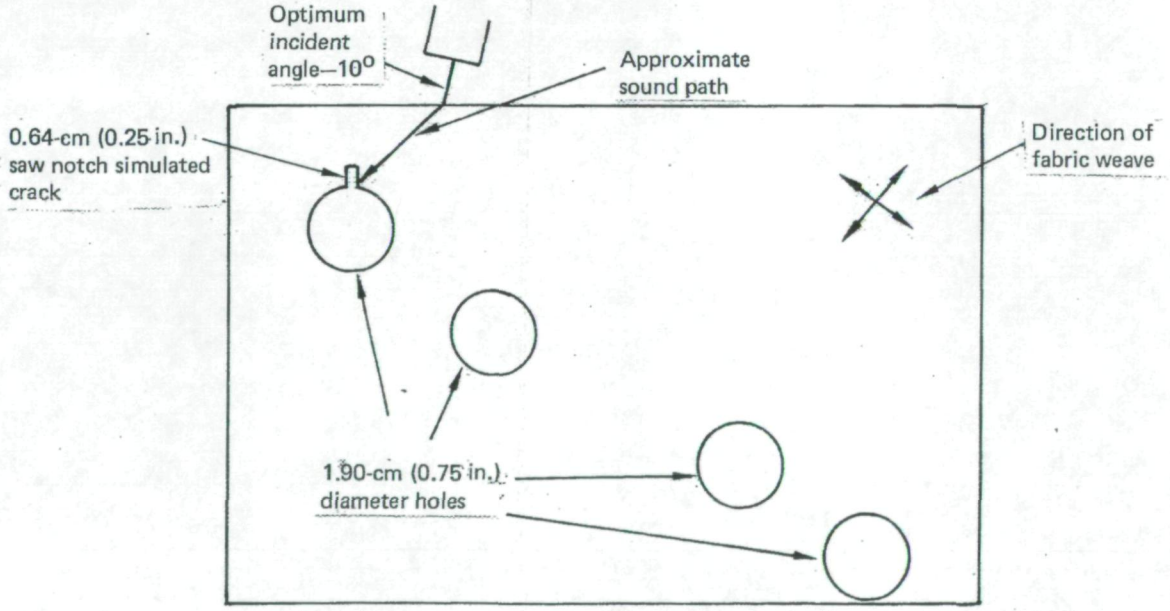

Figure 19. — Ultrasonic Detection of Simulated Lug Hole Fracture in 3.175-cm (1.25-in.) Thick Specimen

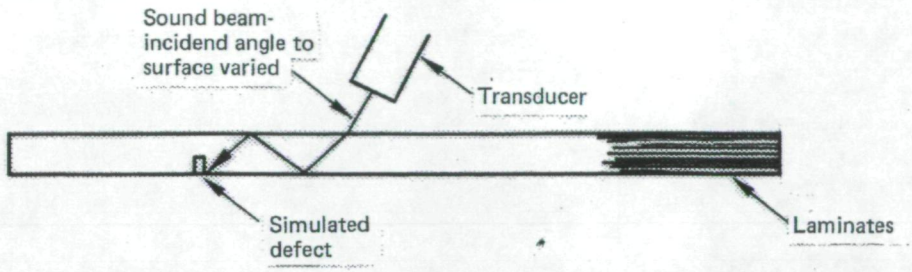

Figure 20. — Ultrasonic Detection of Simulated Crack in Laminate Plate

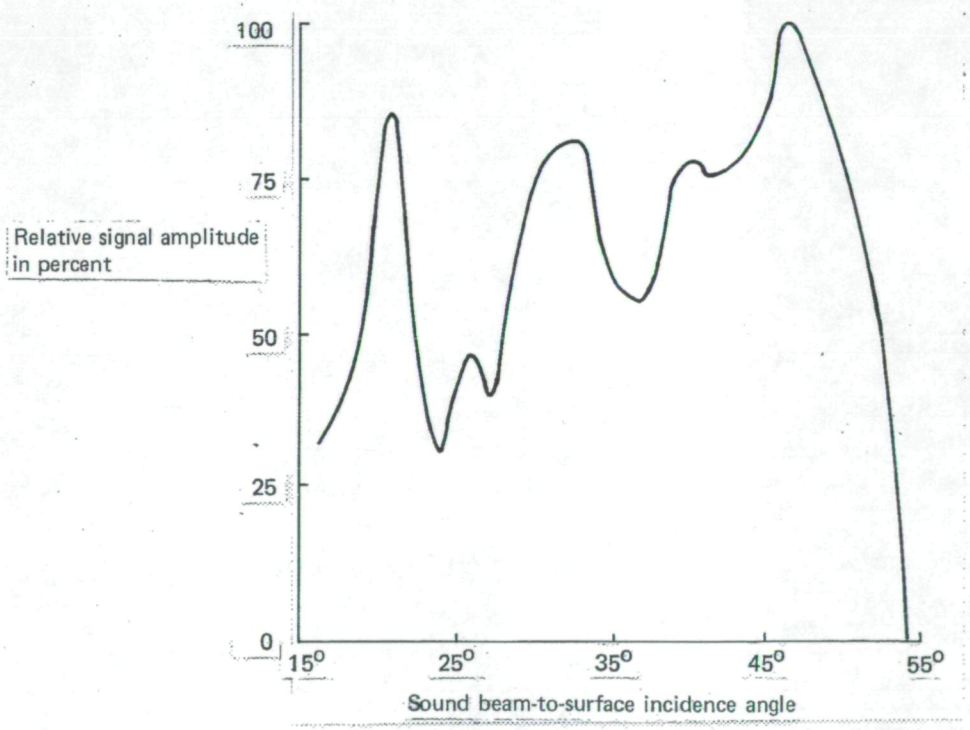

Figure 21. — Relative Ultrasonic Signal Amplitude From a 0.127-cm (0.050-in.) Deep Simulated Crack in a 0.53-cm (0.210-in.) Thick Laminated Plate

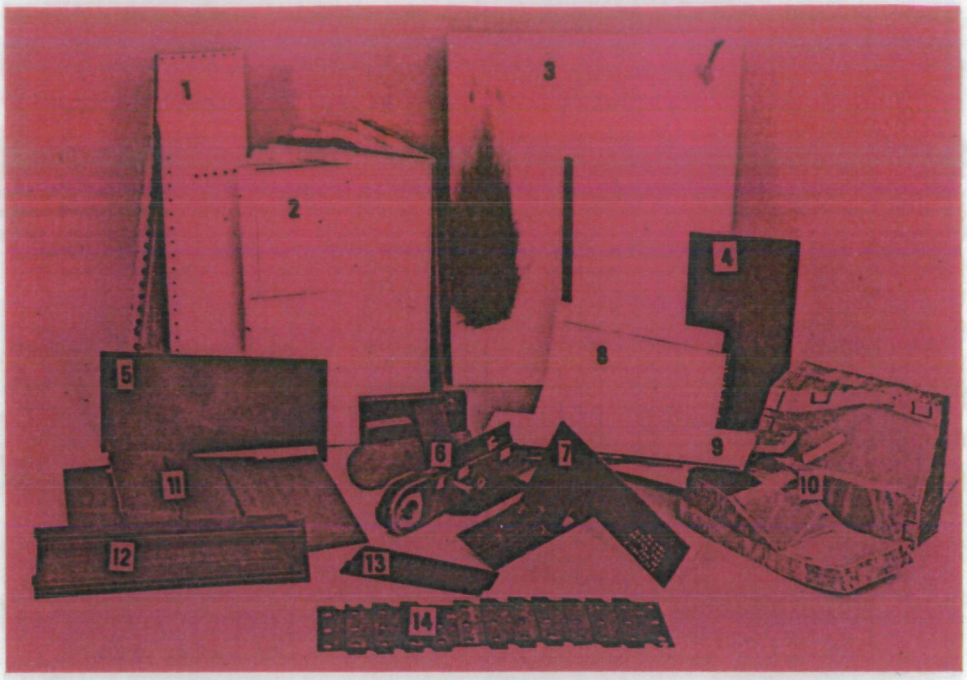

Key	Description	Defects
1	Gr-Ep laminate/Nomex honeycomb skin and rib structure, mechanically fastened, painted two sides. B727 elevator section	Impact damage, fastener hole damage, water-in-honeycomb, rib flange cracks
2	Gr-Ep laminate and Nomex honeycomb painted one side	Delaminate/disbond defects and impact damage defects in honeycomb, laminate, and transition areas
3	Wedge shape, Gr-Ep skin—Nomex honeycomb painted two sides	Impact damage, lightning damage, burn damage
4	Gr-Ep laminate plates, painted one side	Delamination/disbond and impact damage defects, simulated surface cracks
5	Unidirectional Gr-Ep laminate	Simulated surface cracks
6	Gr-Ep laminate lug and thick sections	Fracture in lug, simulated hole cracks
7	Gr-Ep honeycomb panel mechanically fastened to Gr-Ep I-stiffened skin structure	Complete failure (fracture) in flange at one hole
8	Curved Gr-Ep skin and Nomex honeycomb	Impact damage
9	Kevlar and Gr-Ep skin and Nomex honeycomb	Impact damage
10	Kevlar and Gr-Ep skin and septumized Nomex honeycomb—B767 landing gear door sections	Delamination/disbond defects
11	Gr-Ep laminate and aluminum honeycomb or titanium plate	Delamination/disbond defects
12	Gr-Ep laminate I-stiffened skin panel	Impact damage
13	Gr-Ep laminate stepped-thickness X-ray and ultrasonic test part	Varied thicknesses
14	Gr-Ep laminate fatigue specimens	Cracks and hole damage

Figure 22. — Test Parts

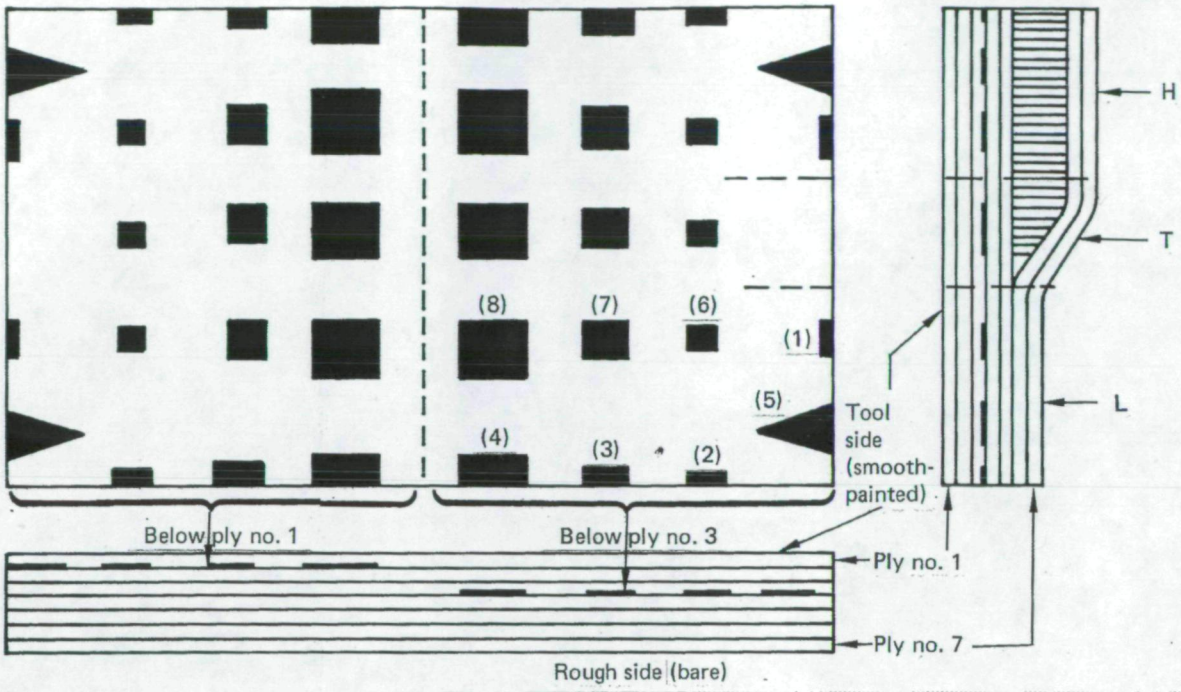

Material: Gr-Ep fabric: type II, class II, style 3K-70-PW
Honeycomb core: Nomex, 4 lb

Defect type: Defects identified by numbers 6, 7, and 8 are 3 plies of 2-mil teflon embedded in the laminate. Numbers 1, 2, 3, 4, and 5 are 3 plies of 2-mil Teflon embedded at the edge and removed after panel fabrication, leaving a voided delamination.

Defect number:	1	2	3	4	5	6	7	8
Defect size:	0.635 cm (0.25 in.) by 2.54 cm (1.0 in.)	1.270 cm (0.5 in.) by 2.54 cm (1.0 in.)	1.905 cm (0.75 in.) by 2.54 cm (1.0 in.)	2.54 cm (1.0 in.) by 3.81 cm (1.5 in.)	3.175 cm (1.25 in.) by 5.08 cm (2.0 in.) (30^{o} wedge)	1.270 cm (0.5 in.) by 1.270 cm (0.5 in.)	2.54 cm (1.0 in.) by 2.54 cm (1.0 in.)	3.81 cm (1.5 in.) by 3.81 cm (1.5 in.)

Defect depth:

No. of plies to defect	From tool side	From rough side
	1 and 3	2 and 4

Defect location:
L Laminate area
H Honeycomb area
T Laminate/honeycomb transition area

Figure 23. — Typical Delamination/Disbond Defect Test Panel of Honeycomb/Laminate Construction

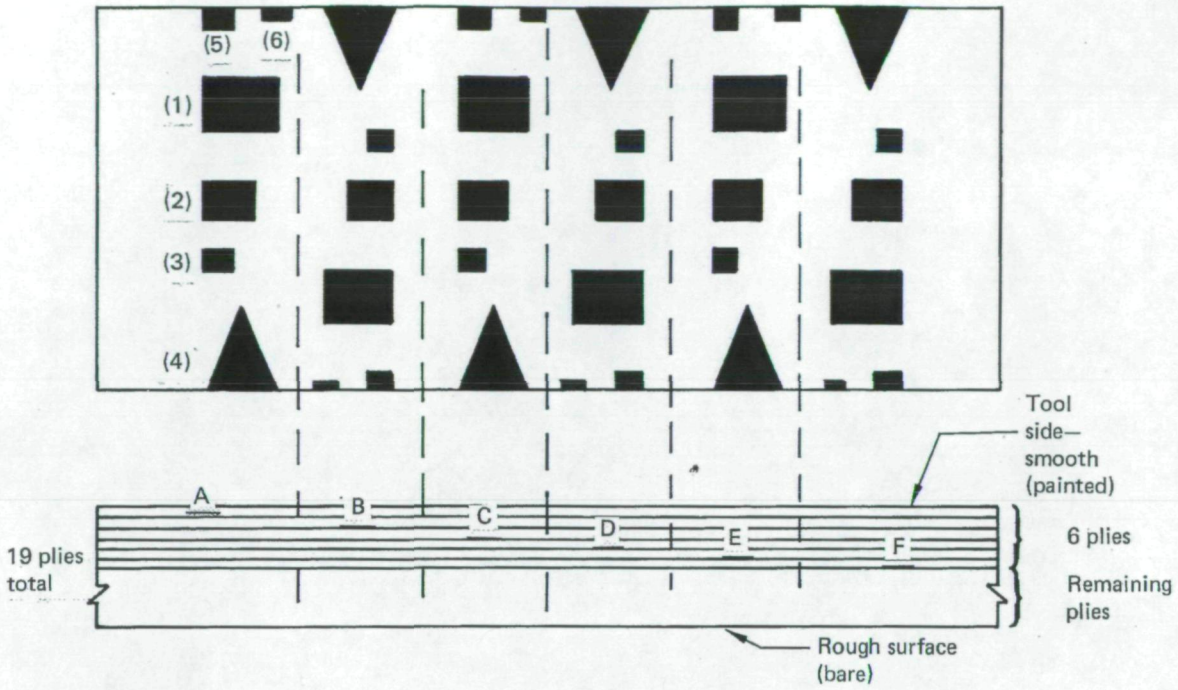

Material:	Gr-ep fabric: type II, class II, style 3K-70-PW.					
Defect type:	Defects identified by numbers 1 through 6—nos. 1, 2, and 3 are 3 plies of 2-mil Teflon embedded in the laminate. Numbers 4, 5, and 6 are 3 plies of 2-mil Teflon embedded at the edge and removed after panel fabrication, leaving a void delamination.					
Defect number:	1	2	3	4	5	6
Defect size:	3.81 cm (1.5 in.) by 3.81 cm (1.5 in.)	2.54 cm (1.0 in.) by 2.54 cm (1.0 in.)	1.270 cm (0.5 in.) by 1.270 cm (0.5 in.)	3.175 cm (1.25 in.) by 5.08 cm (2.0 in.) (30^{O} wedge)	1.270 cm (0.5 in.) by 1.270 cm (0.5 in.)	0.635 cm (0.25 in.) by 1.270 cm (0.5 in.)

Defect depth:

Location		A	B	C	D	E	F
No. of plies to defect	From tool side	1	2	3	4	5	6
	From rough side	18	17	16	15	14	13

Figure 24. — Typical Delamination/Disbond Defect Test Panel of 19-Ply Panel Laminate Construction

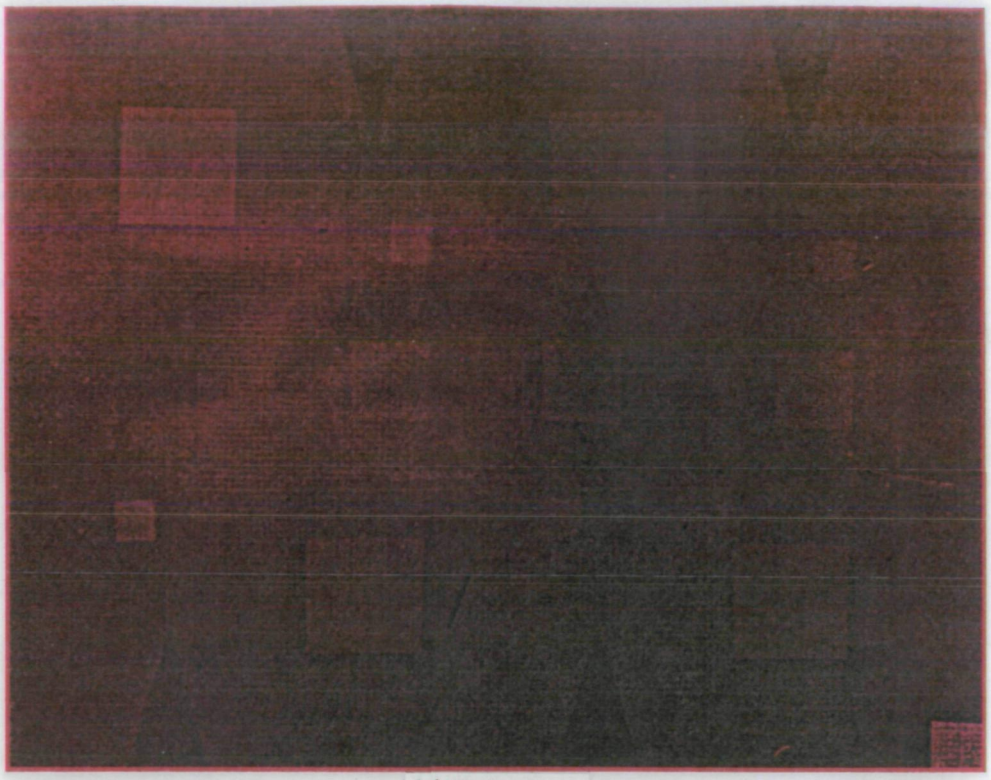

(a) Radiograph

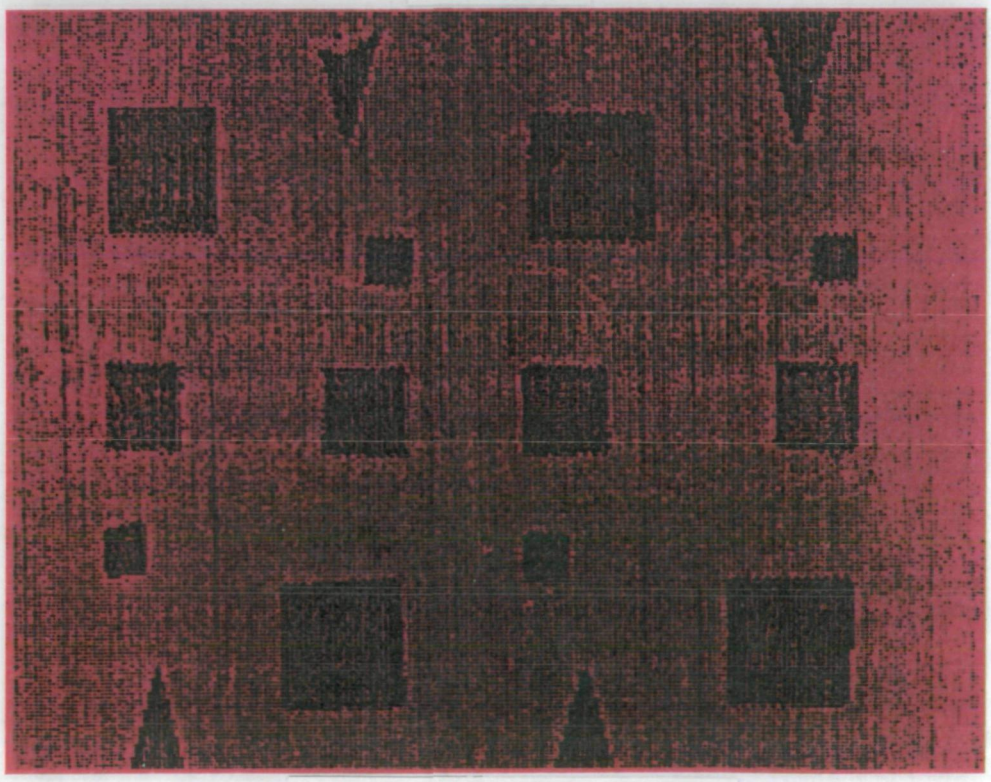

(b) Through Transmission Recording

Figure 25. — Delamination Defect Panel

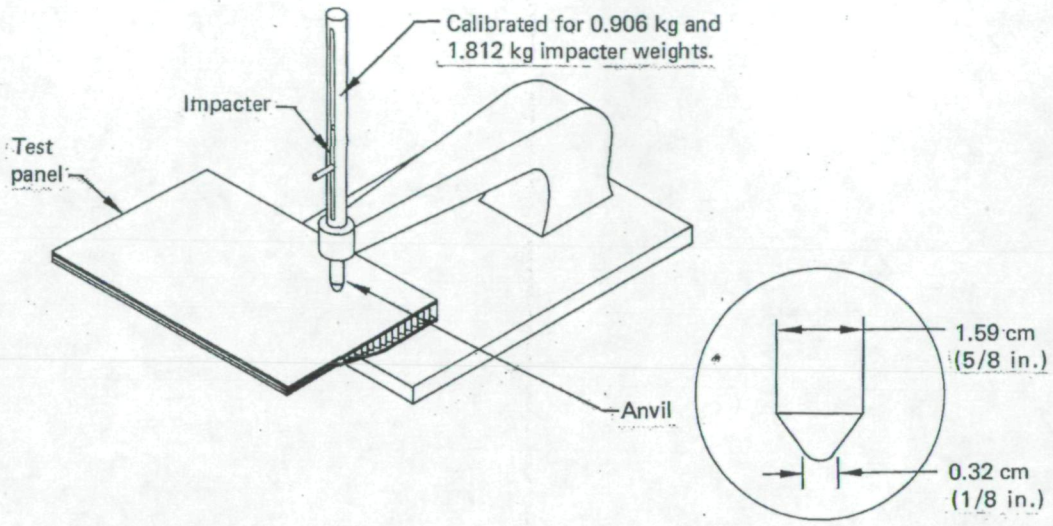

Figure 26. — Impact Damage Tool

Laminate thickness	Skin-to-honeycomb thickness	Impact levels (range)	
		cm / kg	in./lb
0.034	0.016	2.3 to 6.9	2 to 6
0.041	0.024	2.3 to 6.9	2 to 6
0.058	0.040	2.3 to 13.7	2 to 12
0.070	0.057	11.4 to 38.9	10 to 34
0.090	*	2.3 to 27.4	2 to 24
0.157	*	18.3 to 68.6	16 to 60
0.213	*	45.7 to 137.2	40 to 120

*Laminate only

Figure 27. — Impact Defects

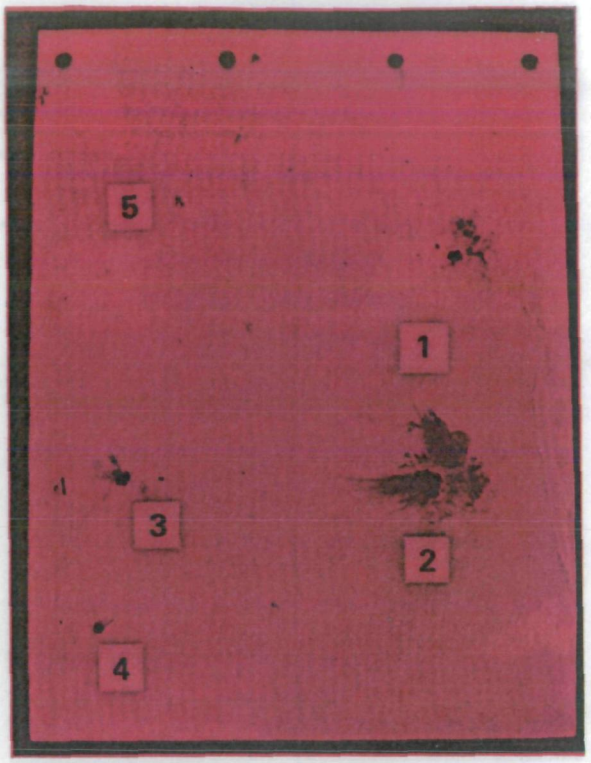

Figure 28. — Lightning Strike Defects

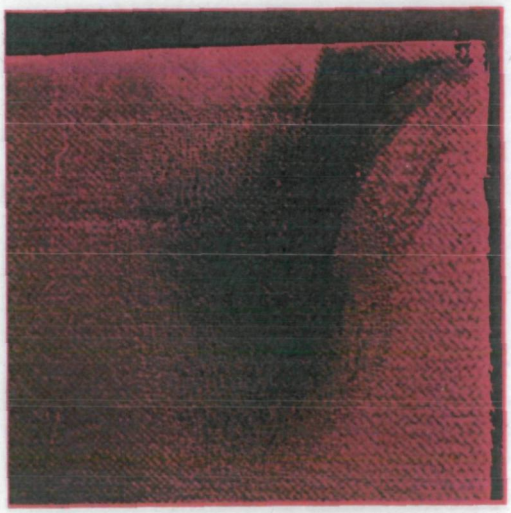

a) SCORCHED, BLISTERED, AND DELAMINATED SKIN

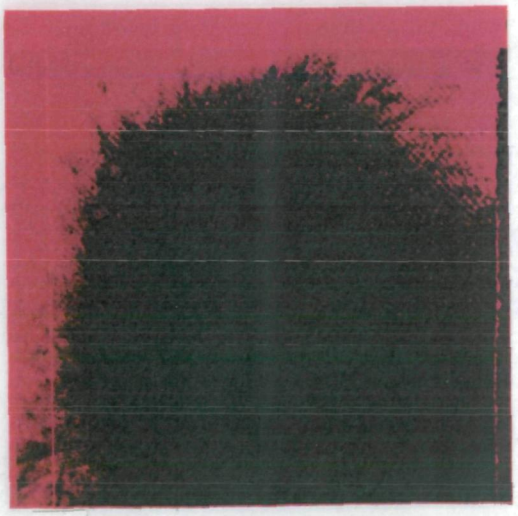

b) SURFACE CHARRED AND SKIN FLAKED OFF

Figure 29. — Heat Damage on Painted Gr-Ep Honeycomb

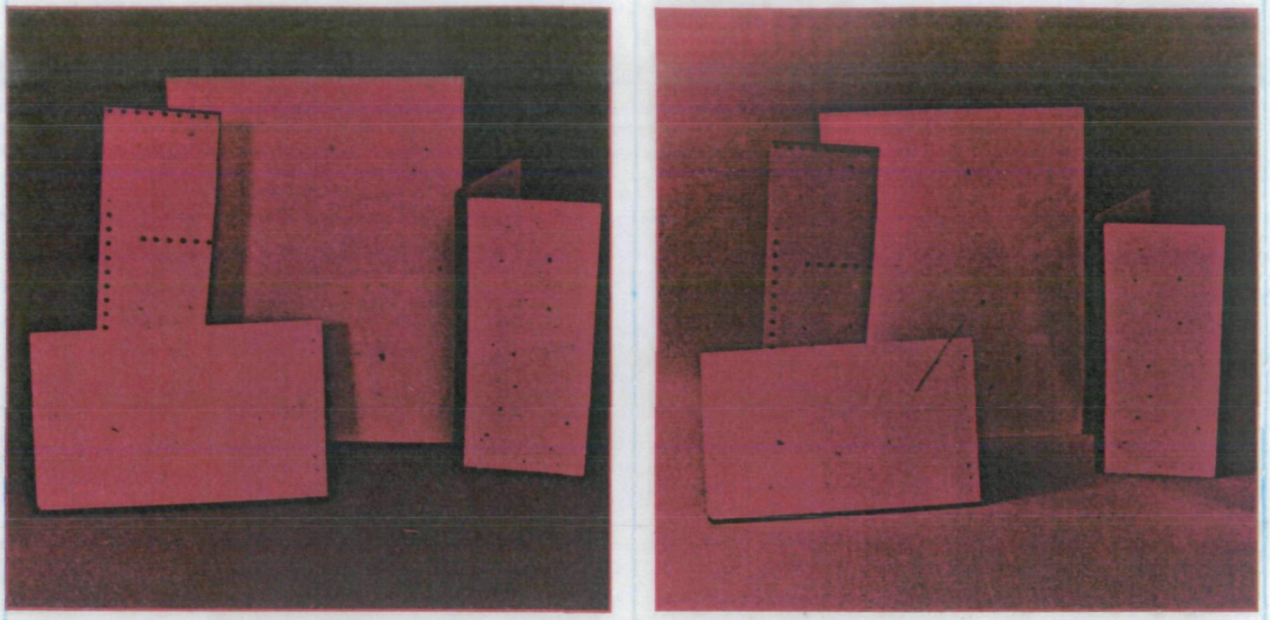

a) DIRECT LIGHT

b) LOW-ANGLE INCIDENCE LIGHT

Figure 30. — Impact Damage Visibility

Panel	Drop height, m	Impact angle	Appearance	Detectability[1]	
				Near visual[2]	Far visual[2]
Skin/ honeycomb	2.74 (9 ft)	90°	Large dent; black Gr-Ep exposed	X	X
	1.82 (6 ft)	90°	Medium dent; black Gr-Ep exposed; small fracture	X	X
	0.914 (3 ft)	60°	Small dent; small fracture	X	?
	0.610 (2 ft)	90°	Small dent; black Gr-Ep exposed; small fracture	X	—
	0.305 (1 ft)	90°	Small dent; small fracture	?	—
Laminate	2.74 (9 ft)	90°	No dent; marred paint	?	—
	2.74 (9 ft)	60°	No dent; black Gr-Ep exposed	X	X
	2.44 (8 ft)	60°	No dent; black Gr-Ep exposed	X	X
	0.914 (3 ft)	60°	No dent; black Gr-Ep exposed	X	?
	0.610 (2 ft)	60°	No dent; black Gr-Ep exposed	X	—

1. X = Detectable ? = Marginal — = Not detectable
2. Near visual: 0 to 1.52m (5 ft) Far visual: 7.62m (25 ft)

Figure 31. — Impact Damage Visibility Results

Group	Materials	Results
I and II	• Post-emulsifiable visible dye	• Poor initial results • Testing discontinued
III	• Water-washable visible dye • Nonaqueous, dry, and wet developers	• Poor sensitivity because of poor contrast with the dark background • Some improvement with developers
IV	• Water-washable fluorescent penetrants • Nonaqueous, dry, and wet developers	• Very good sensitivity on Tedlar, with no enhancement using developers • Good results on bare gr-ep with developer
V	• Post-emulsifiable fluorescent penetrant • Nonaqueous, dry, and wet developers	• Somewhat less sensitive than group IV • More processing steps required

Figure 32. — Penetrant Evaluation Results

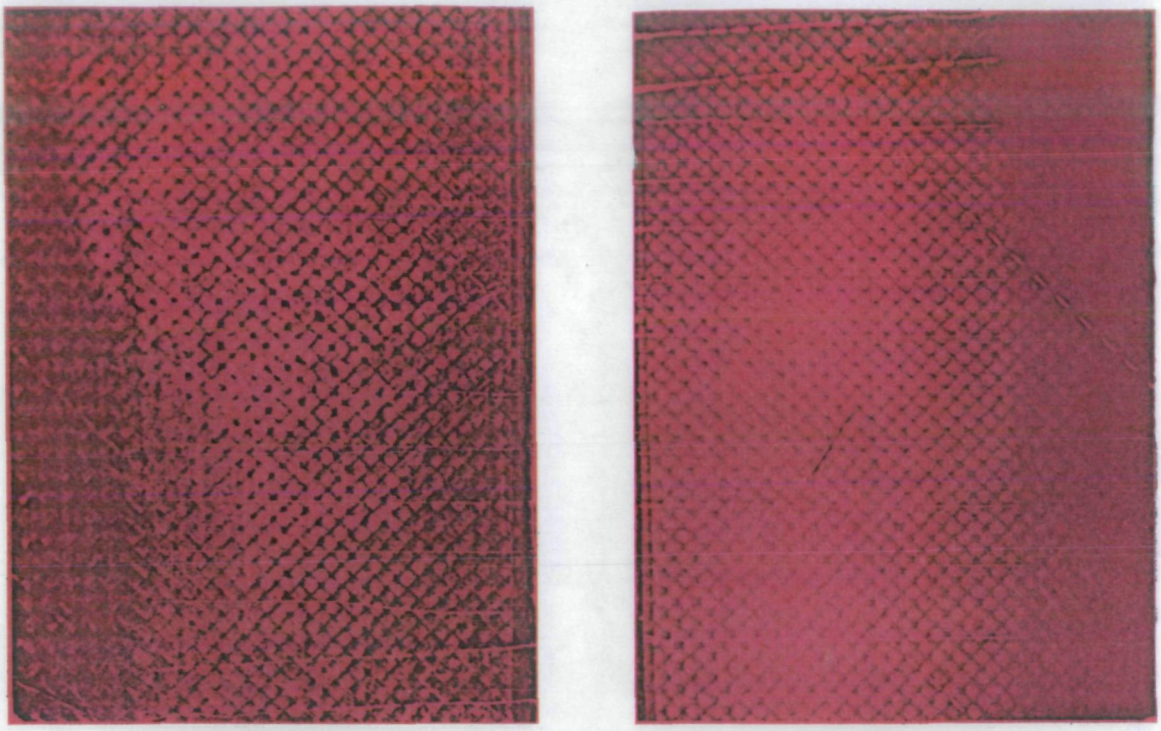

a) VISIBLE DYE

b) FLUORESCENT DYE

Figure 33. – Penetrant Indication on Gr-Ep Panel

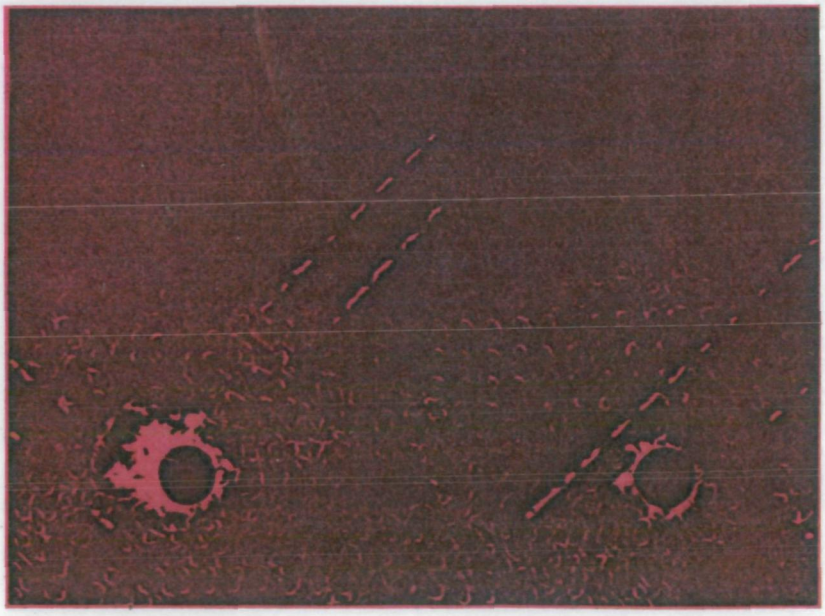

SEVERE HOLE DAMAGE

LIGHT HOLE DAMAGE

Figure 34. – Fluorescent Penetrant Results

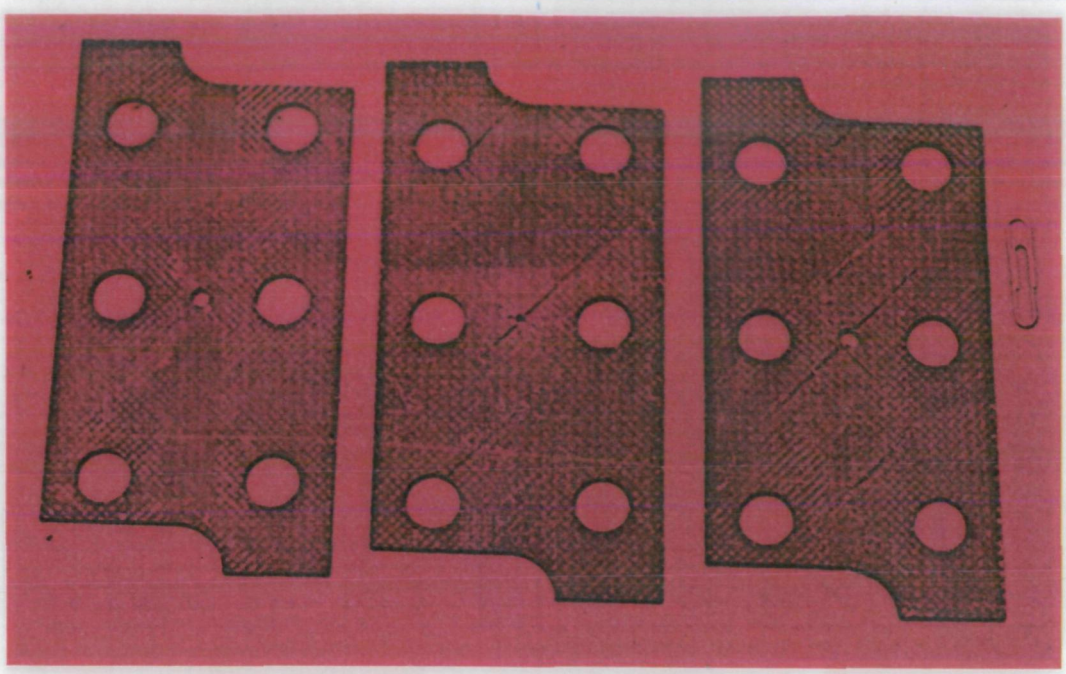

Figure 35. — Fractured Fatigue Specimens

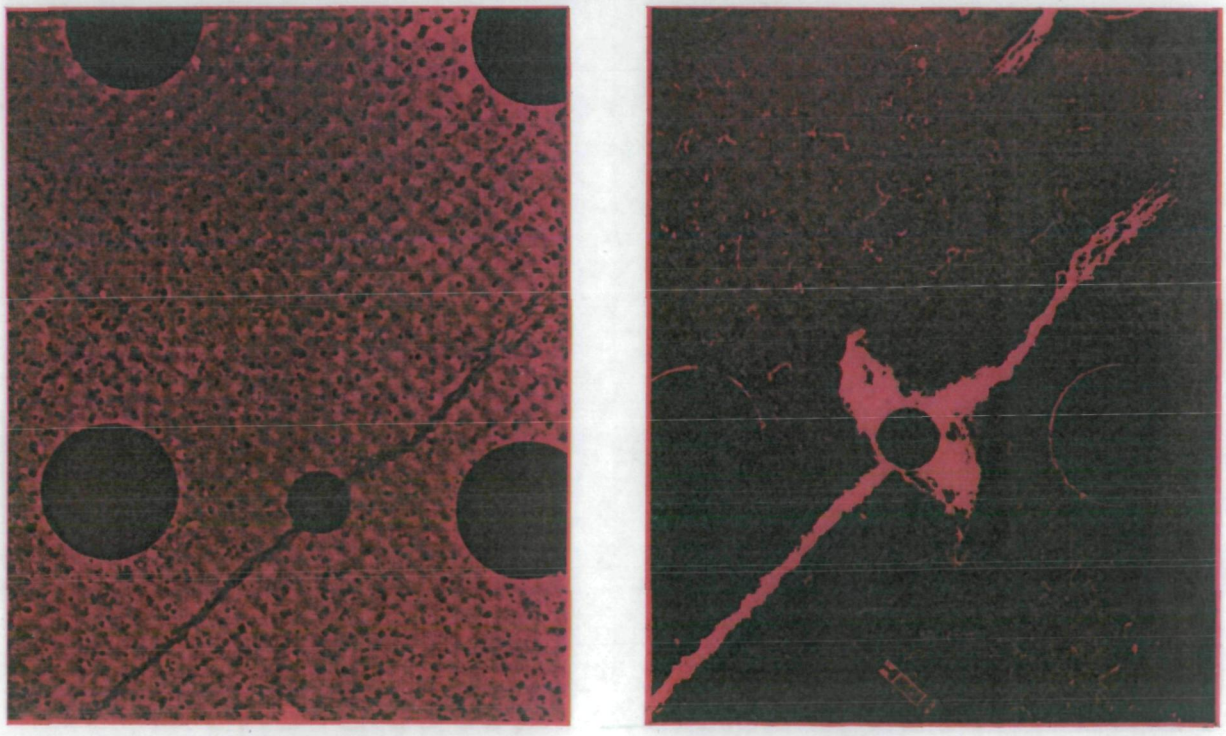

a) NO ENHANCEMENT

b) DIB-ENHANCED

Figure 36. — Cracks in Gr-Ep Specimen

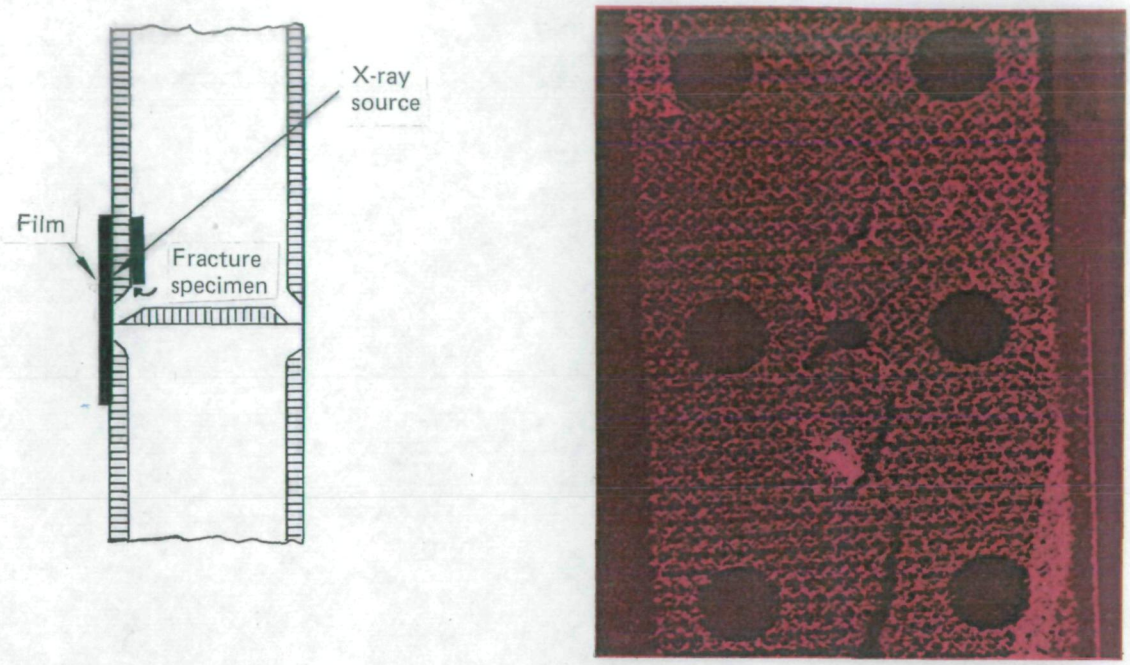

Figure 37. — Radiograph of Simulated Large Fractures in Honeycomb Skin

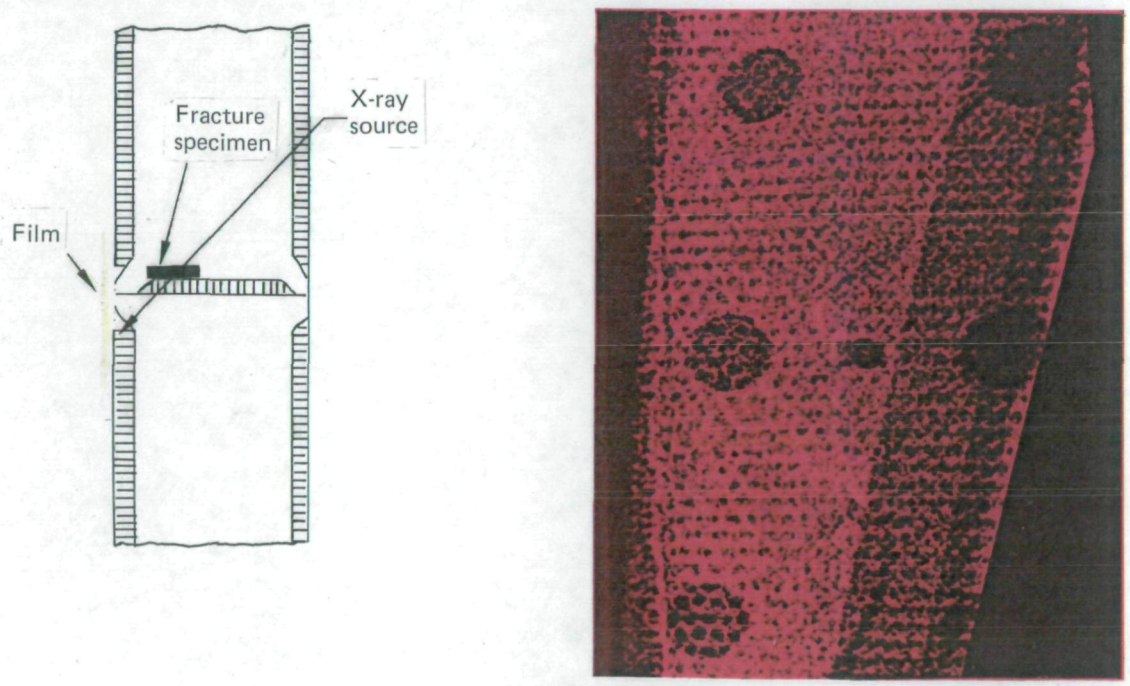

Figure 38. — Radiograph of Simulated Large Fractures in Honeycomb Rib

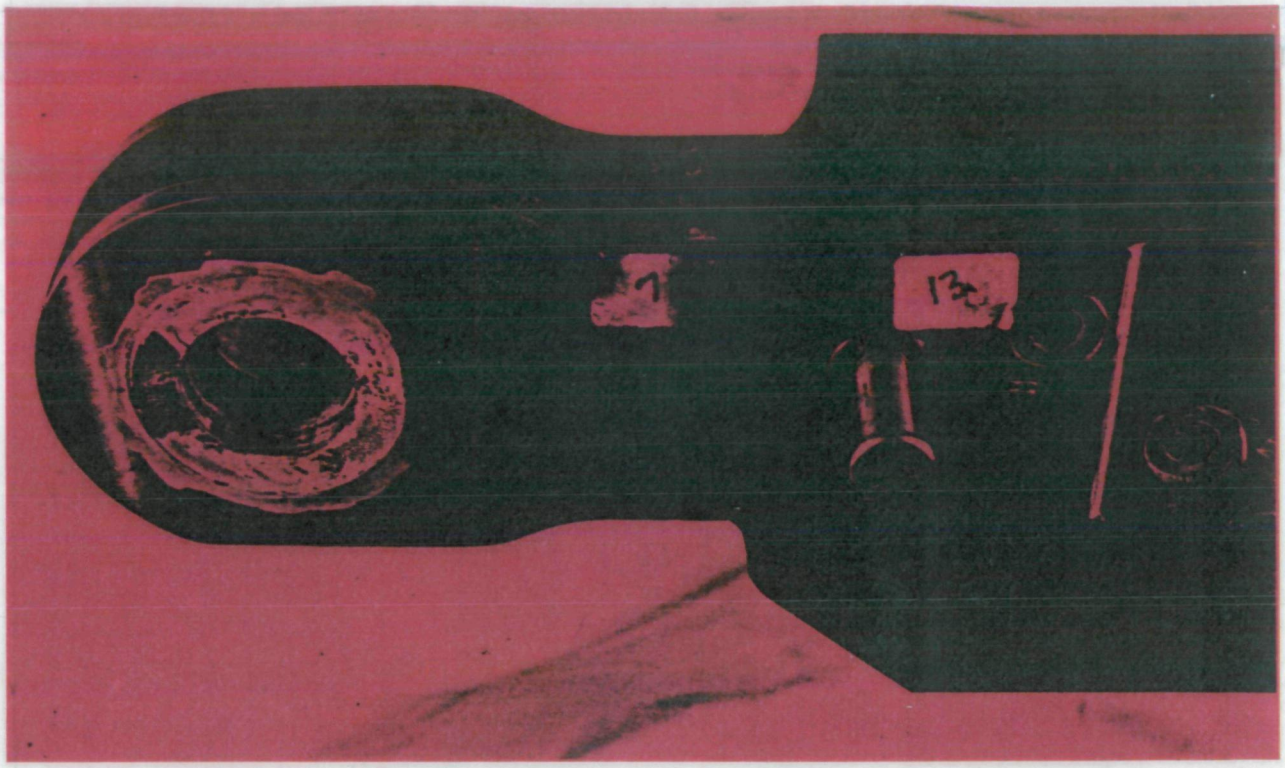

Figure 39. — Fractured Lug Specimen

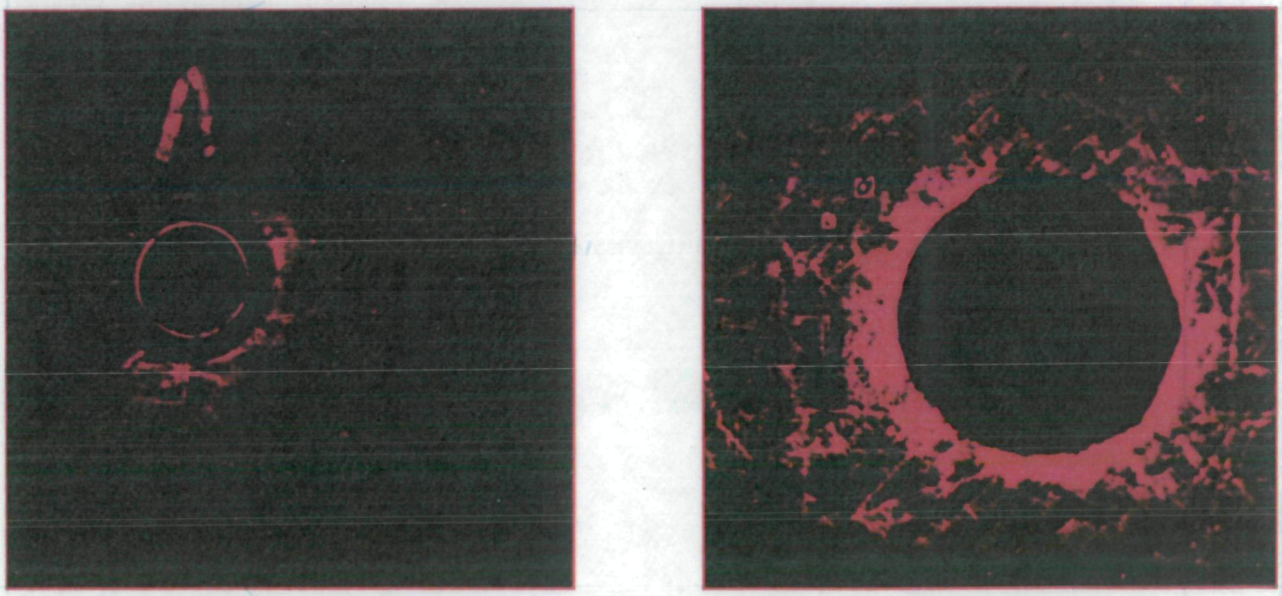

a) LIGHT DAMAGE

b) SEVERE DAMAGE

Figure 40. — Hole Damage Revealed by Radiography With DIP Enhancement

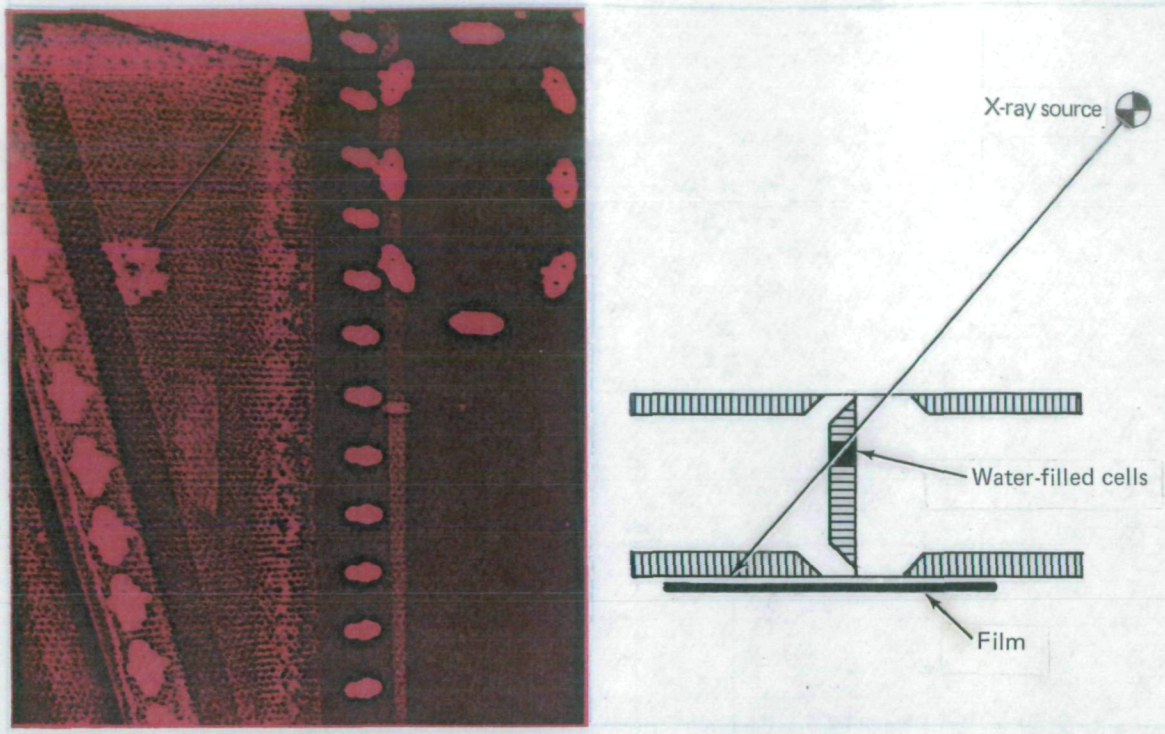

Figure 41. — Radiographic Detection of Water in Honeycomb Rib

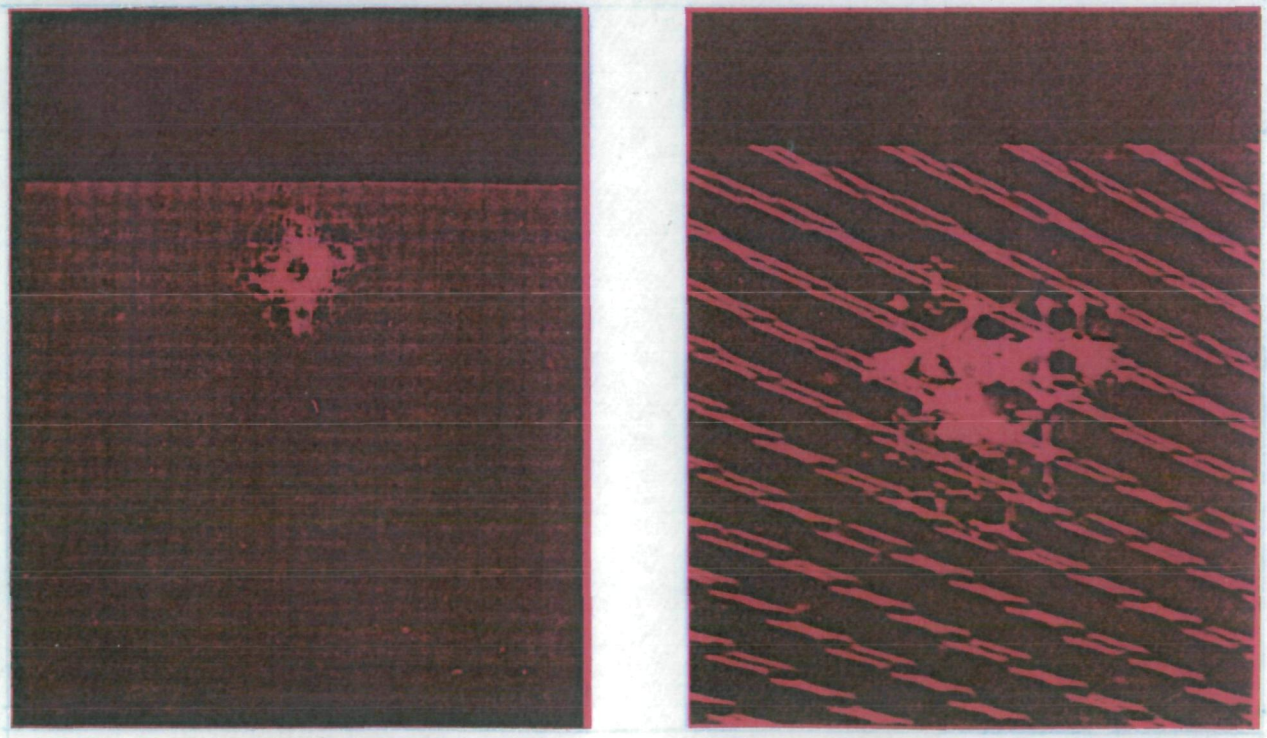

a) LAMINATE PART

b) HONEYCOMB PART

Figure 42. — Radiographs of DIB-Enhanced Impact Damage

Figure 43. — Manual TTU Inspection With Yoke

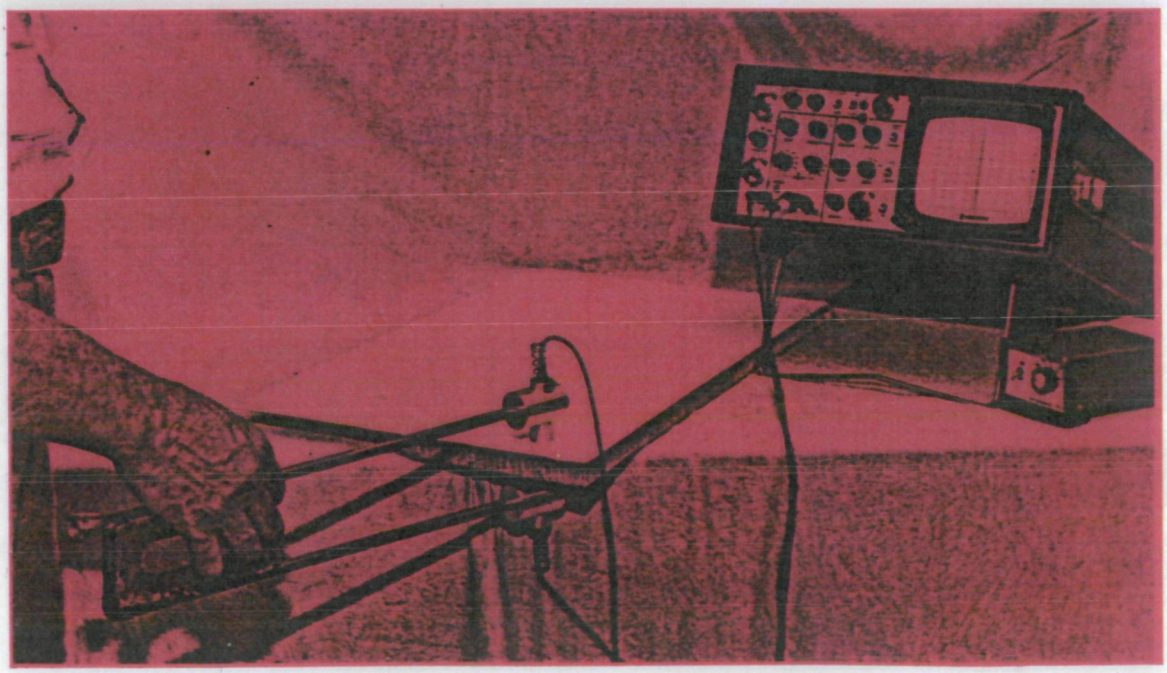

Figure 44. — TTU Sonatest/Shadow

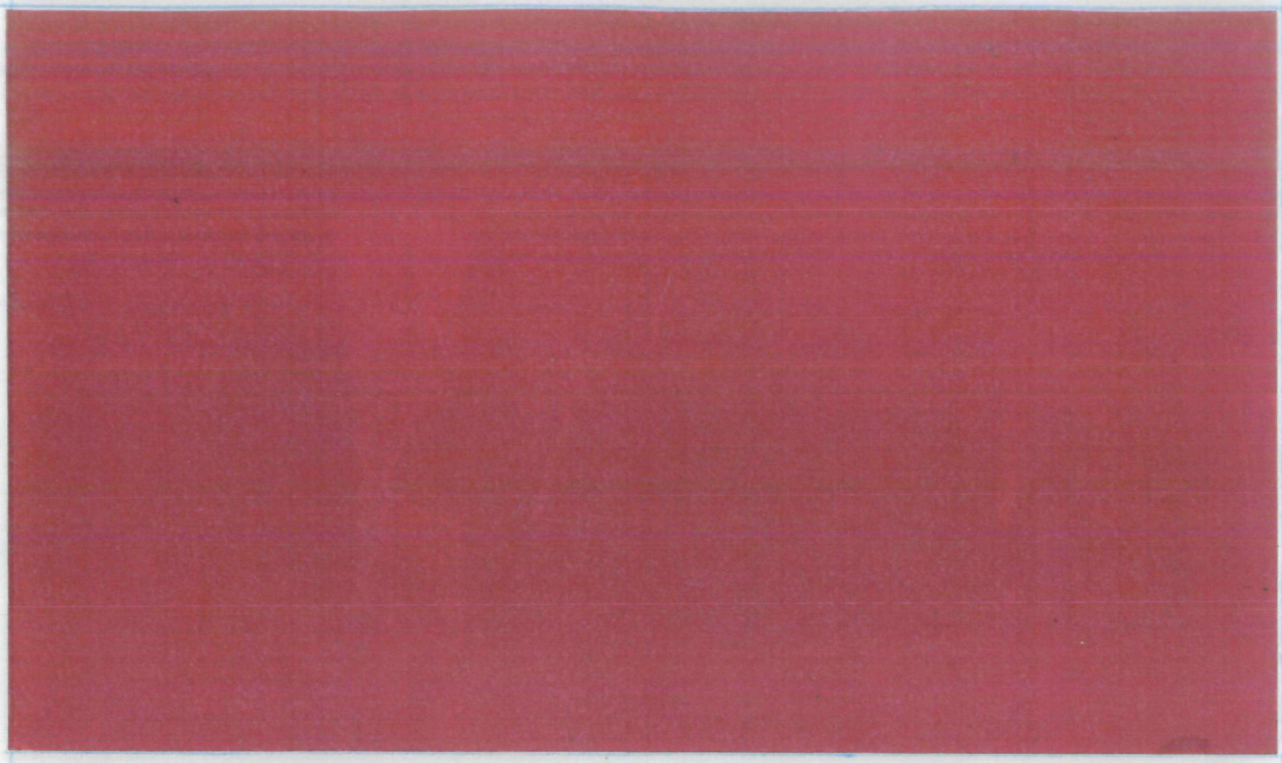

Figure 45. — Ultrasonic Thickness Gage

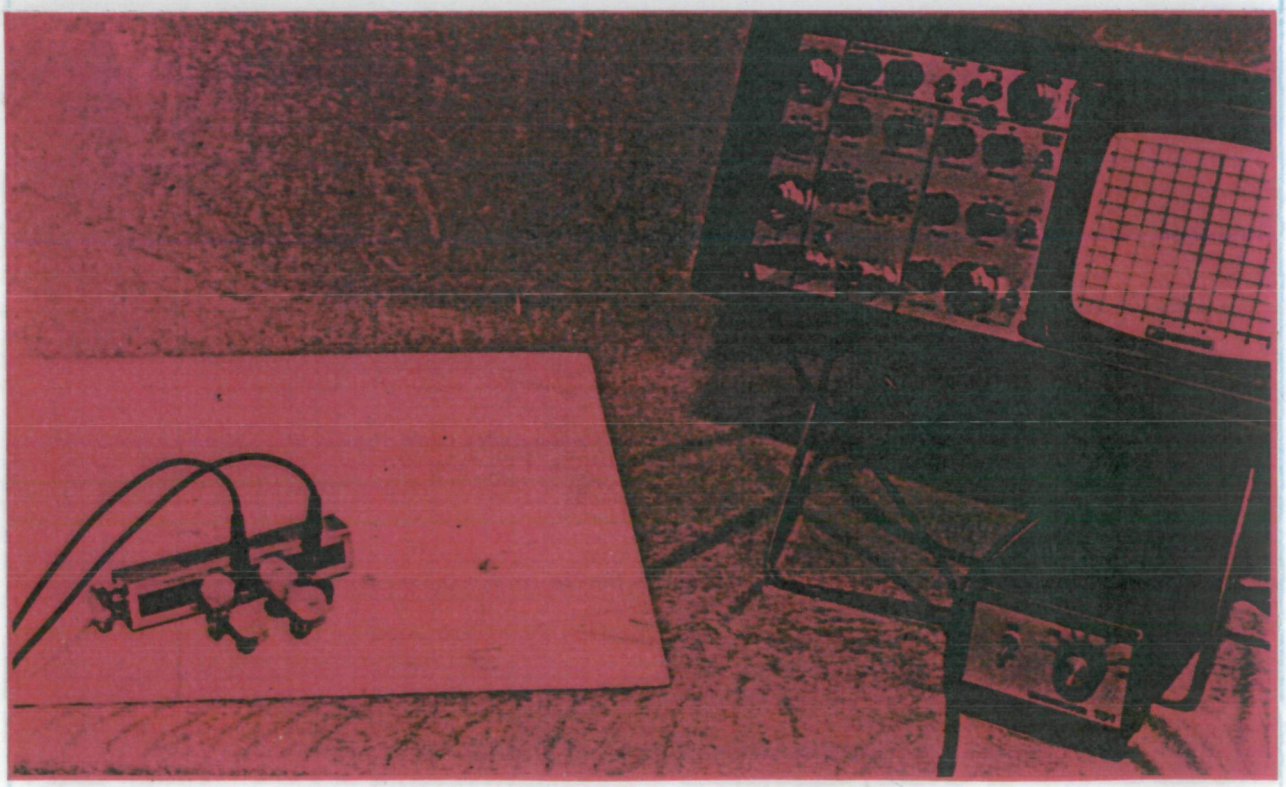

Figure 46. — Single-Side Sonatest/Shadow

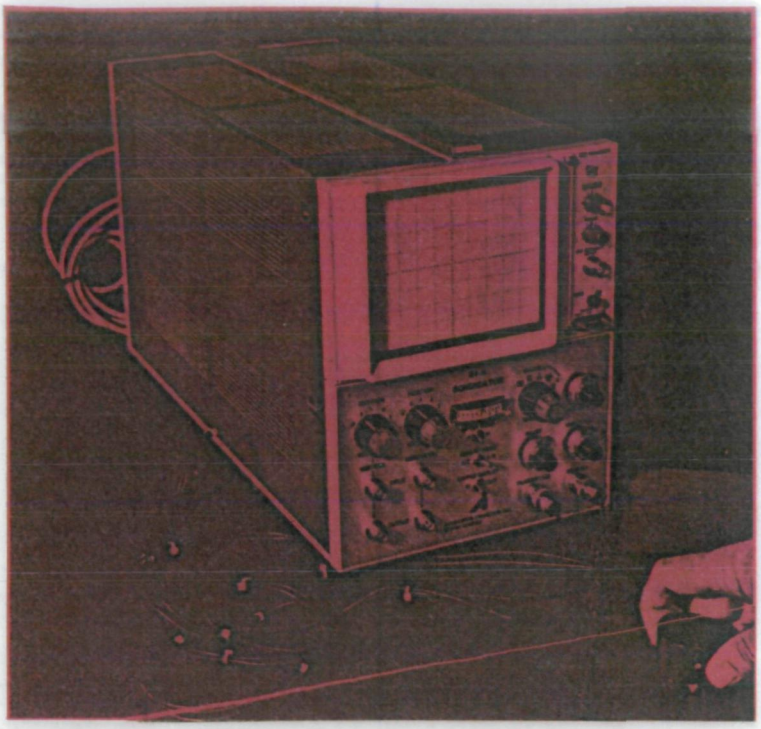

Figure 47. — S1-A Sondicator

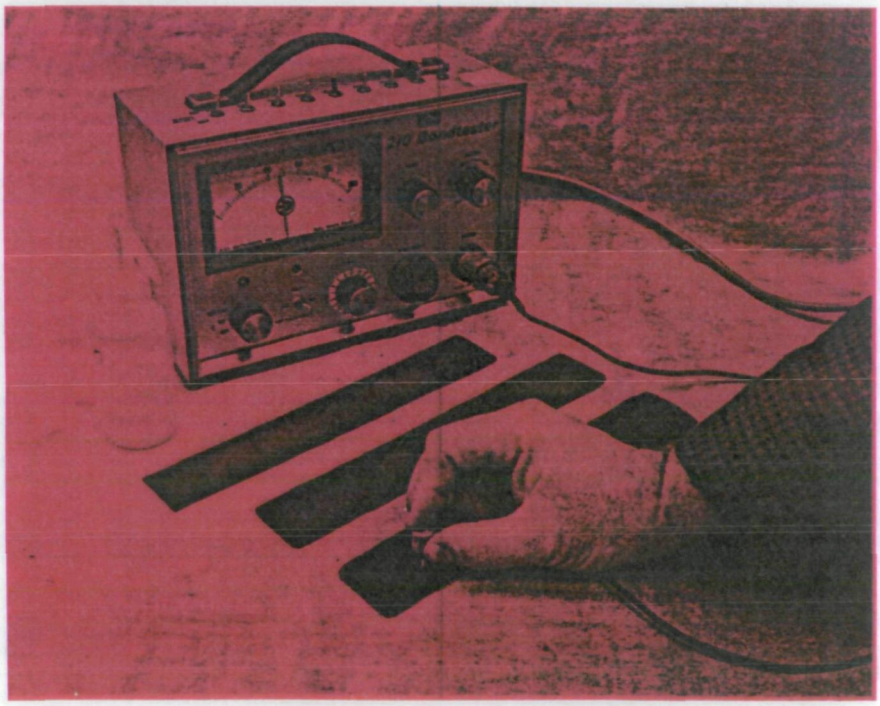

Figure 48. — 210 Bondtester

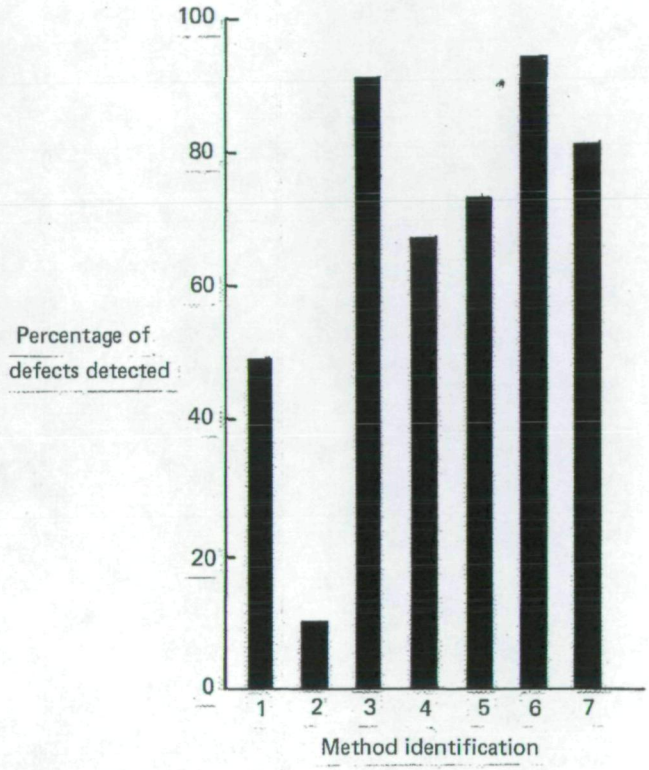

Method identification key:

1. Visual
2. Tap test
3. TTU
4. TTU Sonatest/Shadow
5. Single-side Sonatest/Shadow
6. 210 Bondtester
7. S1-A Sondicator

Figure 49. — Impact Damage Detection Capability

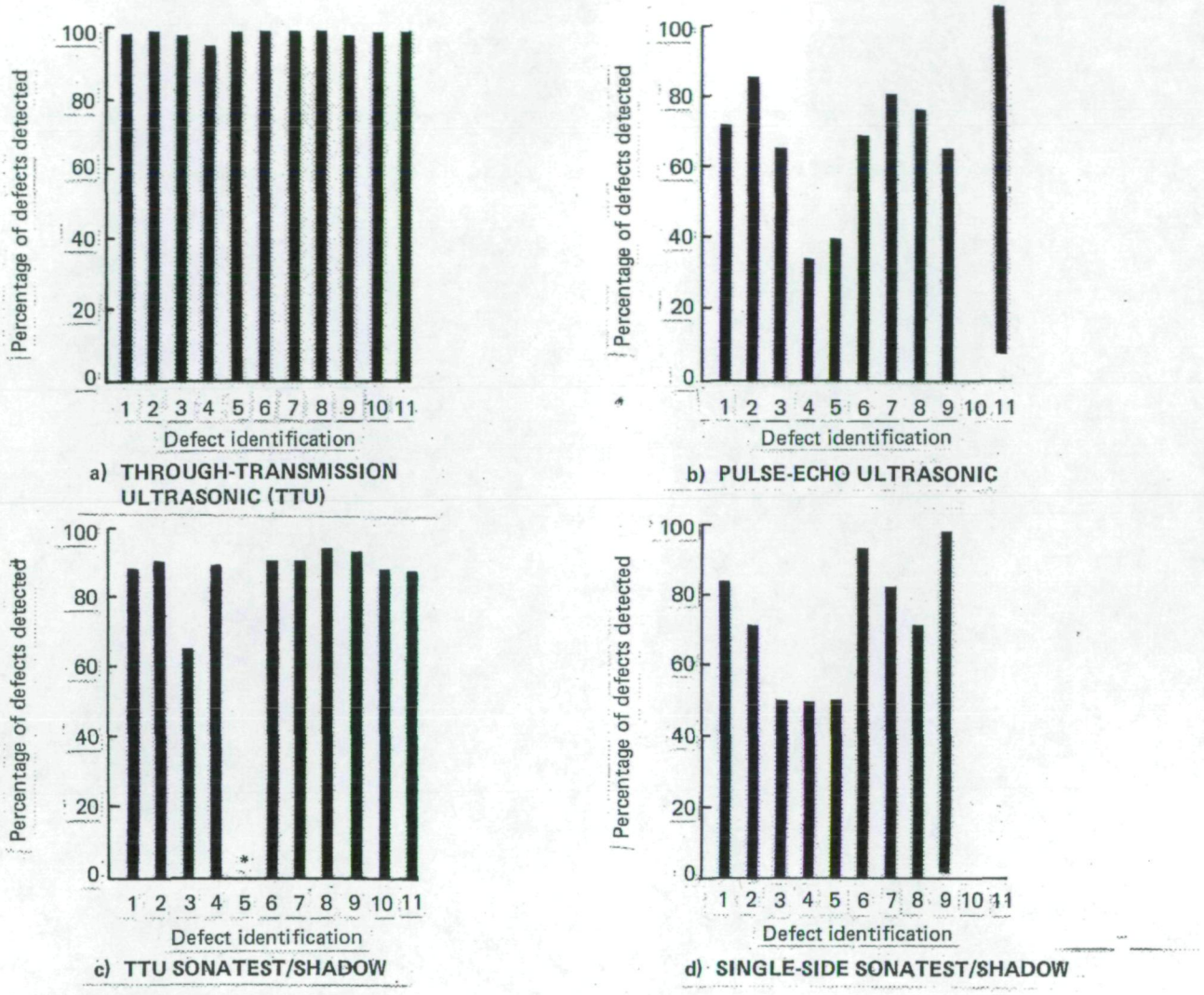

* Omitted—temporary yoke could not accommodate the transition area

Defects Detected—Key:

1. Total defects
2. Small defects
3. Edge defects
4. Laminate/honeycomb defects
5. Transition zone defects
6. First eight plies
7. Nine plies or more
8. Rough side
9. Tool side
10. Gr-Ep—aluminum honeycomb defects
11. Gr-Ep—titanium plate defects

Figure 50. — Delamination/Disbond Defect Detection Capability

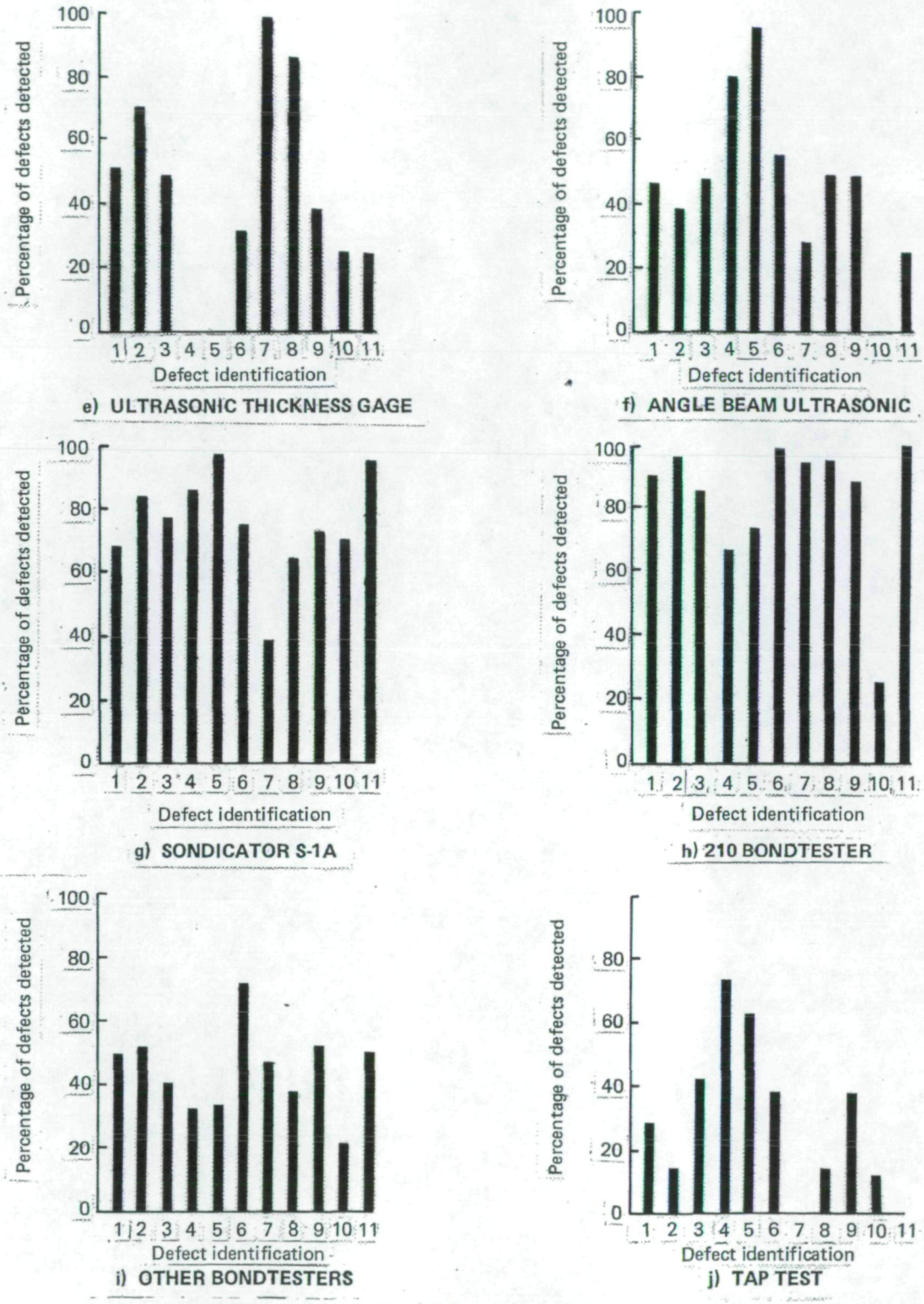

Figure 50. — Delamination/Disbond Defect Detection Capability (Concluded)

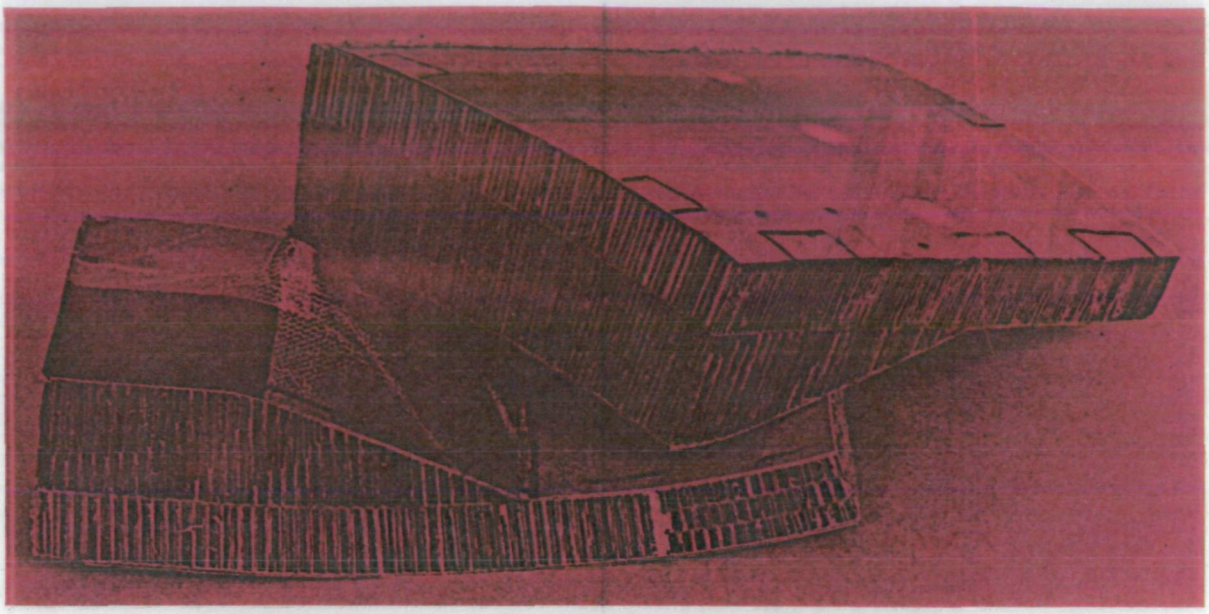

Figure 51. — Septumized Honeycomb Landing-Gear Door Sections

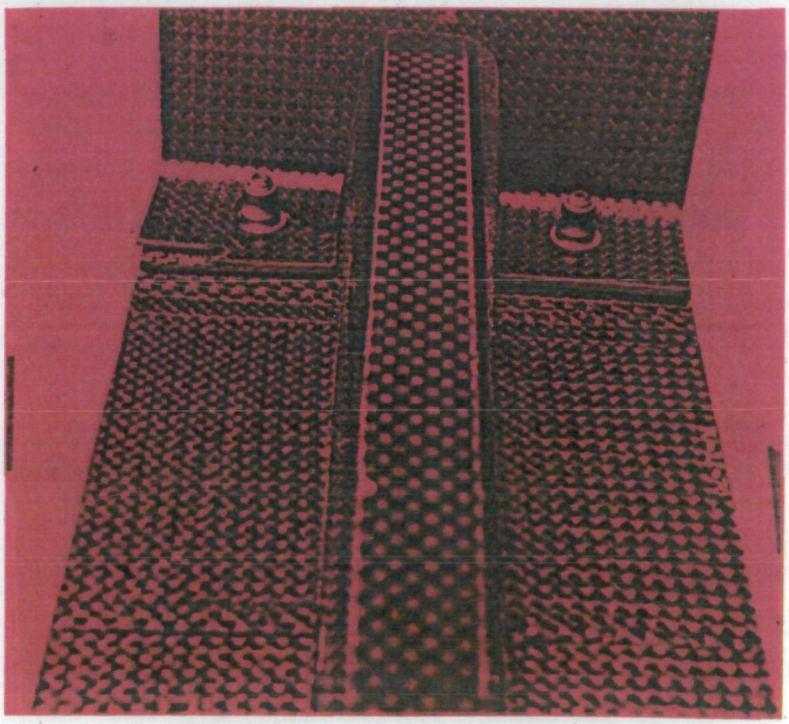

Figure 52. — Fractured Rib Flange

Method	Area*	On-aircraft inspection time, hr	Suspension of maintenance	Reference standards required	Labor hours	Materials, including reference standards
Radiography	S	1.5	Yes	No	6.0	$ 18
	L	13.0	Yes	No	28.5	$300
Ultrasonic TTU (with yoke)	S	1.5	No	Yes	3.0	$130
	L	6.0	No	Yes	12.0	$130
Ultrasonic or bondtester with couplant	S	1.0	No	Yes	2.0	$130
	L	5.0	No	Yes	10.0	$130
Ultrasonic or bondtester without couplant	S	0.75	No	Yes	1.5	$130
	L	4.0	No	Yes	8.0	$130
Eddy current	S	0.5	No	Yes	1.0	$130
	L	3.5	No	Yes	7.0	$130
Fluorescent penetrant	S	0.5	No	No	1.0	—
	L	Not applicable to large areas				
Far visual (1 person)	S	0	No	No	0.25	—
	L	0	No	No	0.25	—
Close visual and tap test	S	0.25	No	No	0.50	—
	L	1.0	No	No	2.0	—

*S = Small localized area

L = Large area: 18.5 linear meters (50 ft) along rib and spar

Figure 53. — Comparative Costs of Different Inspection Methods

Figure A-1. – EM-4300 and Probes

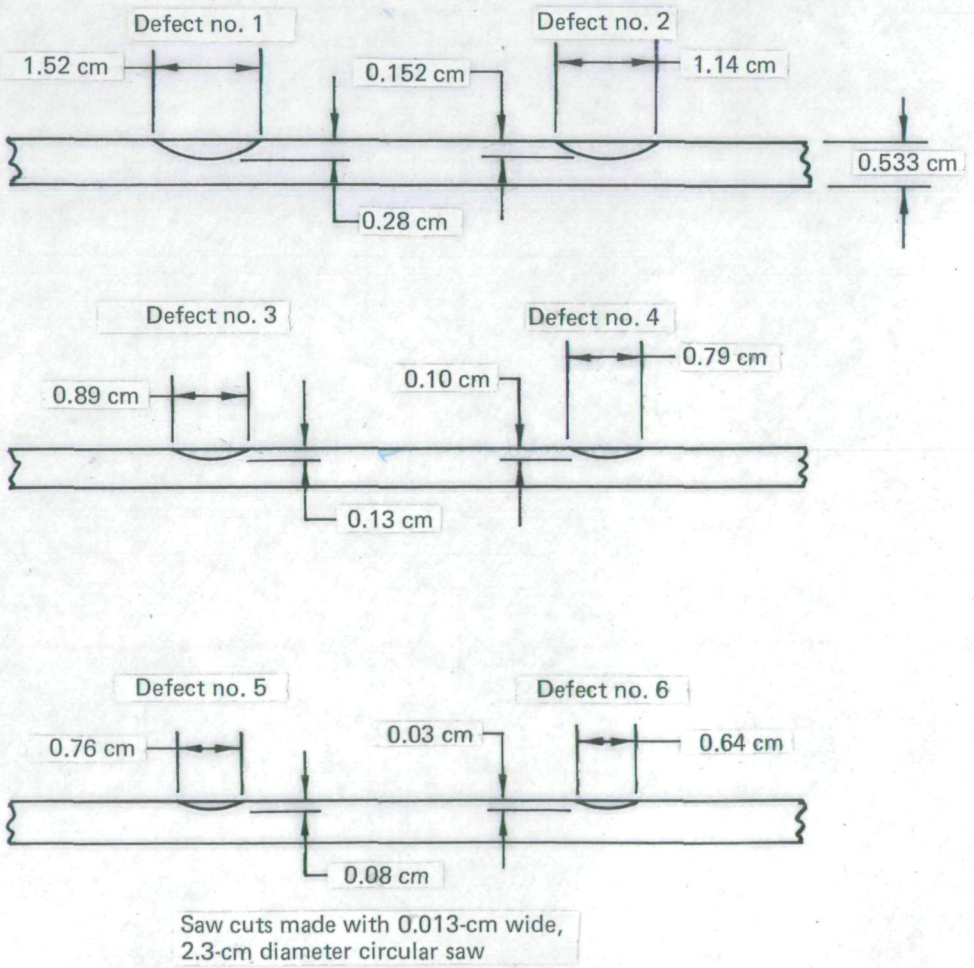

Figure A-2. – Gr-Ep Test Panel Cross Section Views

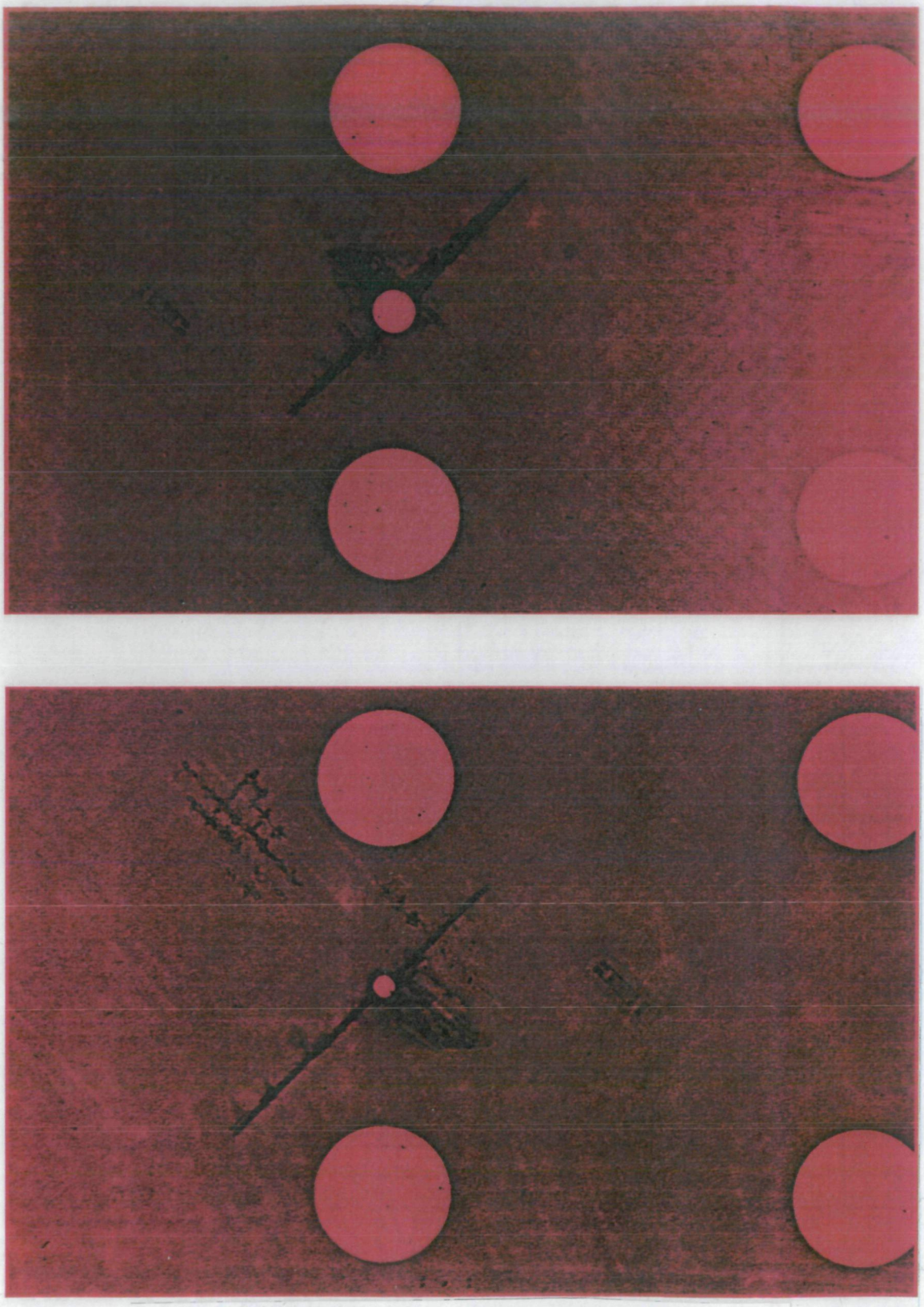

Figure A-3. — X-ray Negatives of Fractures in Fatigue Specimens

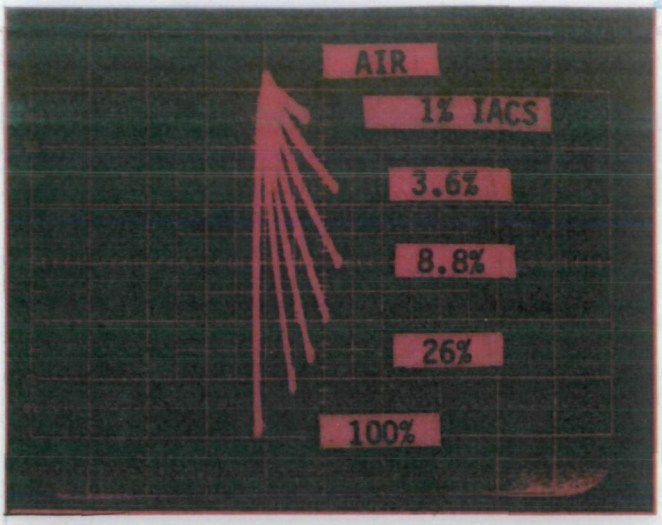

a) TYPICAL CONDUCTIVITY RELATIONSHIPS (AT 60 kHz)

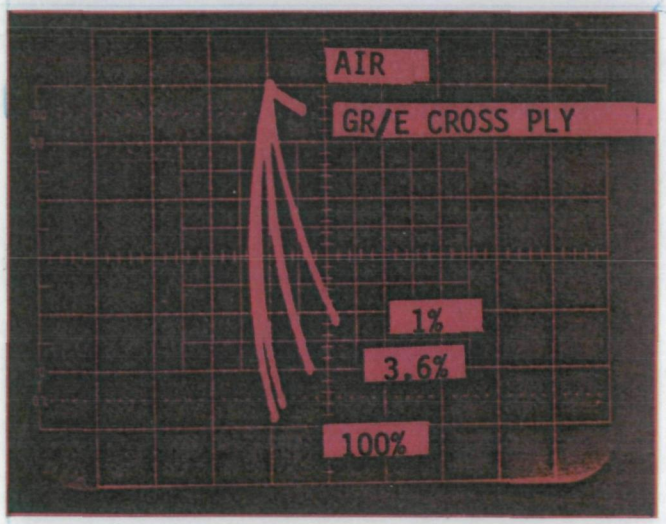

b) Gr-Ep CONDUCTIVITY MUCH LESS THAN 1.0% IACS (AT 2 MHz)

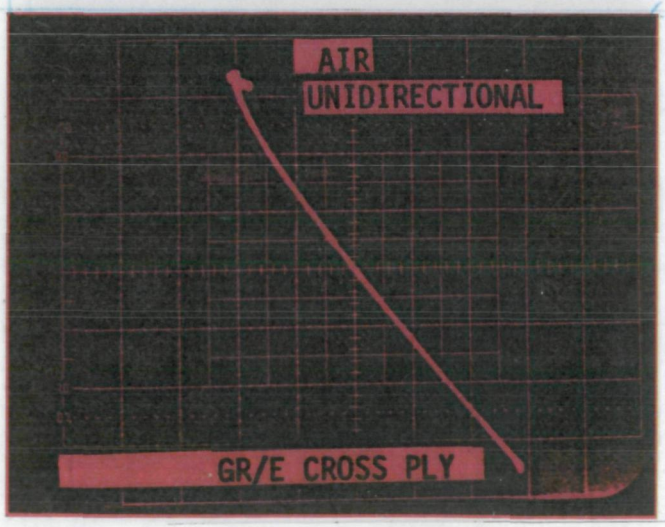

c) UNIDIRECTIONAL Gr-Ep LAMINATE, CONDUCTIVITY MUCH LESS THAN CROSS-PLY FABRIC CONSTRUCTION (AT 2 MHz)

Figure A-4. – Conductivity Comparisons by Impedance Plane Presentation

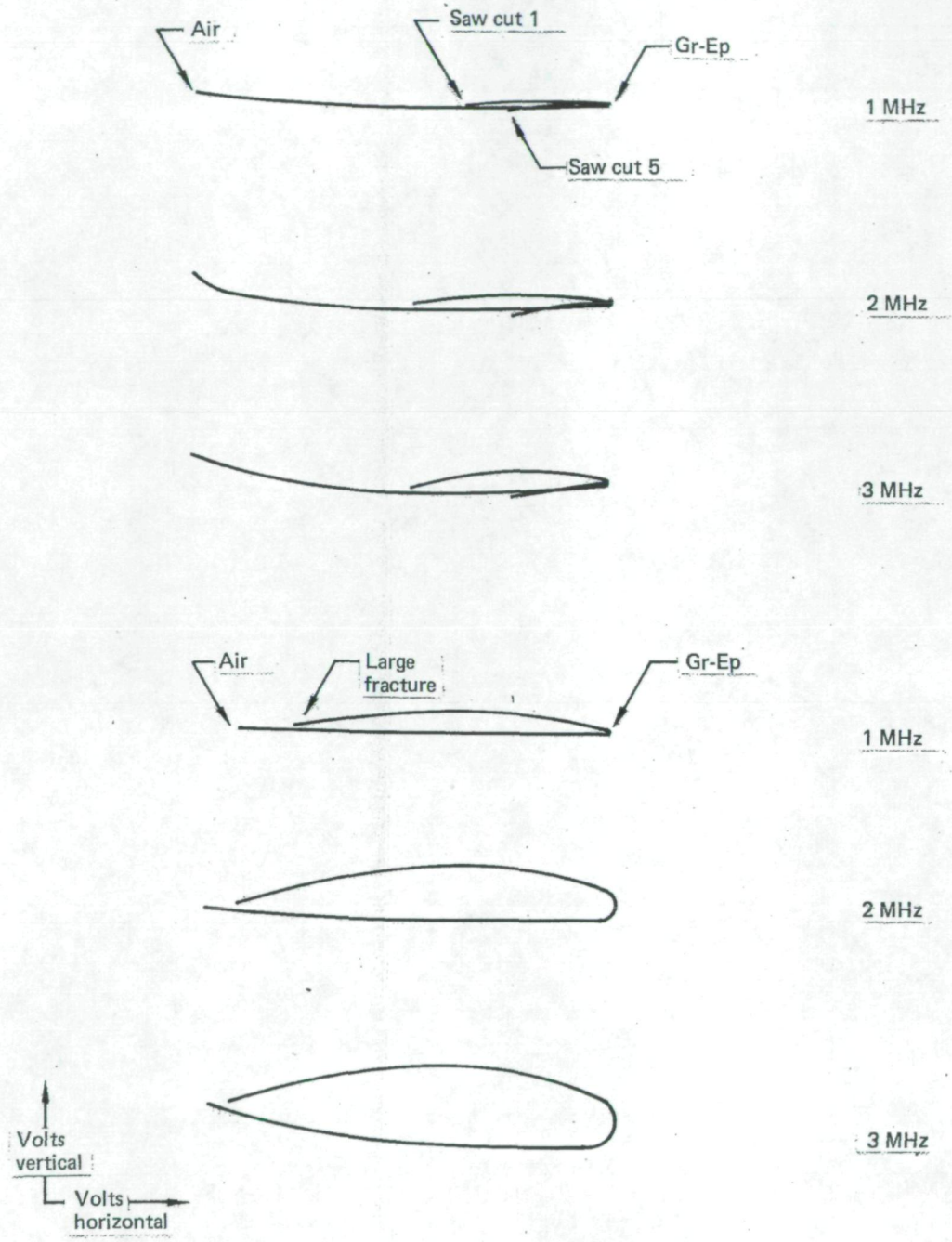

Figure A-5. — Phase Angle Versus Frequency and Fracture Size

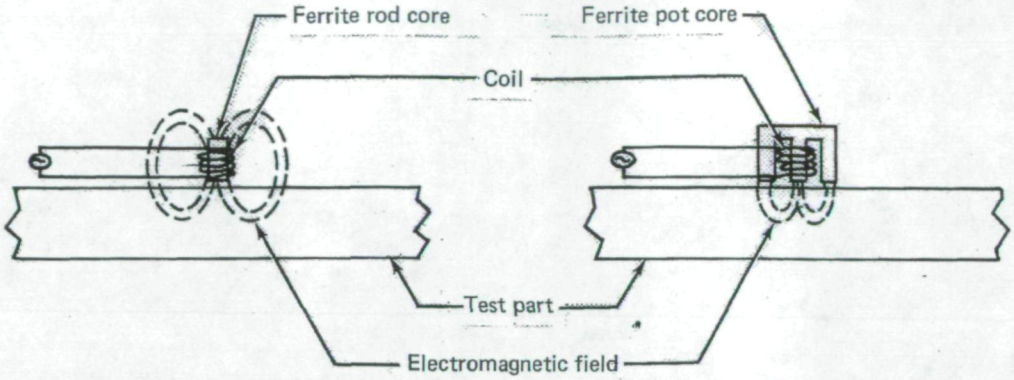

Probe identification	Type of ferrite core and diameter, cm	Coil height, cm	Coil outer diameter, cm	Wire gage	Number of turns	Coil resistance Ω	Coil inductance μH
Zetec 6 MHz	Rod	–	–	–	–	0.5	1.4
No. 1	0.08 Rod	–	0.10	No. 41	15	0.5	0.08
No. 2	0.08 Rod	–	0.09	No. 41	7	–	–
No. 3	0.28 Rod	–	0.38	No. 38	7	0.34	0.08
No. 4	0.08 Rod	0.05	0.30	No. 38	20	0.36	1.4
No. 5	0.12 Rod	0.09	0.46	No. 35	30	0.4	4
No. 6	0.69 Pot	–	0.69	No. 32	14	0.73	3.5
FLEX EC II USEC, Inc.	0.13 Rod		0.30			2.3	80
ED-1	0.69 Pot	–	0.69	No. 38	60	3	80
ED-2	0.69 Pot	–	0.69	No. 39	80	3.7	91
ED-3	0.69 Pot	–	0.69	No. 39	70	3.3	80
ED-4	0.08 Rod	0.09	0.66	No. 38	130	3.6	68
ED-5	0.13 Rod	0.18	0.51	No. 38	190	5	118
ED-6	0.13 Rod	0.13	0.58	No. 38	160	4.5	95
ED-7	1.40 Pot	–	1.40	No. 35	110	3.5	417
ED-8	1.40 Pot	–	1.40	No. 32	55	1	99

Figure A-6. — Probe Description

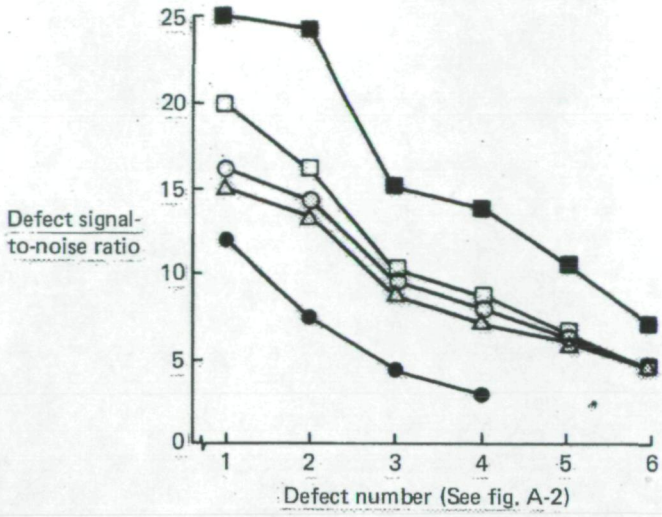

Symbol	Probe	Instrument	Comment
●	6	EM-4300	Liftoff Suppressed
○	6	EM-4300	Liftoff Maximized
△	6	EM-4300	Liftoff Maximized and tuned coil
□	FLEX II	ED 520	Liftoff maximized
■	ED 3	ED 520	Liftoff maximized

Figure A-7. — Instrument Sensitivity to Surface Defects Shown in Figure A-2

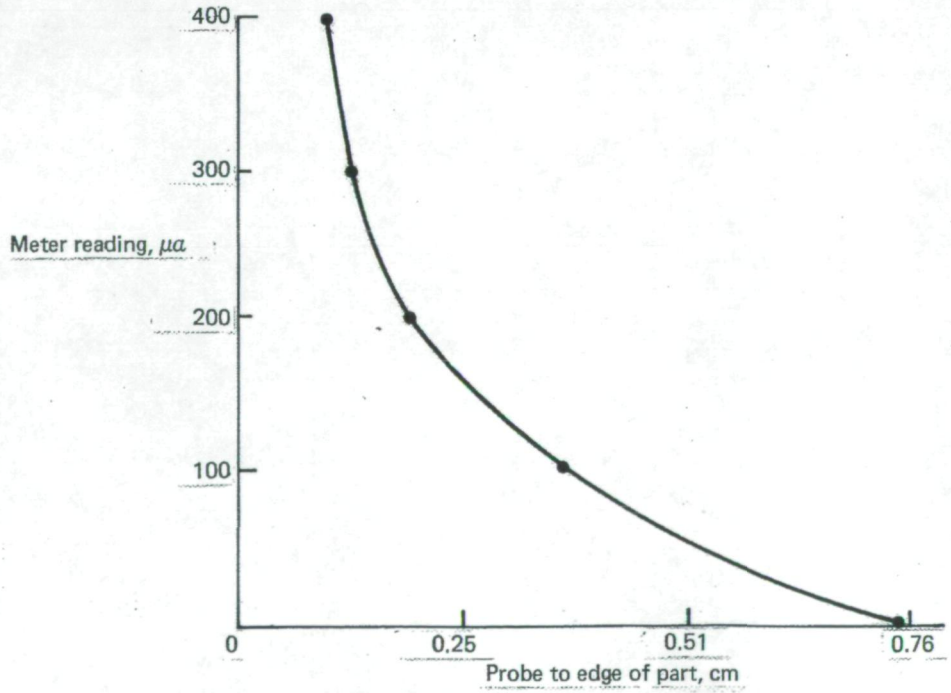

Figure A-8. — Edge Effect for Surface Inspection

Figure A-9. — Hole Damage

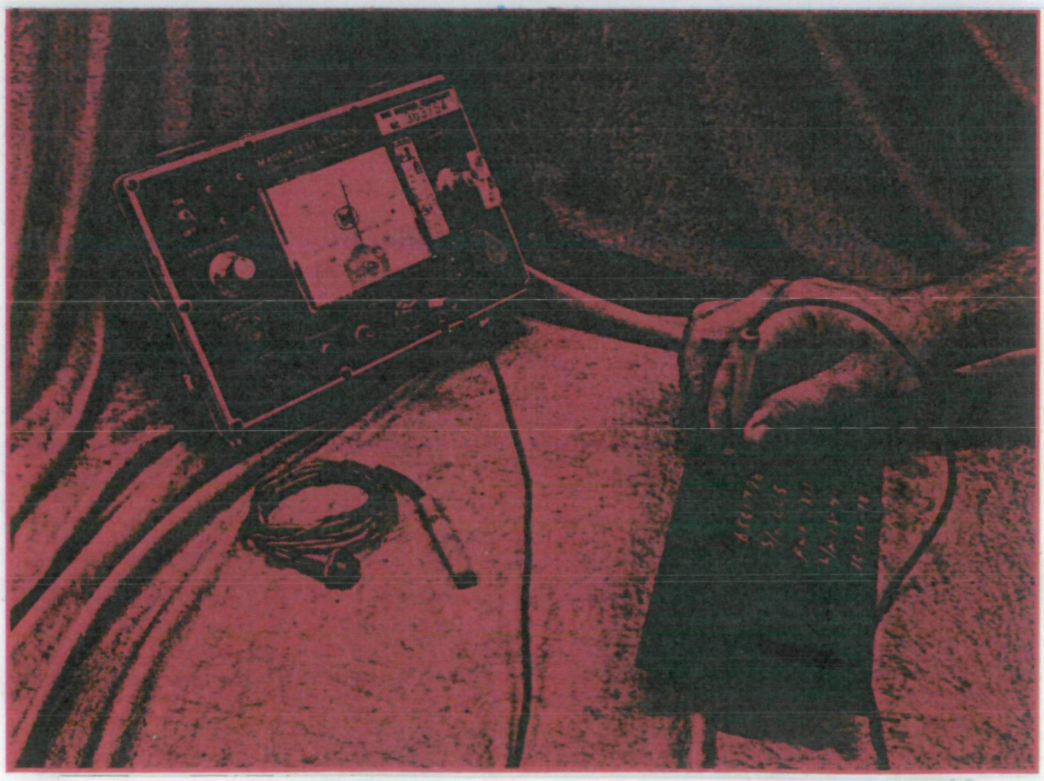

Figure A-10. — Inspection for Surface Fractures Out of Fastener Holes

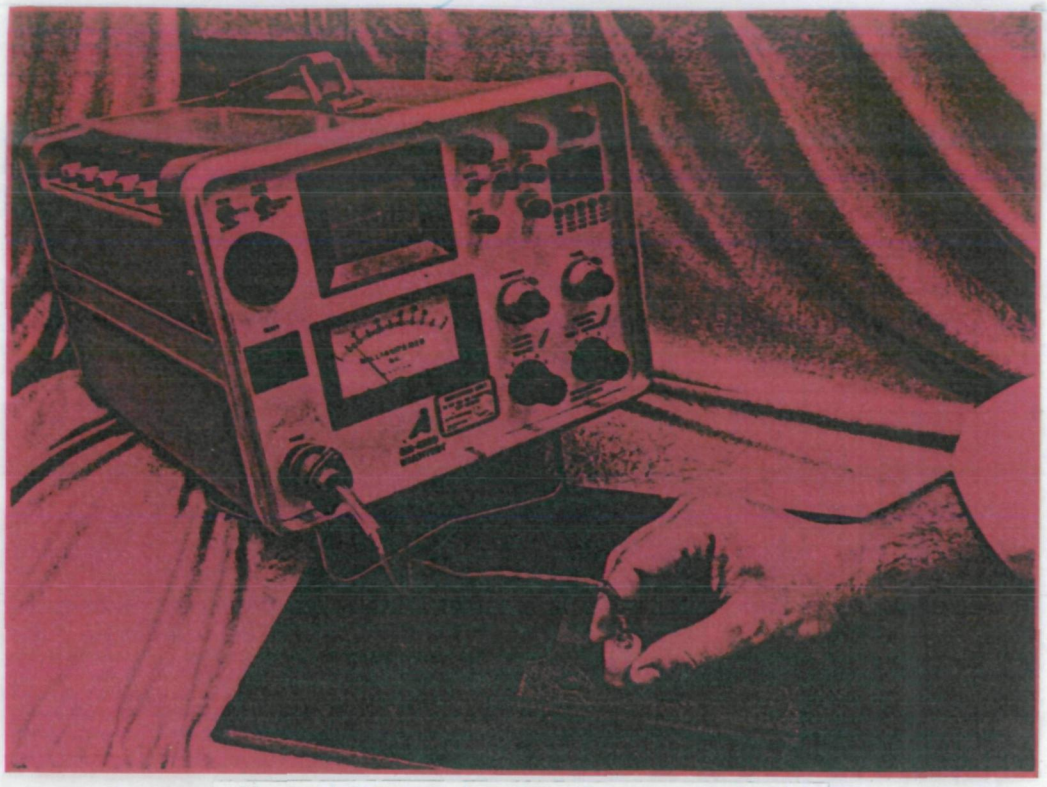

Figure A-11. — Subsurface Fracture Evaluation

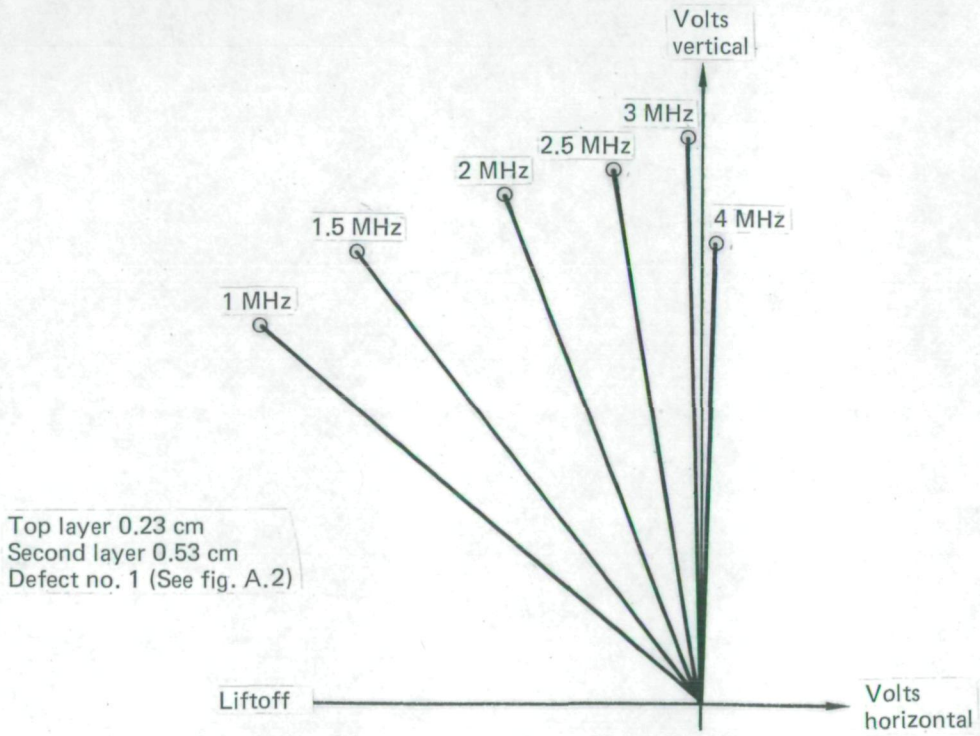

Figure A-12. — Second-Layer Defect Detection Versus Frequency

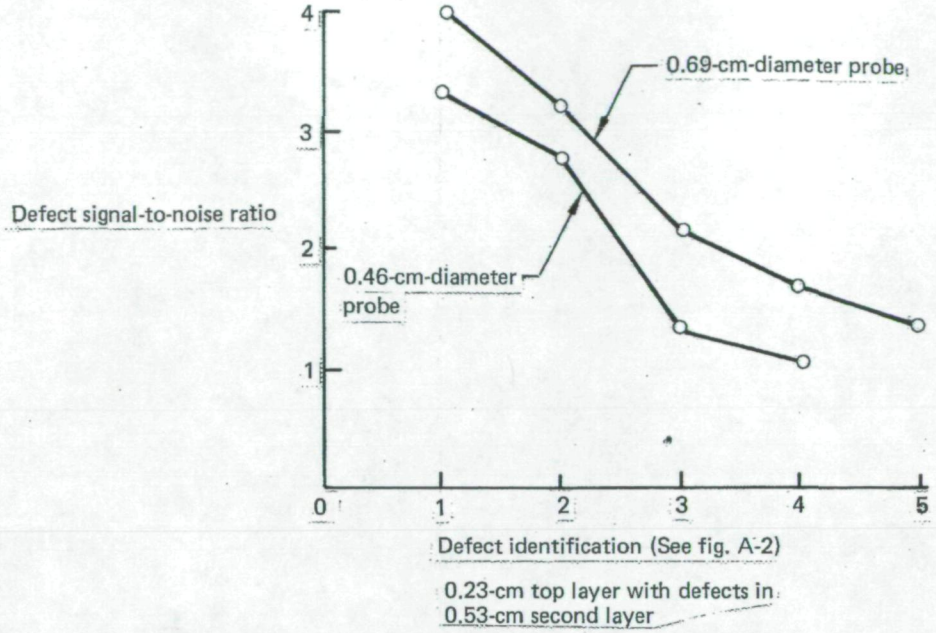

Figure A-13. — Probe Diameter Versus Sensitivity

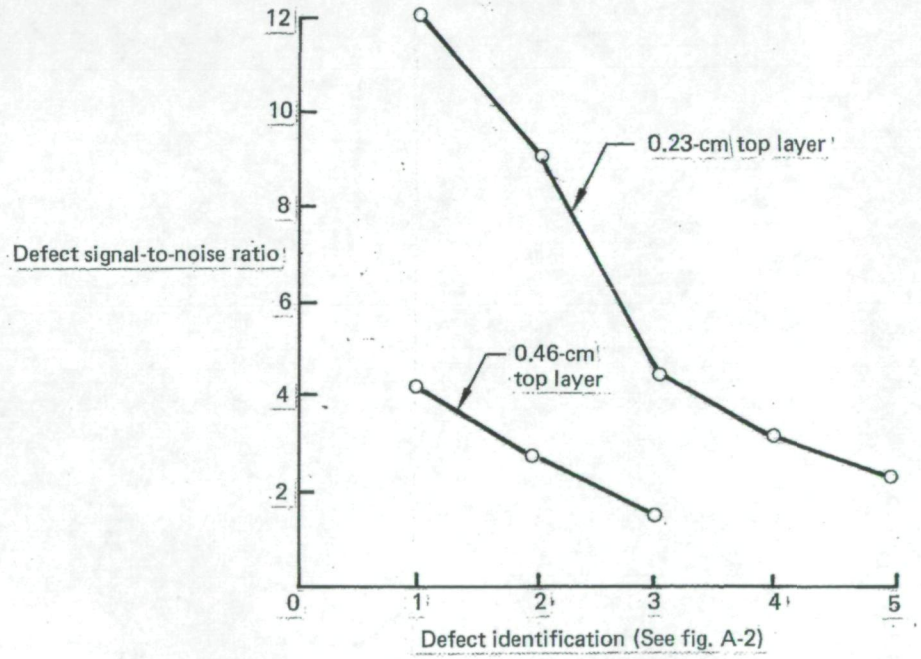

Figure A-14. — Second-Layer Defect Detection With Probe 8

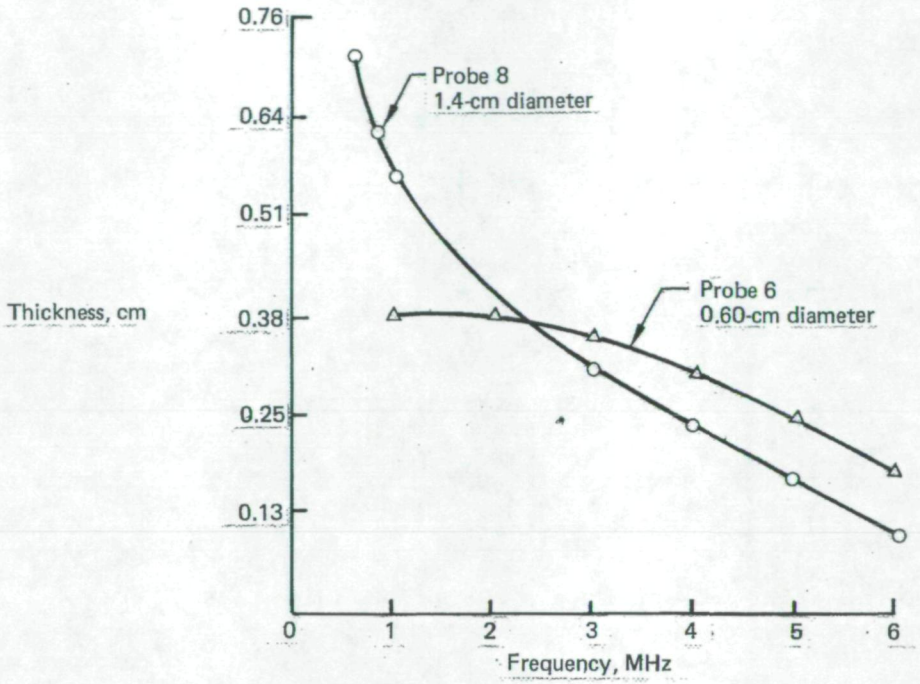

Figure A-15. — Penetration Versus Frequency

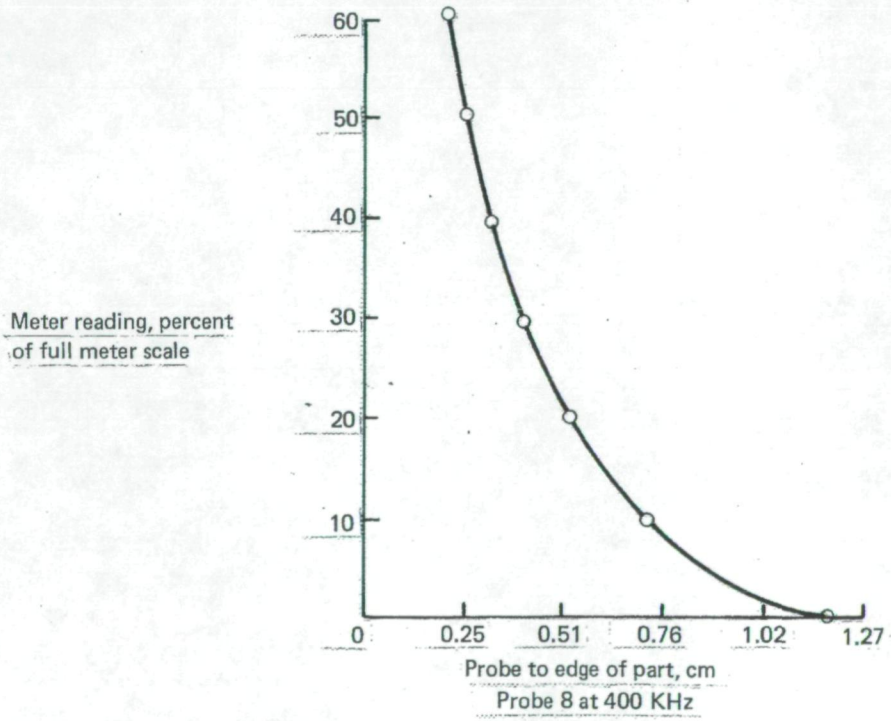

Figure A-16. — Top-Layer Edge Effect For Subsurface Inspection

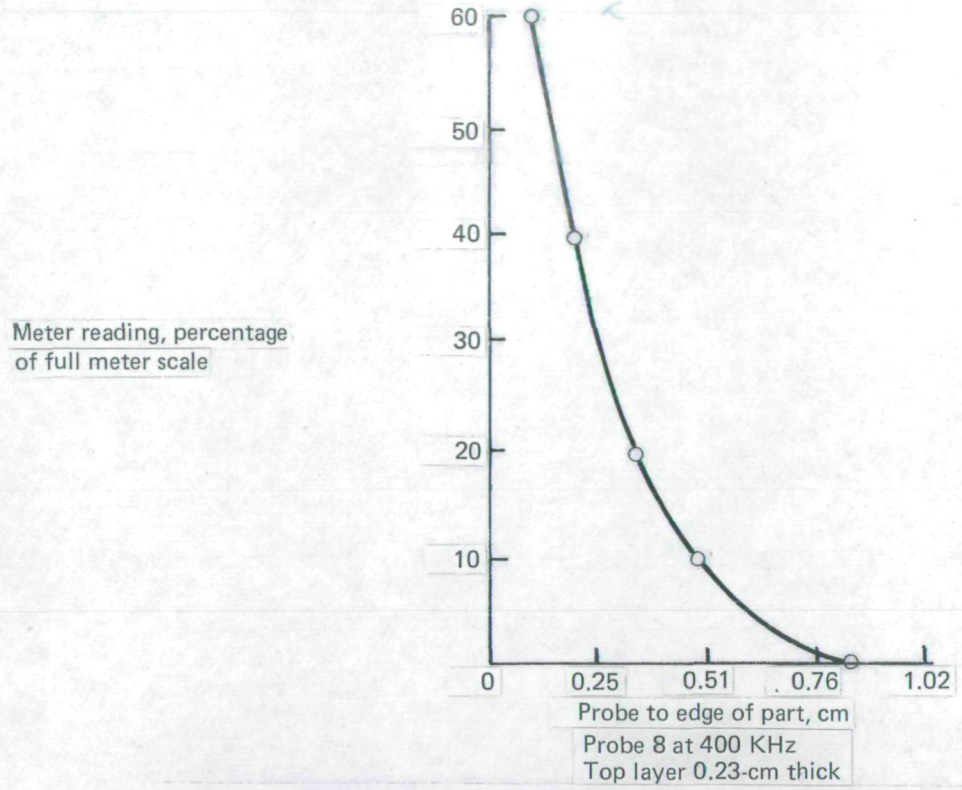

Figure A-17. – Second-Layer Edge Effect For Subsurface Inspection

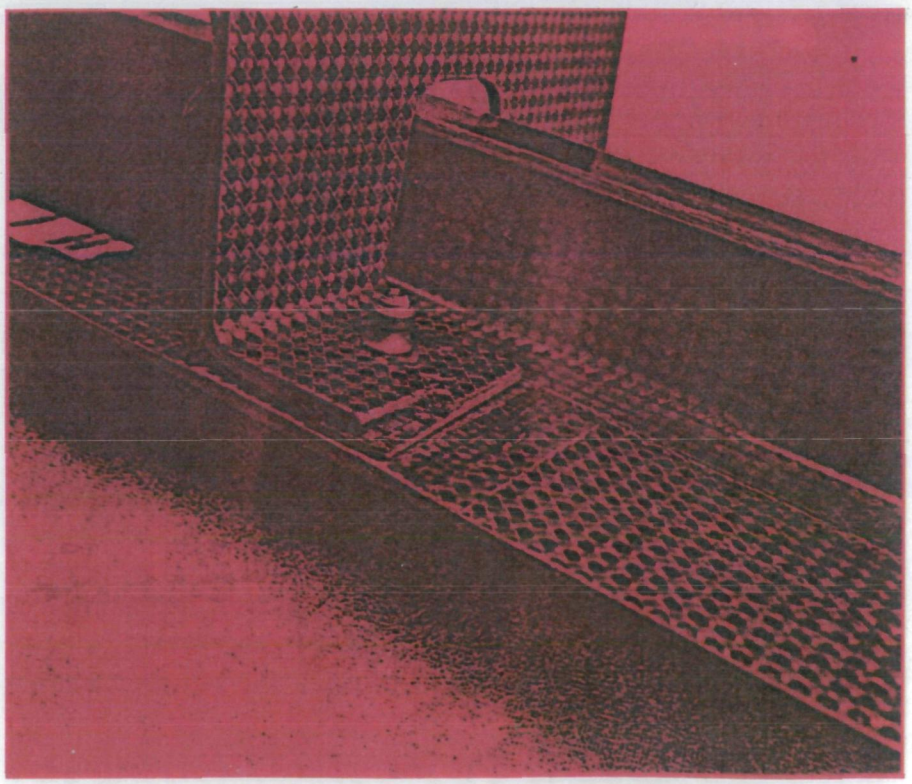

Figure A-18. – Structure With Second-Layer Fracture at Hole

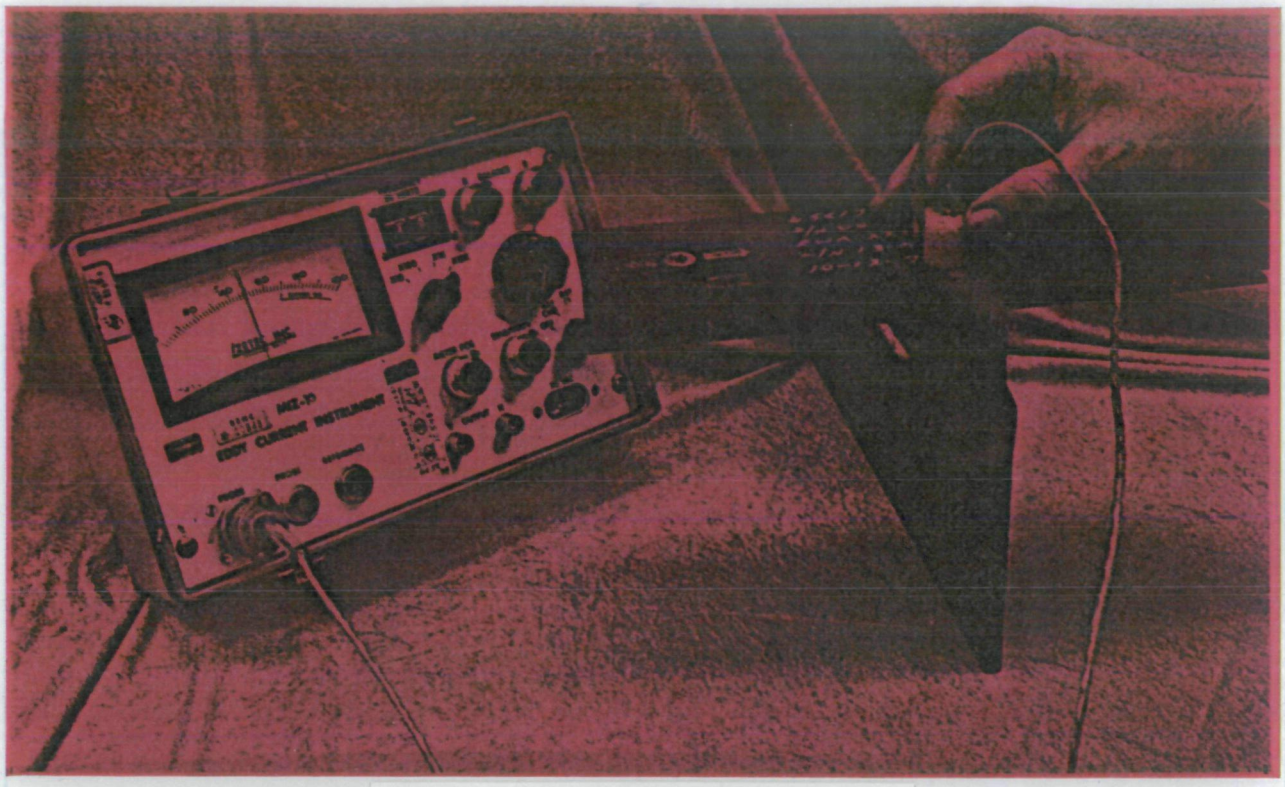

Figure A-19. — Second-Layer Inspection

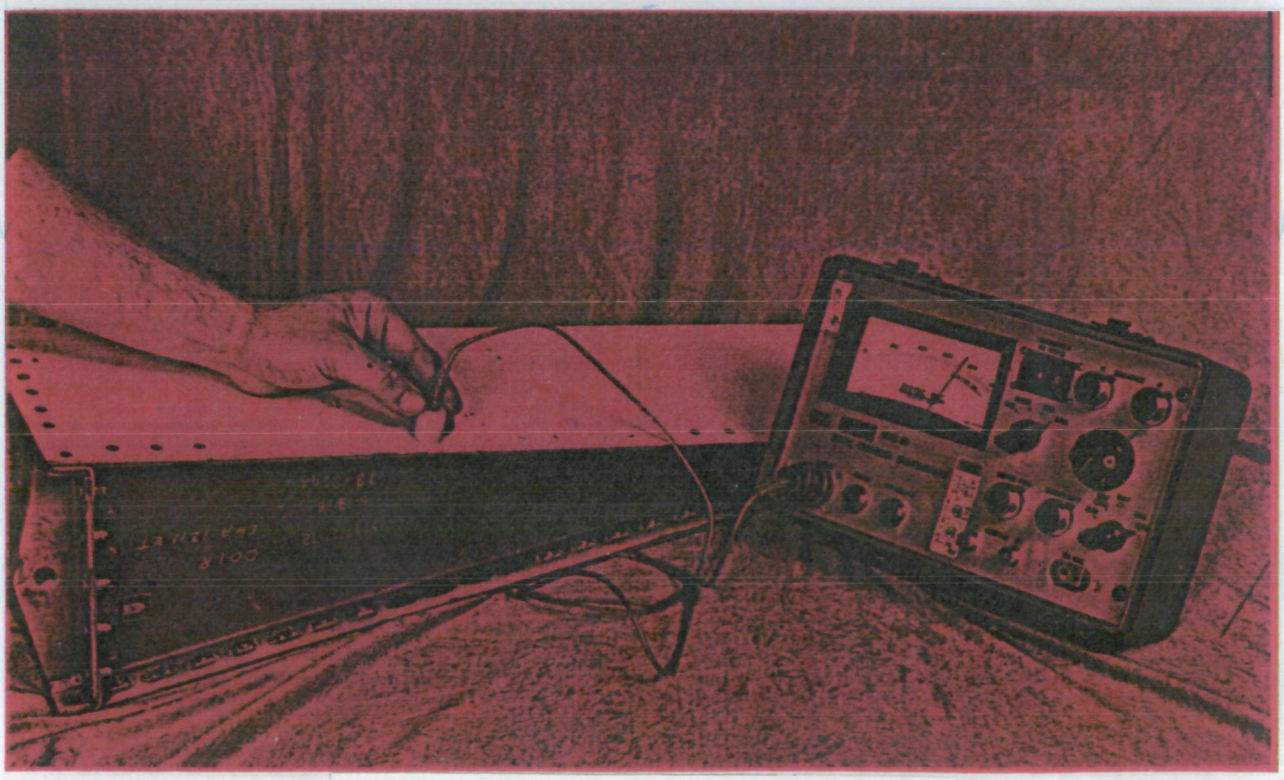

Figure A-20. — Boeing 727 Elevator Inspection

Panel identification	Material	Number of plies	Defect number	Impact, cm-kg
I 11	Graphite-epoxy/ fabric type II, class II, style 3K-70-PW per BMS 8-212	11	1	11.3
			2	22.6
			3	33.9
			4	45.2
			5	56.4
			6	67.7
			7	79.0
I 27	Graphite-epoxy/ fabric type II, class II, style 3K-70-PW per BMS 8-212	27	1	225.8
			2	248.4
			3	270.9
			4	293.5
			5	316.1
			6	338.7
			7	361.2
HI 325	Graphite-epoxy/ fabric type II, class II, style 3K-70-PW per BMS 8-212, with 3/4-in Nomex core	5	1	11.3
			2	22.6
			3	33.9
	No core		6	33.9
			7	39.5
			8	45.2

Figure A-21. — Impact Damage Panels

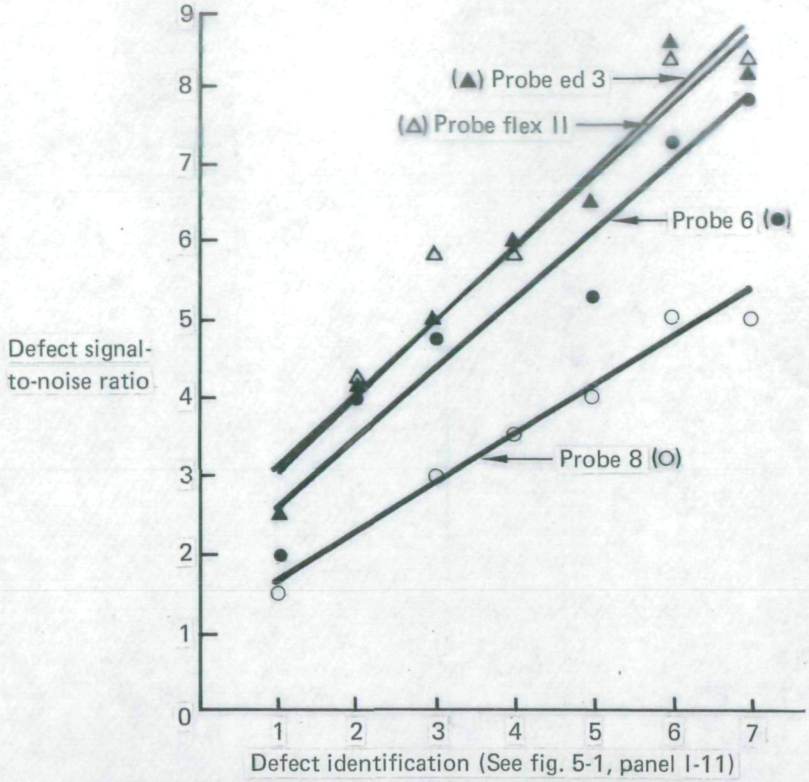

Figure A-22. — Impact Damage Detection on Panel I-11

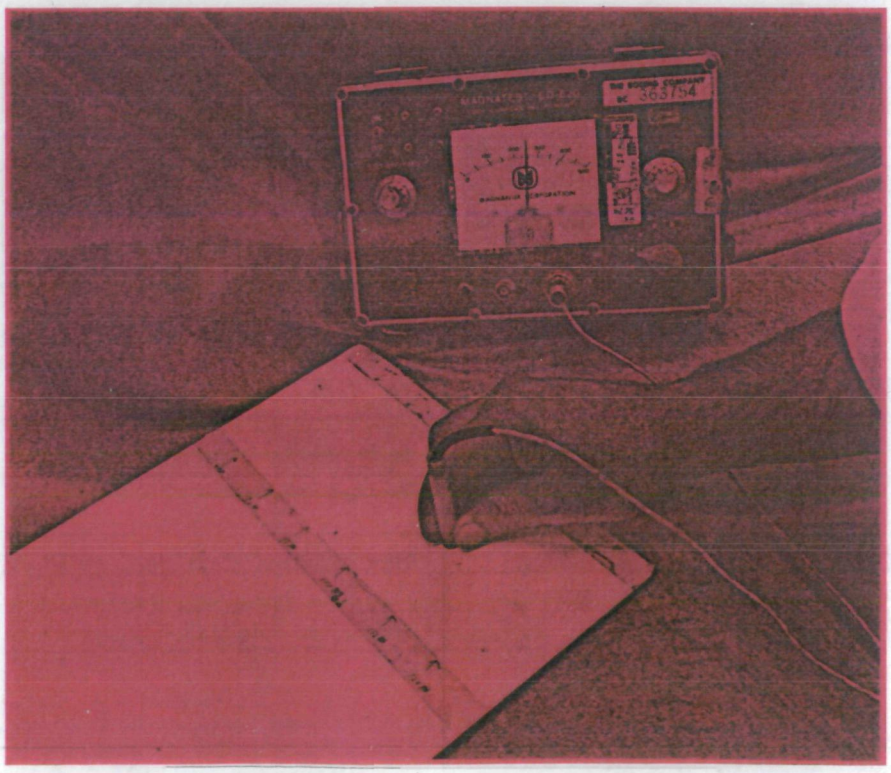

Figure A-23. — Impact Damage Inspection

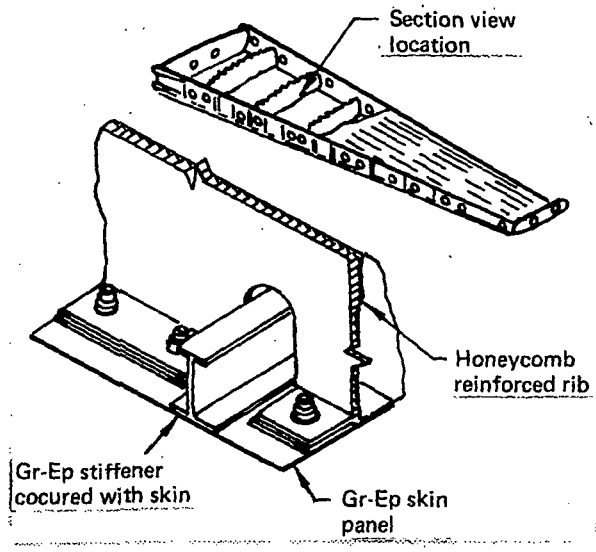

a) I-STIFFENER, RIB, AND SKIN DETAIL

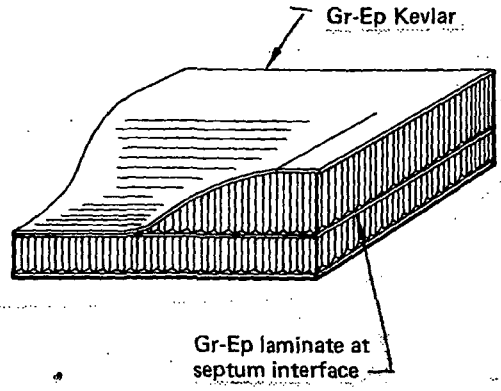

b) SEPTUMIZED HONEYCOMB

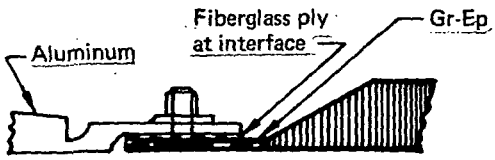

c) ALUMINUM-TO-Gr/Ep JOINT DETAIL

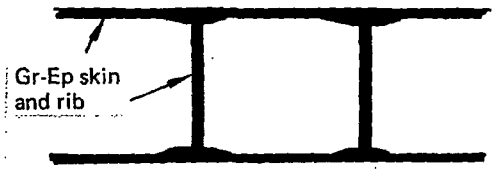

d) COCURED RIB AND SKIN DETAIL (NO ADHESIVE BOND JOINT)

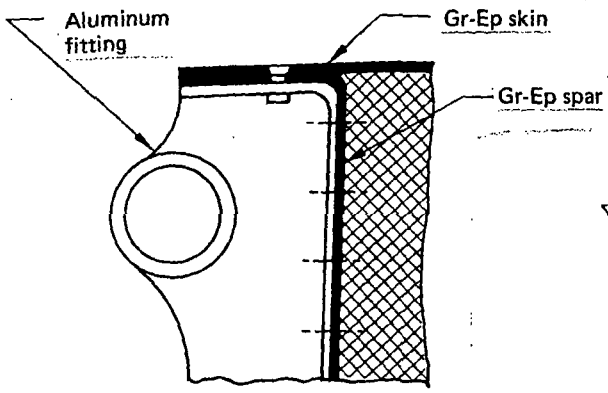

e) HINGE FITTING TO Gr-Ep STRUCTURE DETAIL

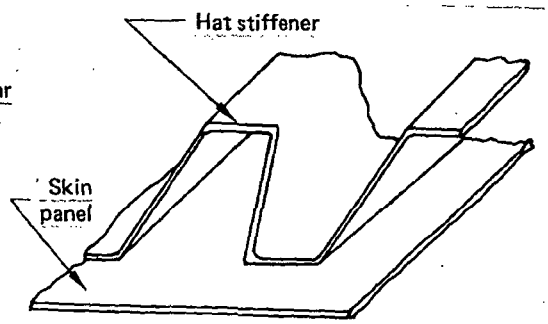

f) ALL Gr-Ep HAT-STIFFENED SKIN (COCURED; NO ADHESIVE BOND)

Figure B-1. — Detailed Structural Configurations of Typical Gr-Ep Structures

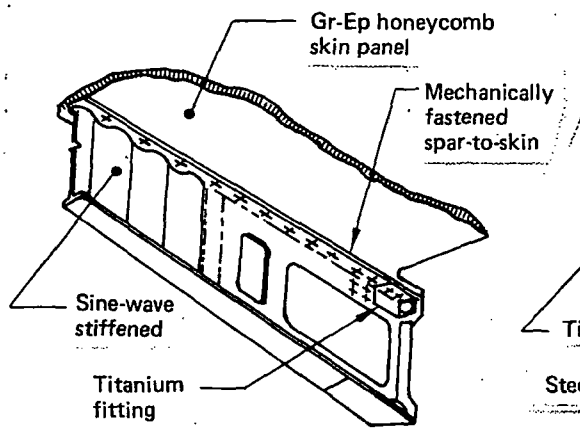

g) SINE WAVE-STIFFENED SPAR/SKIN ATTACH FITTING DETAIL

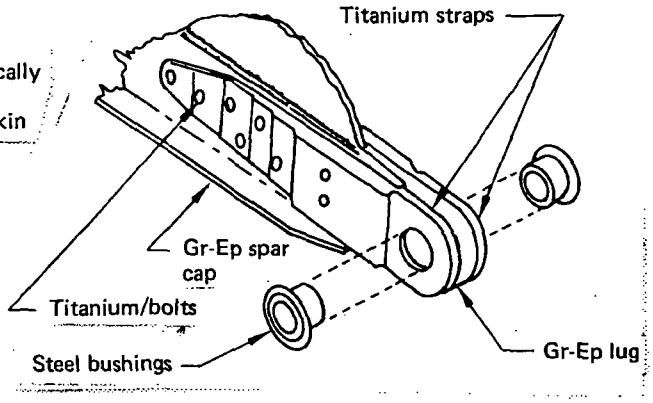

h) LUG FITTING

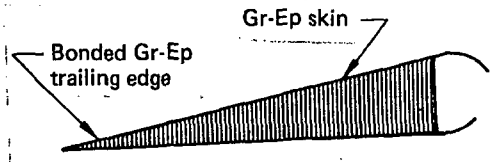

i) FULL DEPTH HONEYCOMB (NOMEX OR HRP CORE)

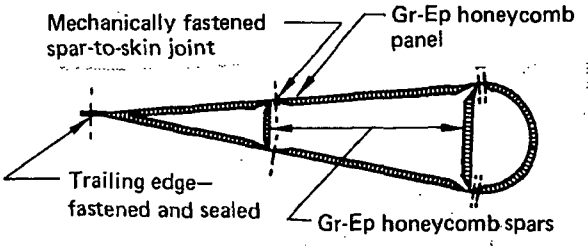

j) MECHANICALLY FASTENED GR-EP HONEYCOMB SKIN AND SPARS

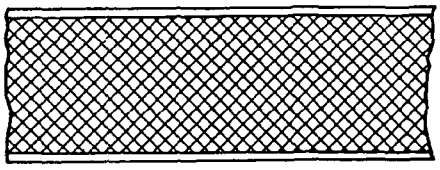

k) GR-EP SKINS AND SYNTACTIC CORE

Figure B-1. — (Concluded)

STRUCTURES	DEFECTS									
	Delamination/ disbond	Impact damage	Fastener hole damage	Lightning damage	Burn damage	Fractures, surface	Fractures, subsurface and substructure	Internal structure damage—access through doors	Internal structure damage—inaccessible	Water-in-honeycomb
Laminated skin	1)D,E 2)D,E	1)A,B 2)B,C, D,E,G	1)A,B 2)B,H,G	1)A,B 2)B,E,D	1)A,B 2)B,E,D	1)A,B,H 2)H,D,F	1)H,D,F 2)B,F, G,E,H	1)B 2)B,F, G,E,H	1)F 2)F	—
Skin/honeycomb panel	1)E,D 2)E,D	1)A,B 2)A,D E,H,G	1)A,B 1)B,H,G	1)A,B 2)B,E, D,F	1)A,B 2)B,E, D,F	1)A,B,H 2)B,H,I	1)B 1)H,D,F	1)F 2)B,F, E,H	1)F 2)F	1)F,E 2)F,E
Skin-to-stiffner joint	1)D,E 2)D,E	1)A,B 2)B,D E,H,G	1)A,B 2)B,H,G	1)A,B 2)B,D E,F	1)A,B 2)B,D E,F	—	—	1)B 2)B,I	—	—
Skin-to-metal joint	1)D,E 2)D,E	1)A,B 2)B,D E,H,G	1)A,B 2)B,H,G	1)A,B 2)B,D, E,F	1)A,B 2)B,D, E,F	—	—	1)B 2)B,I	—	—
Skin-to-skin trailing edge joint	1)C,E,D 2)B,D,I	1)A,B 2)B,C, D,H,I	1)A,B 2)B,H, G,I	1)A,B 2)B,C, D,E	1)A,B 2)B,D, C,E	—	—	—	—	1)C,E, D,F 2)C,E, D,F
Honeycomb ribs, spars, and skin stiffeners	—	—	1)A,B 2)B,H,G	1)A,B 2)B,D,E	1)A,B 2)B,D,E	—	1)F 2)F	1)B 2)B,F, G,H,E	1)F 2)F	1)F 2)F
Laminated ribs, spars, and skin stiffeners	—	—	1)A,B 2)B,H,G	1)A,B 2)B,D,E	1)A,B 2)B,D,E	—	1)F 2)F	1)B 2)B,F, G,E,H	1)F 2)F	—
Full-depth honeycomb	1)E,C,D 2)E,C,D	1)A,B 2)B,D, E,H,G	—	1)A,B 2)B,E,D	1)A,B 2)B,E,D	1)A,B,H 2)B,H,I	1)F 2)F	—	1)C,E, D,F 2)C,E, D,F	1)F,C,E 2)F,C,E
Septumized honeycomb	1)E,C,D 2)D,E,C	1)A,B 2)B,D, E,H,G	—	1)A,B 2)B,E,D	1)A,B 2)B,E,D	1)A,B,H 2)B,H,I	1)F 2)F	—	1)D,C, E,F 2)D,C, E,F	—
Lugs and thick sections	1)D,F,G 2)G,F,G	—	1)D,F,G 2)D,F,G	1)D,F,G 2)D,F,G	1)D,F,G 2)D,F,G	1)A,B,H 2)B,H,I	1)D,F 2)D,F	—	1)F 2)F	1)F,D,E 2)F,D,E

Key:
Inspection method:

A Far visual
B Near visual, optical tap test
C Ultrasonic TTU
D *Ultrasonic pulse echo*
E Bondtester
F Low KV X-ray
G DIB enchanced X-ray
H Eddy current
I Penetrant

Task:
1) Detection
2) Evaluation

Figure B-2.—Method Selection

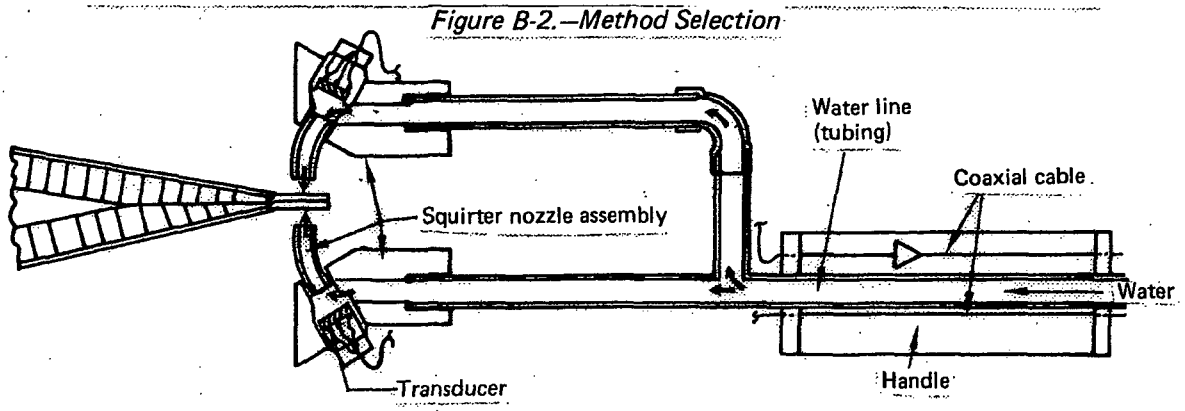

Figure B-3. — Ultrasonic Through-Transmission Yoke Assembly for Trailing-Edge Disbond Inspection

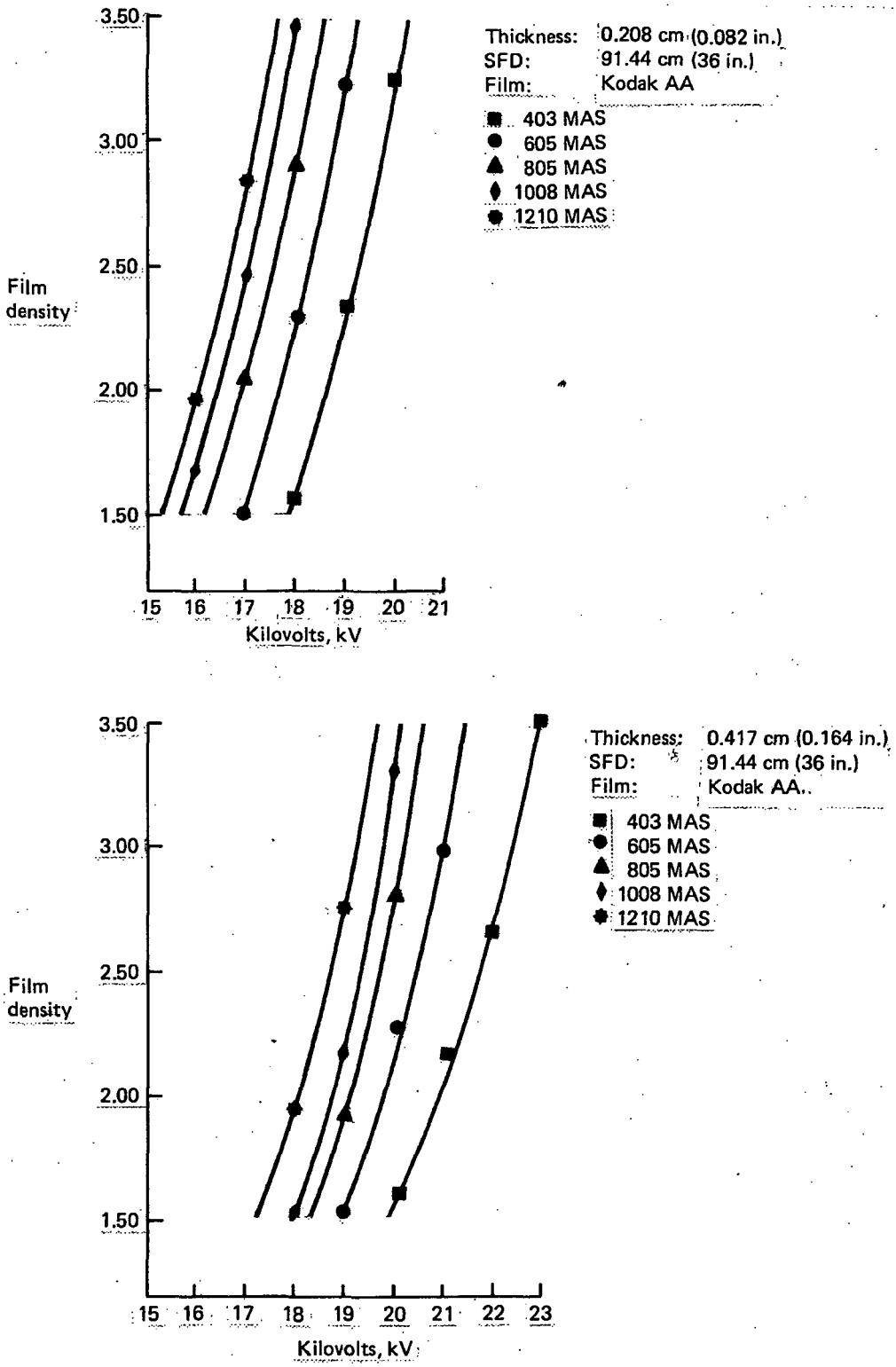

Figure B-4. — Exposure Curves

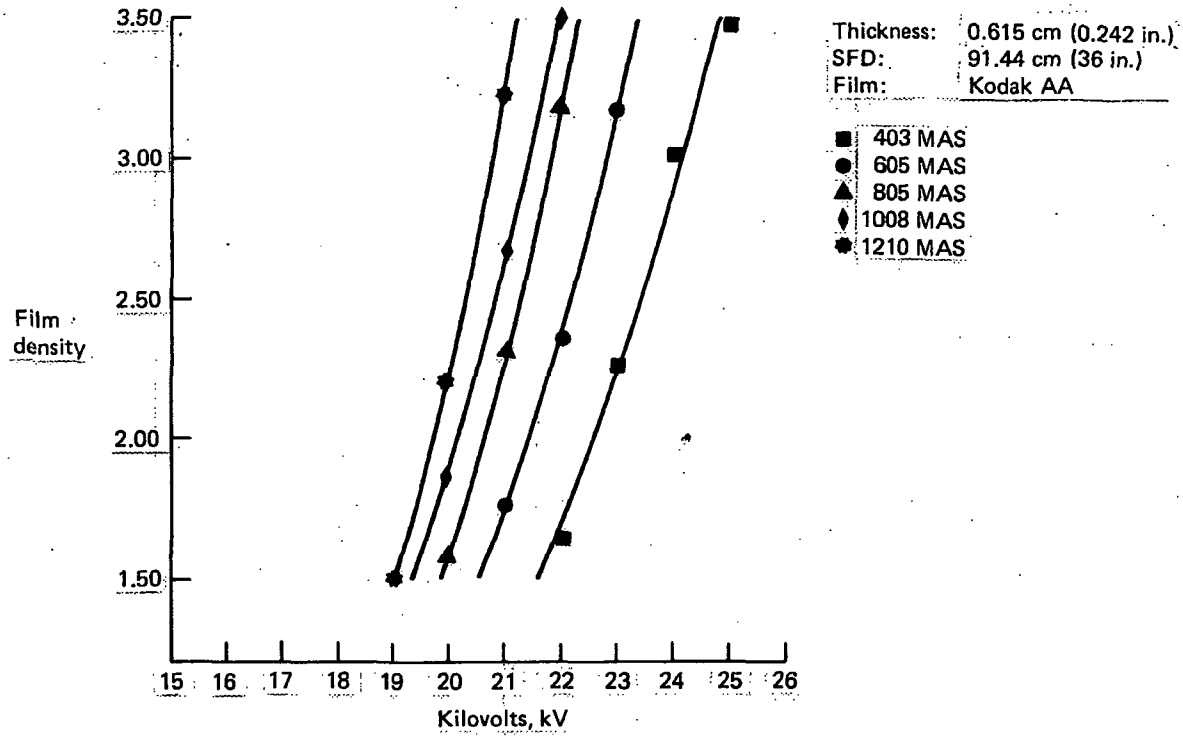

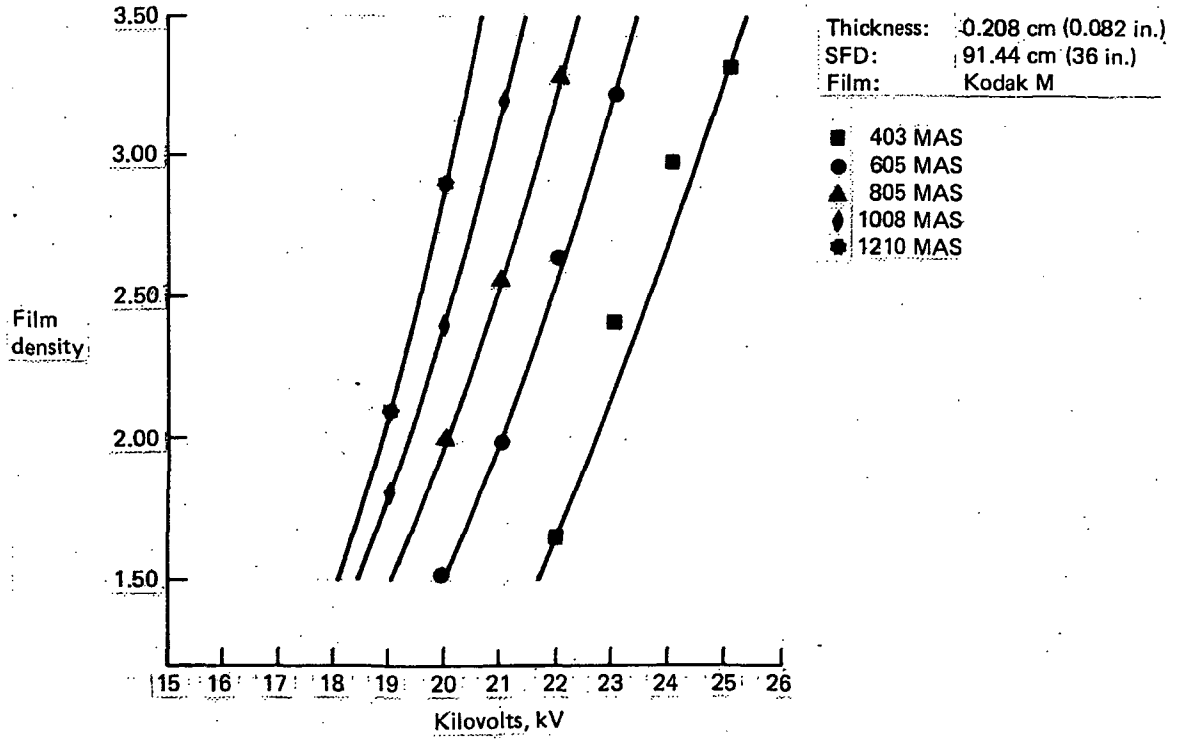

Figure B-4. — (Continued)

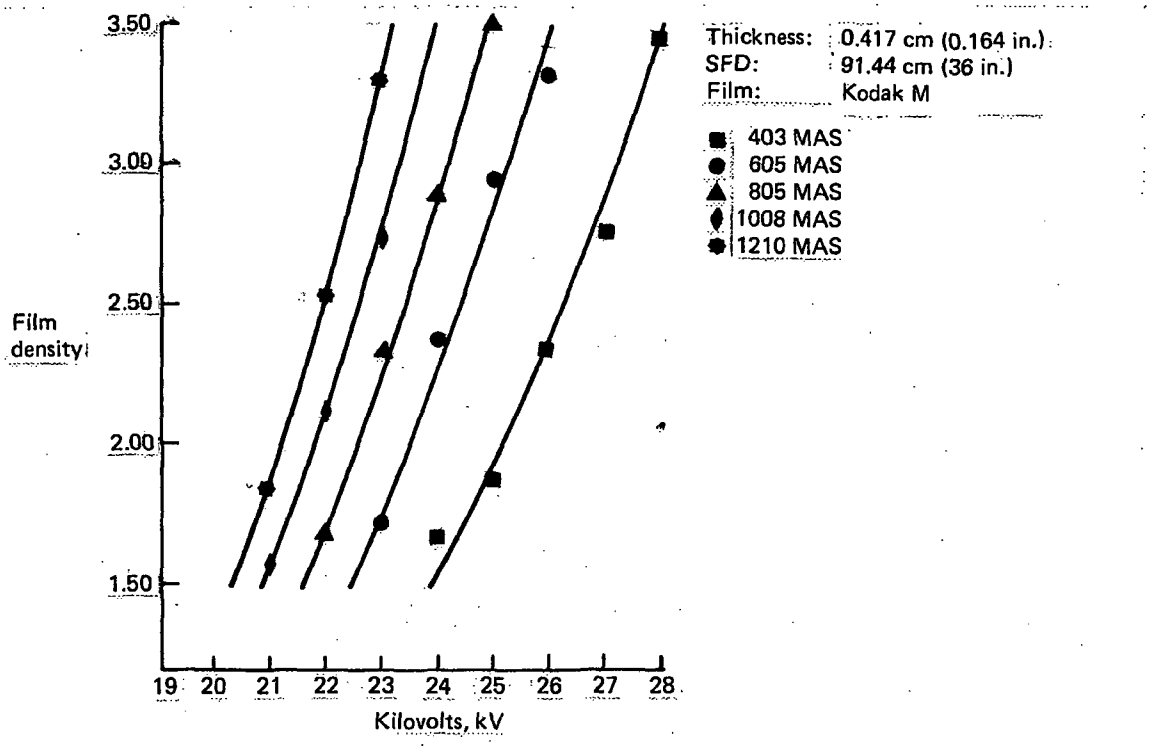

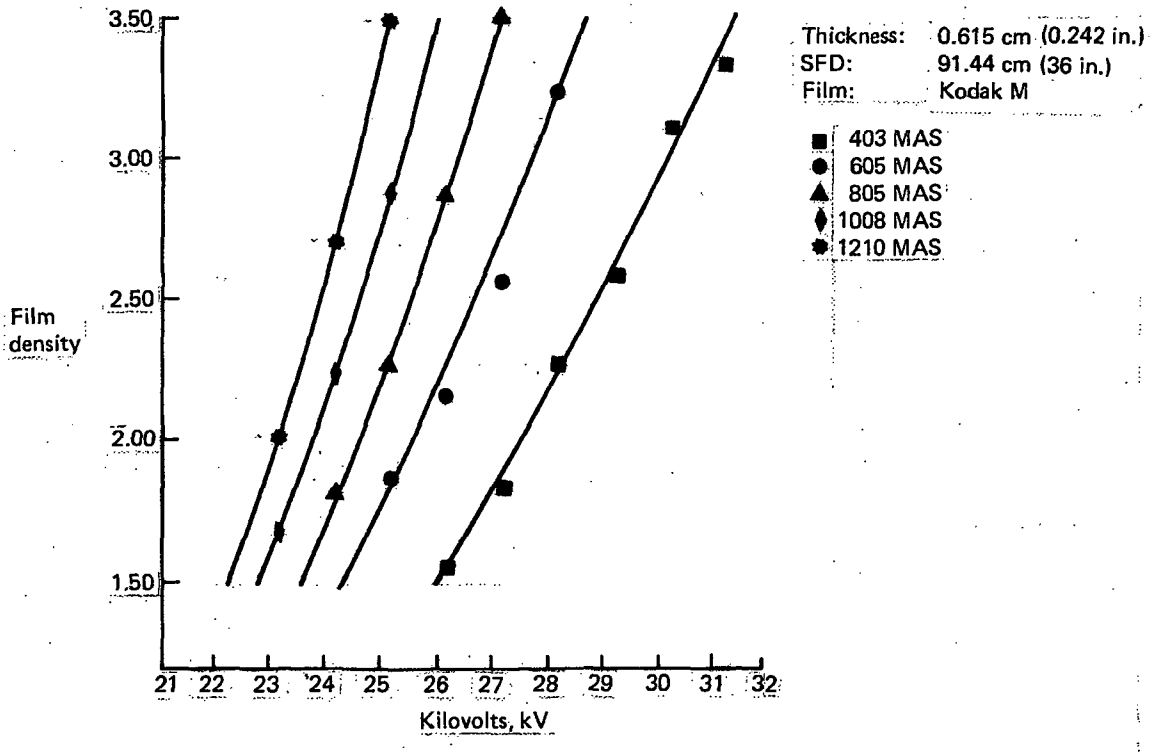

Figure B-4. — (Continued)

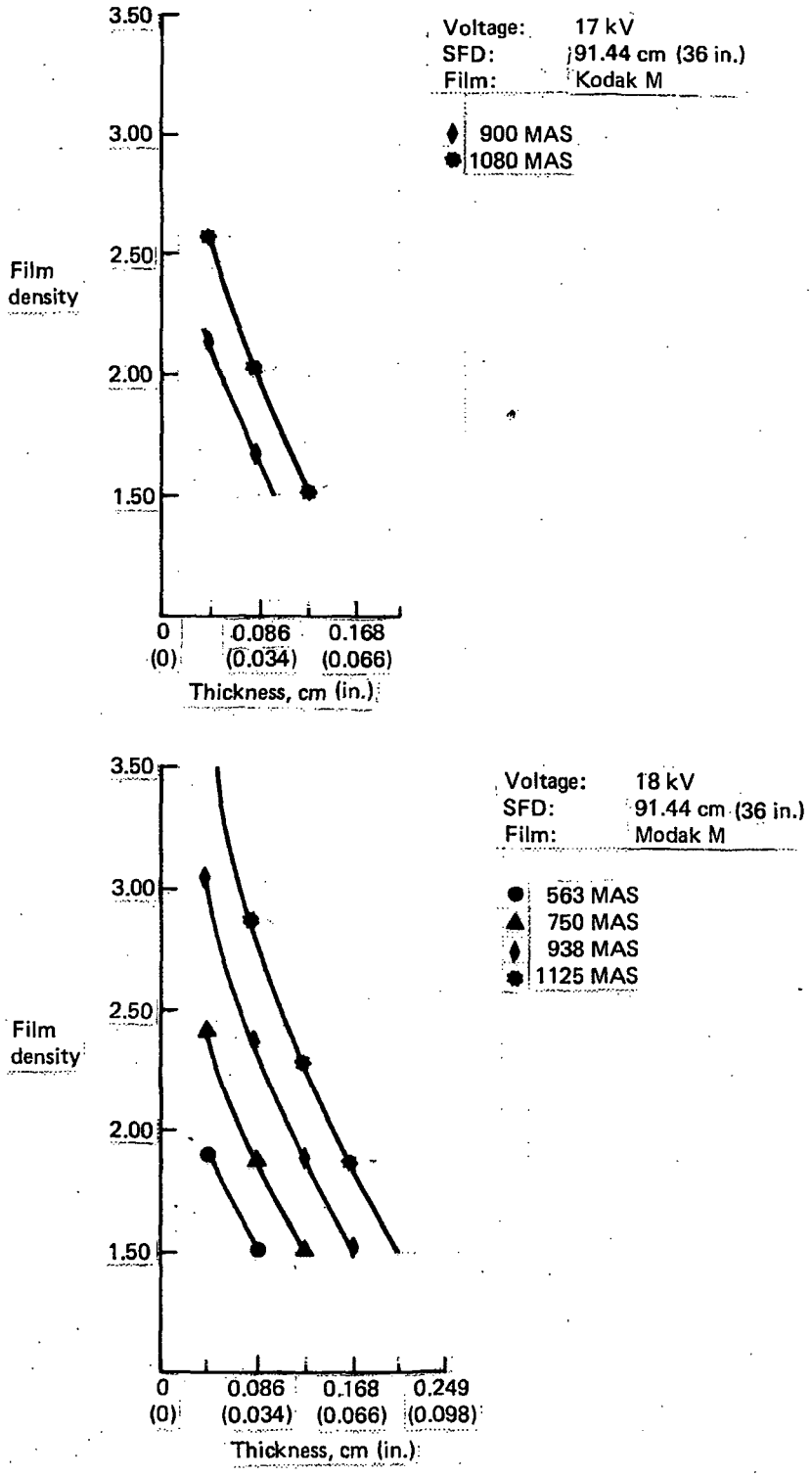

Figure B-4. — (Continued)

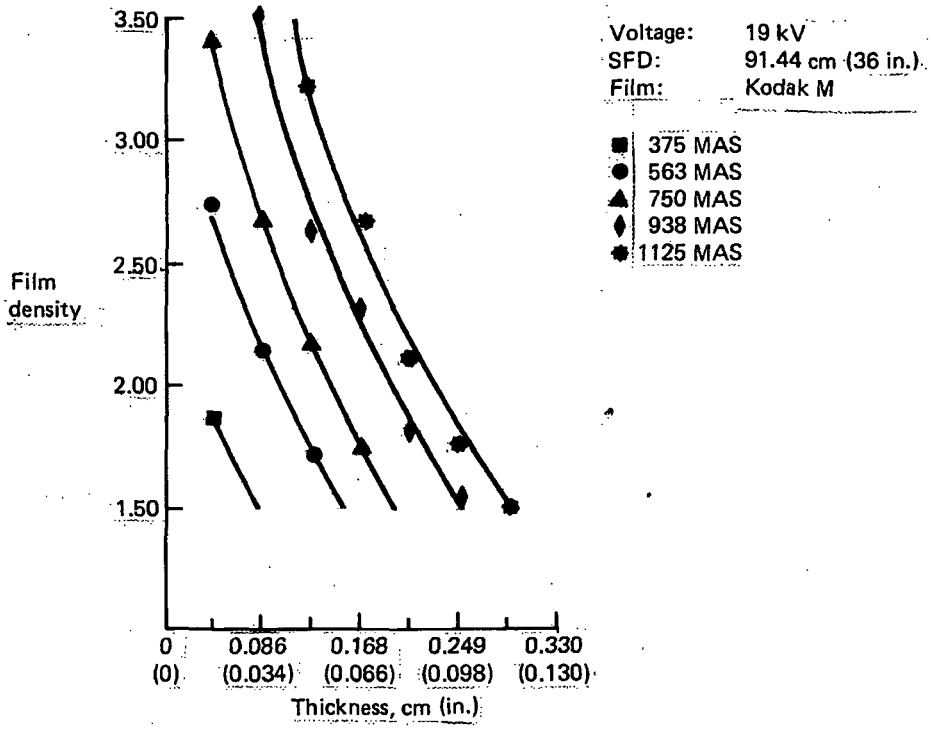

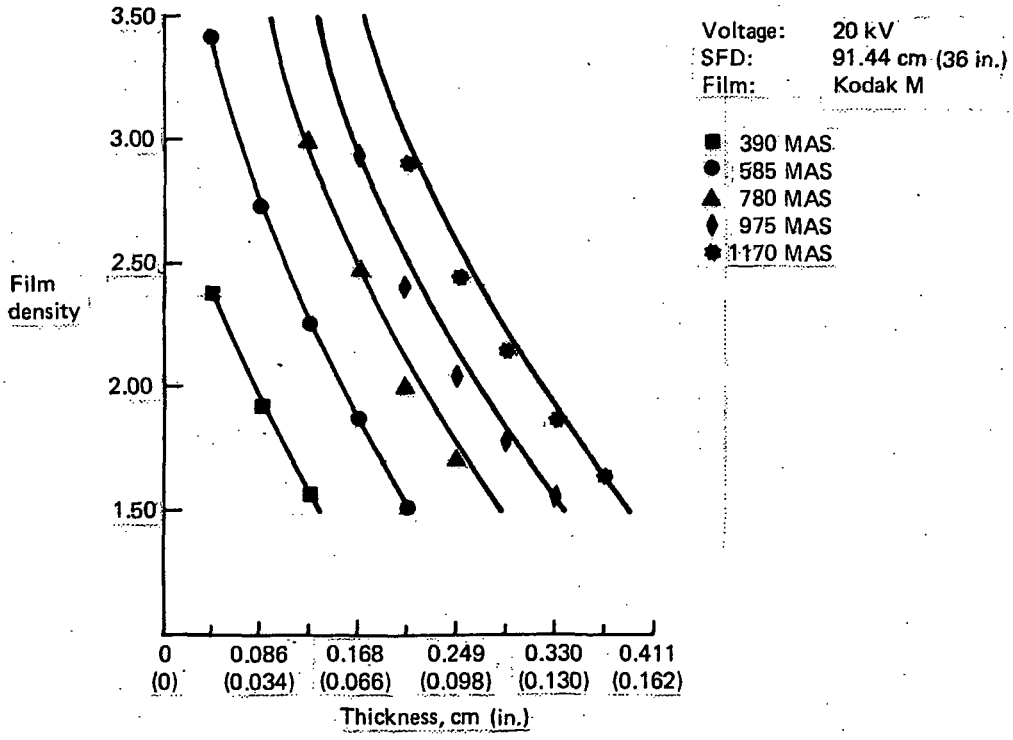

Figure B-4. — (Continued)

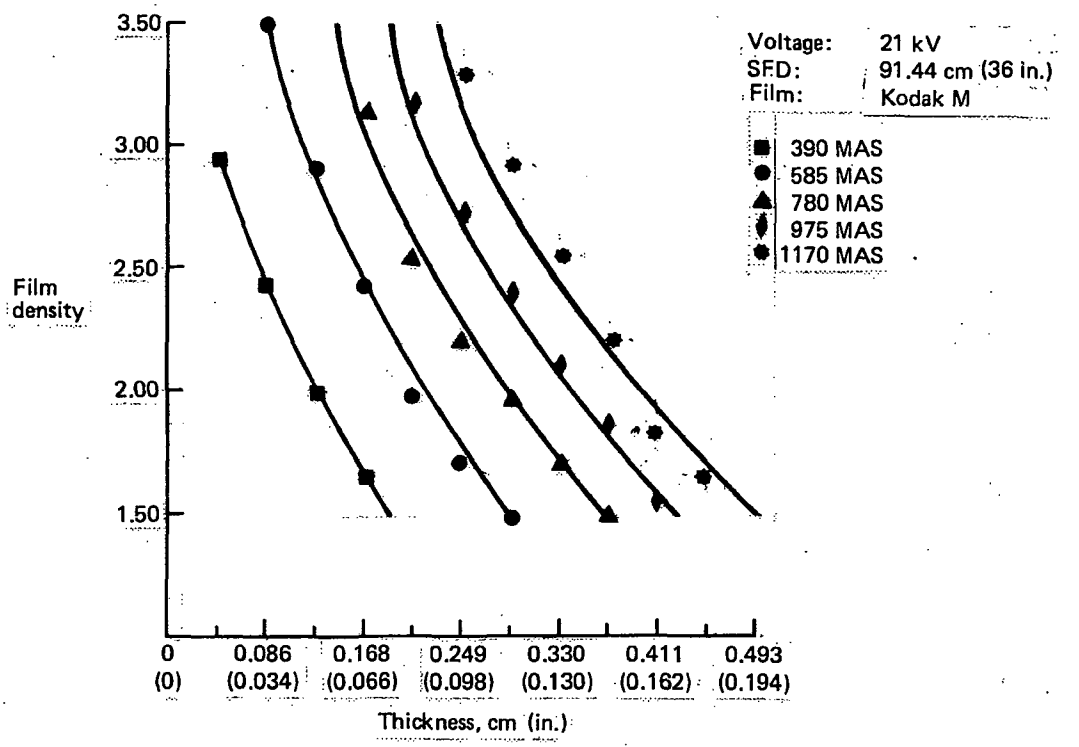

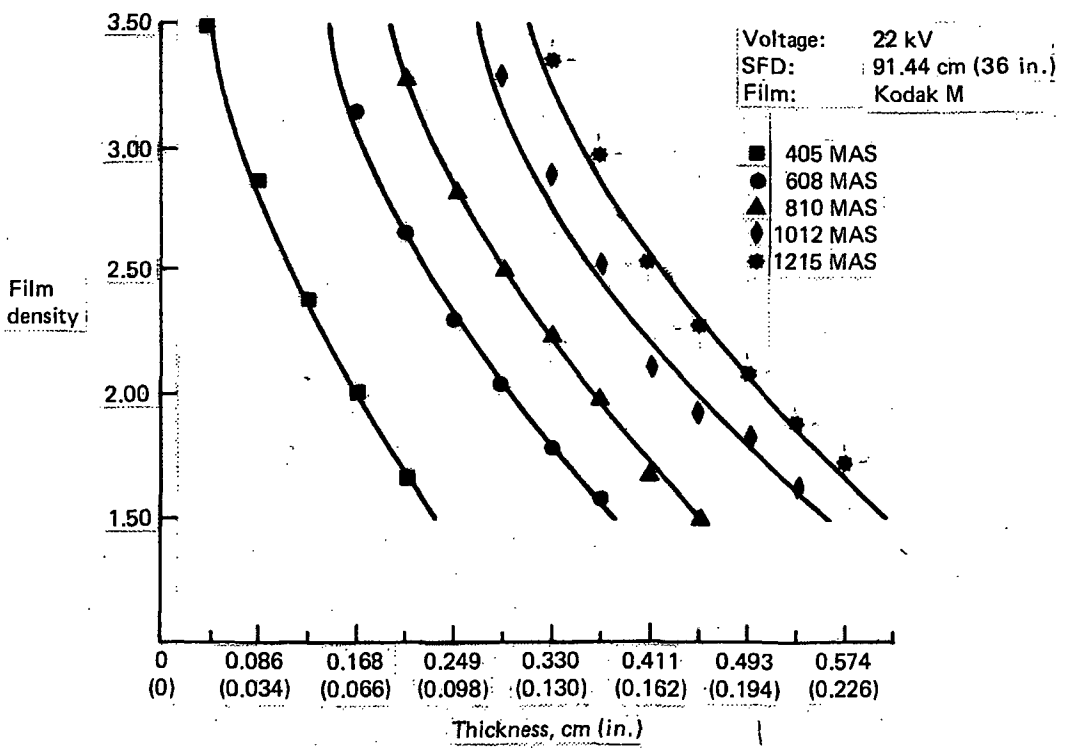

Figure B-4. — (Continued)

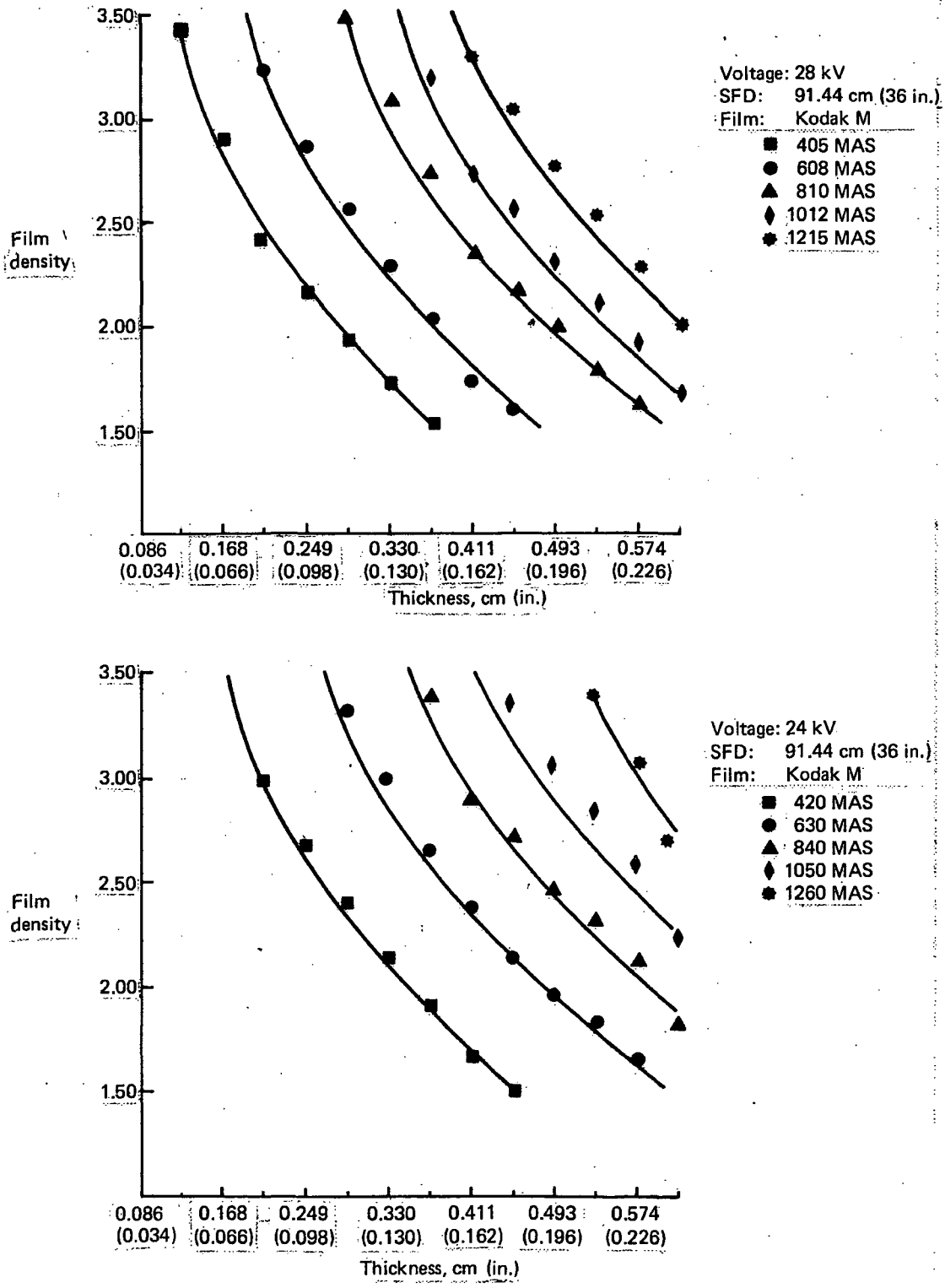

Figure B-4. — (Continued)

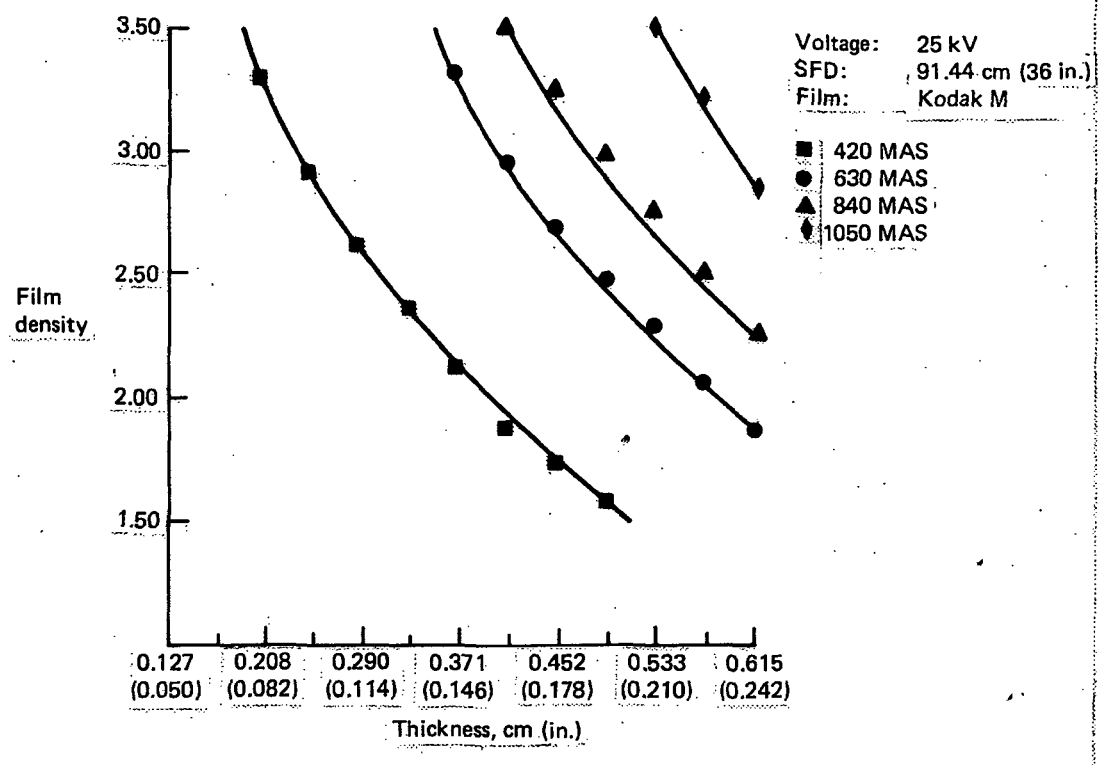

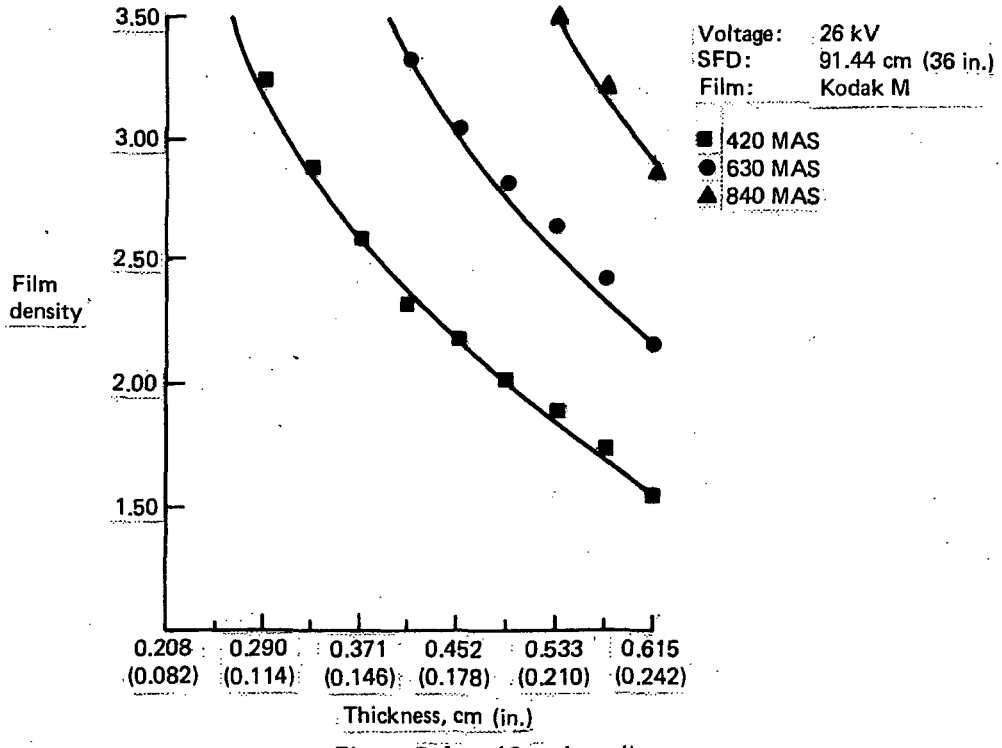

Figure B-4. — (Continued)

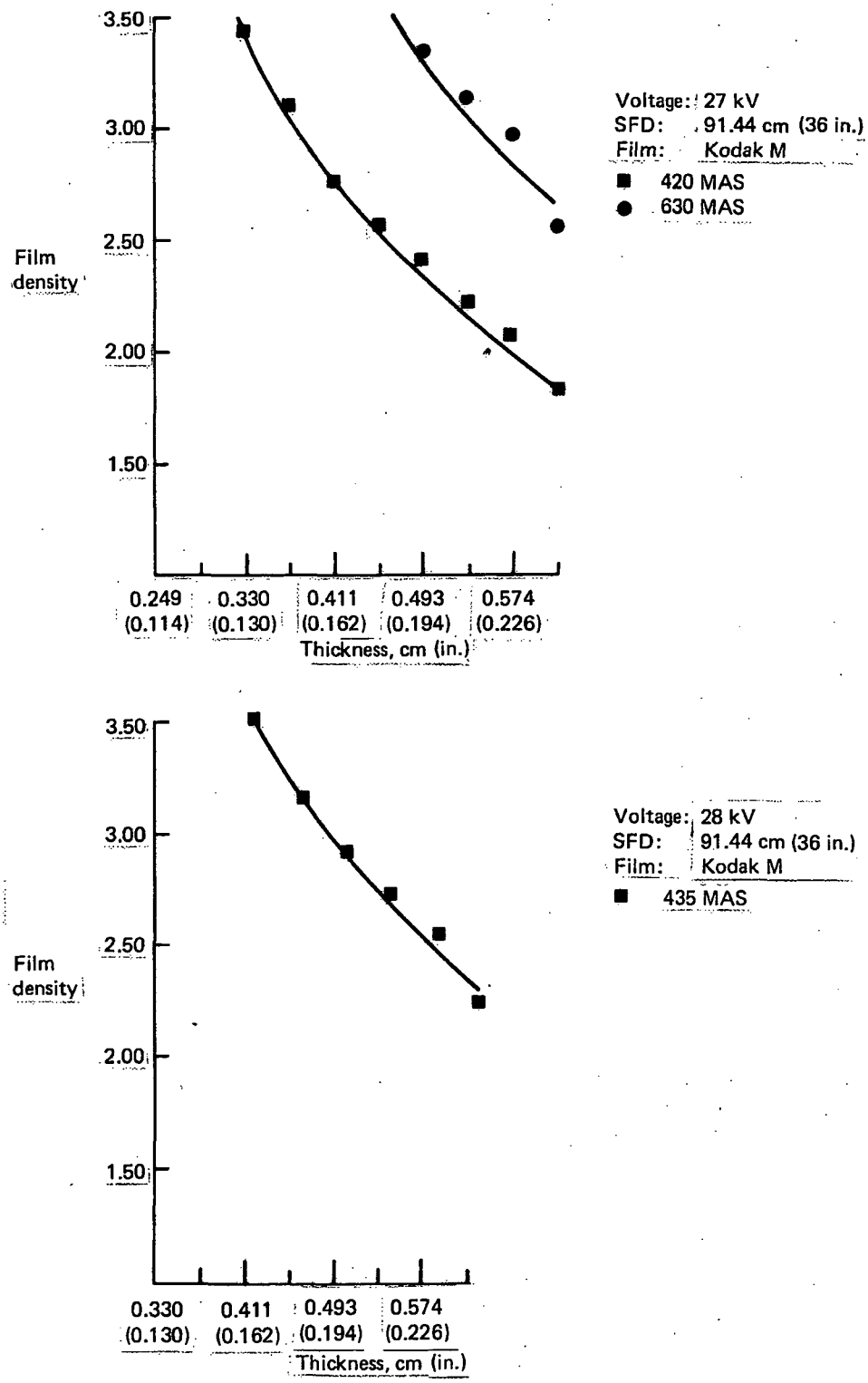

Figure B-4. — (Continued)

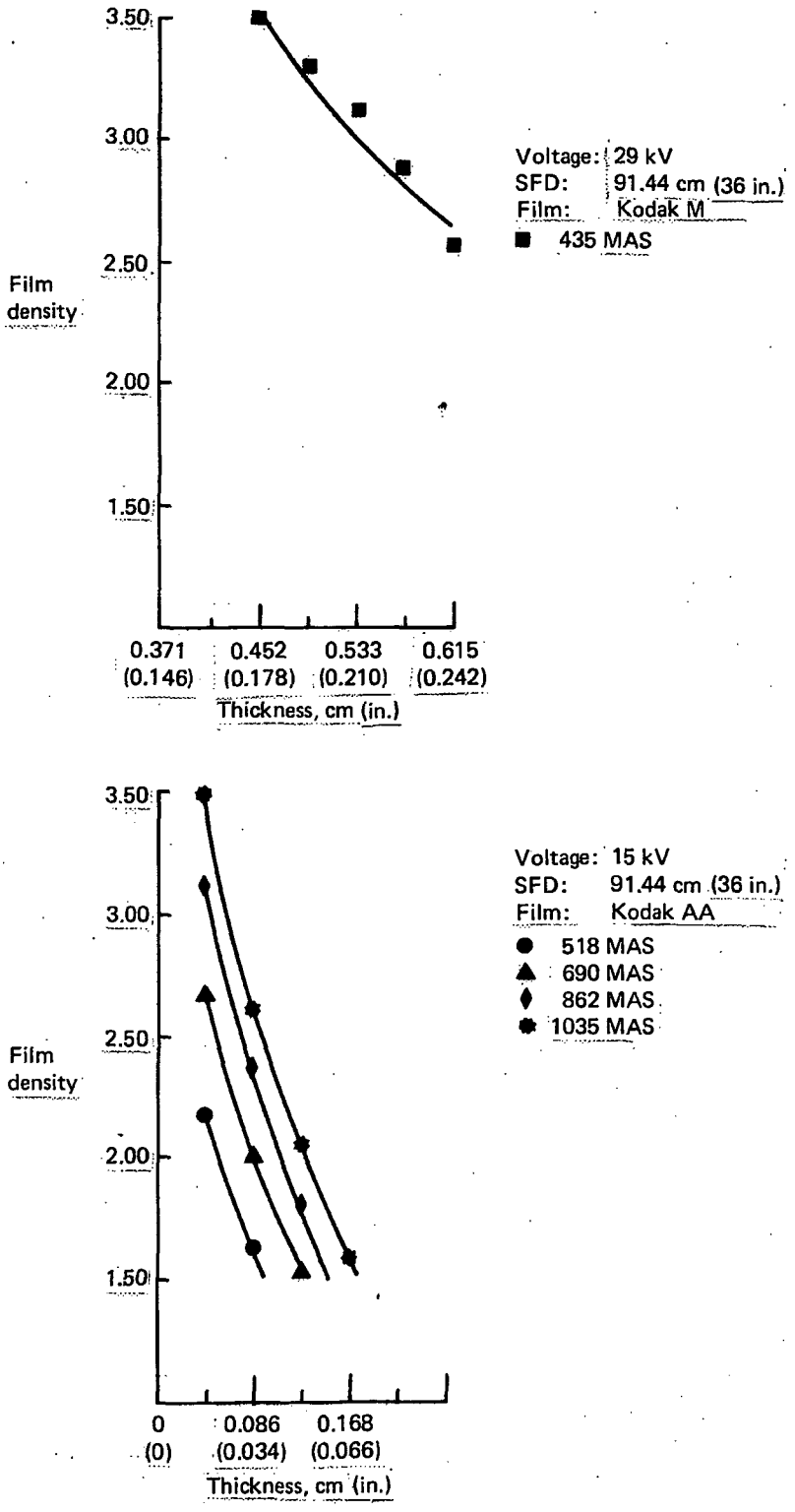

Figure B-4. — (Continued)

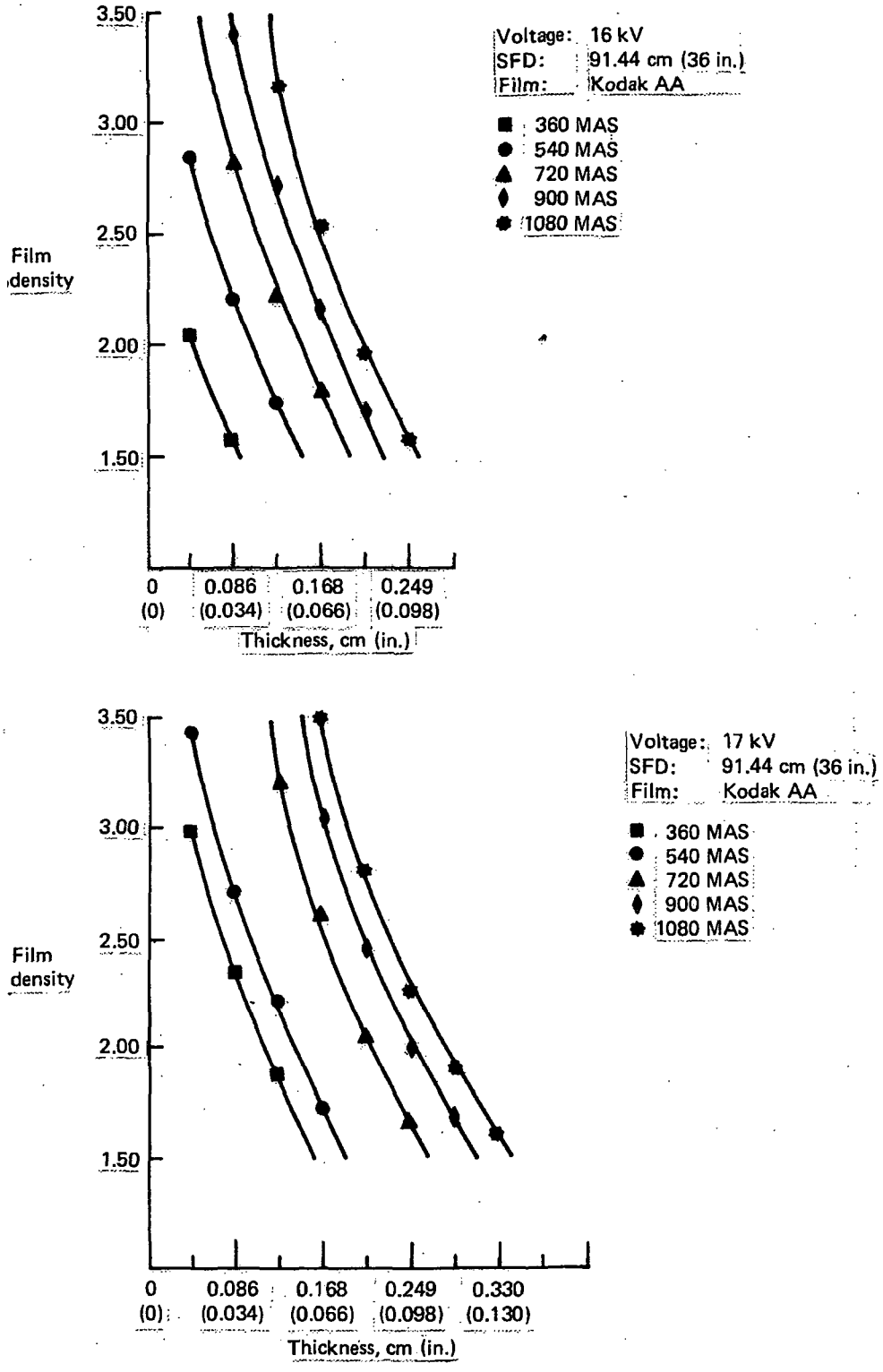

Figure B-4. — (Continued)

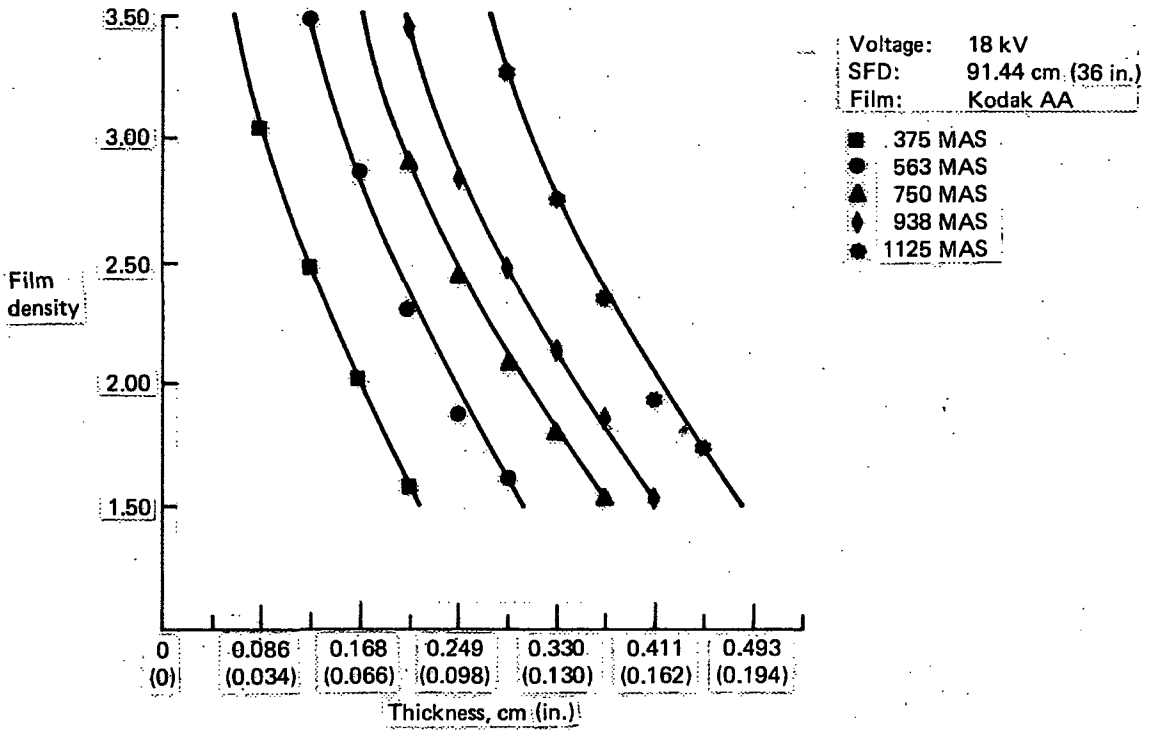

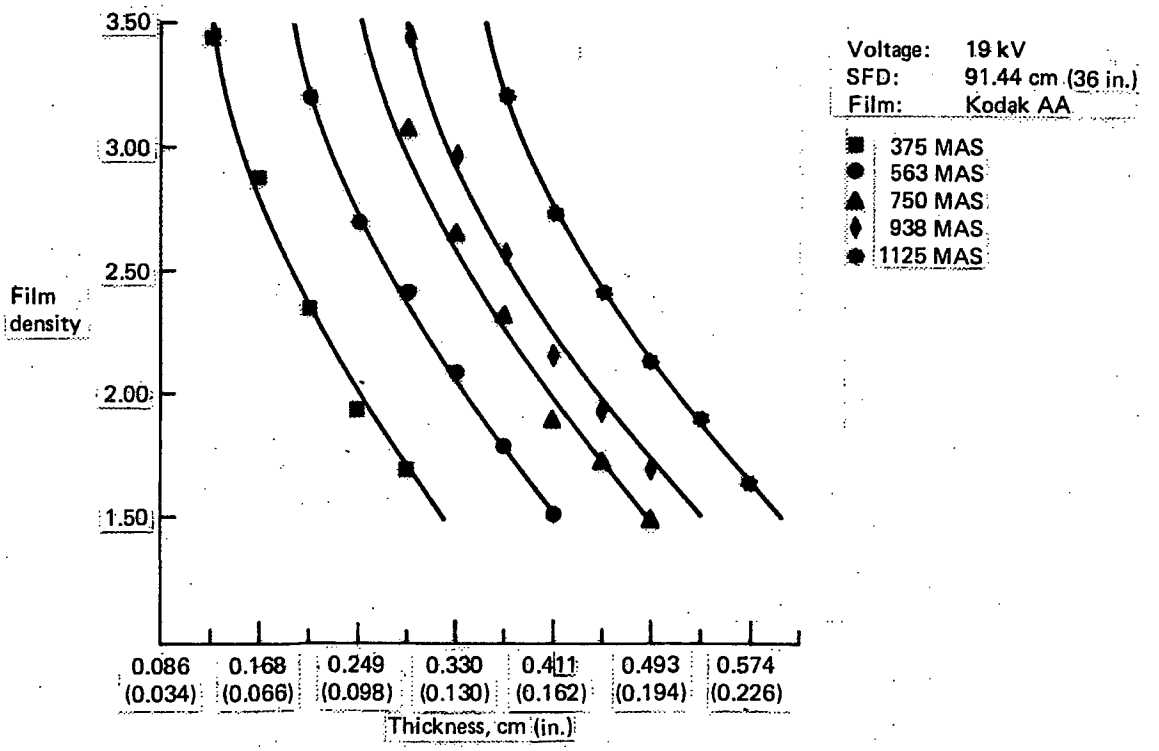

Figure B-4. — (Continued)

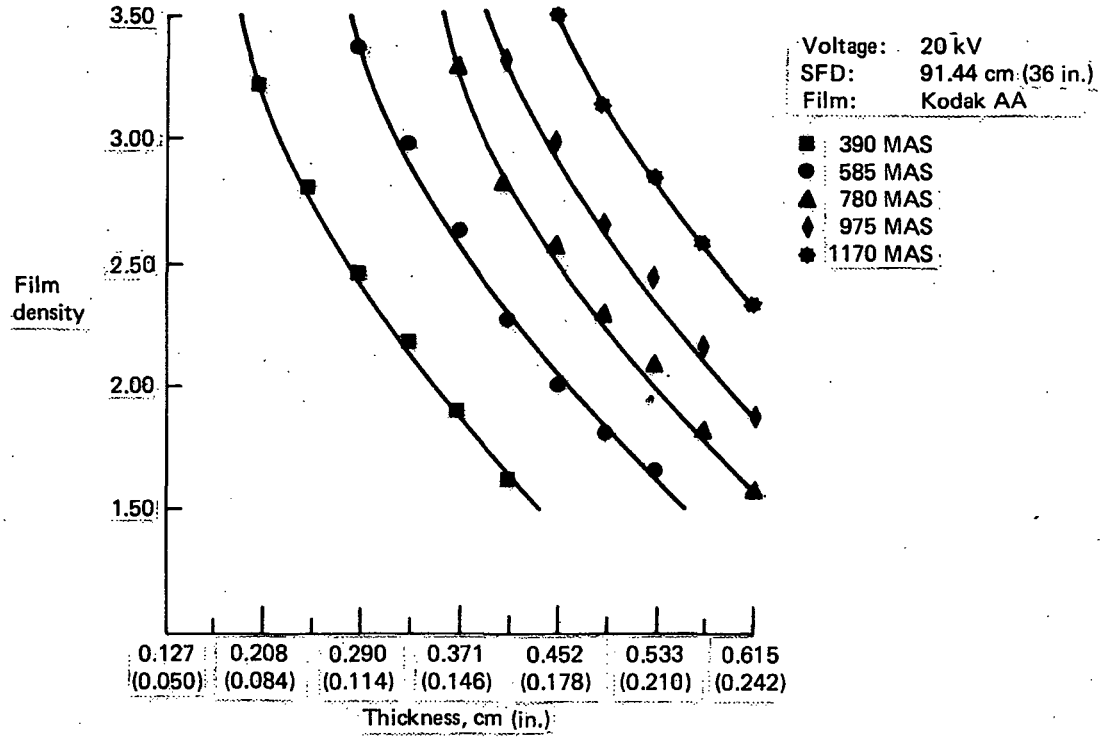

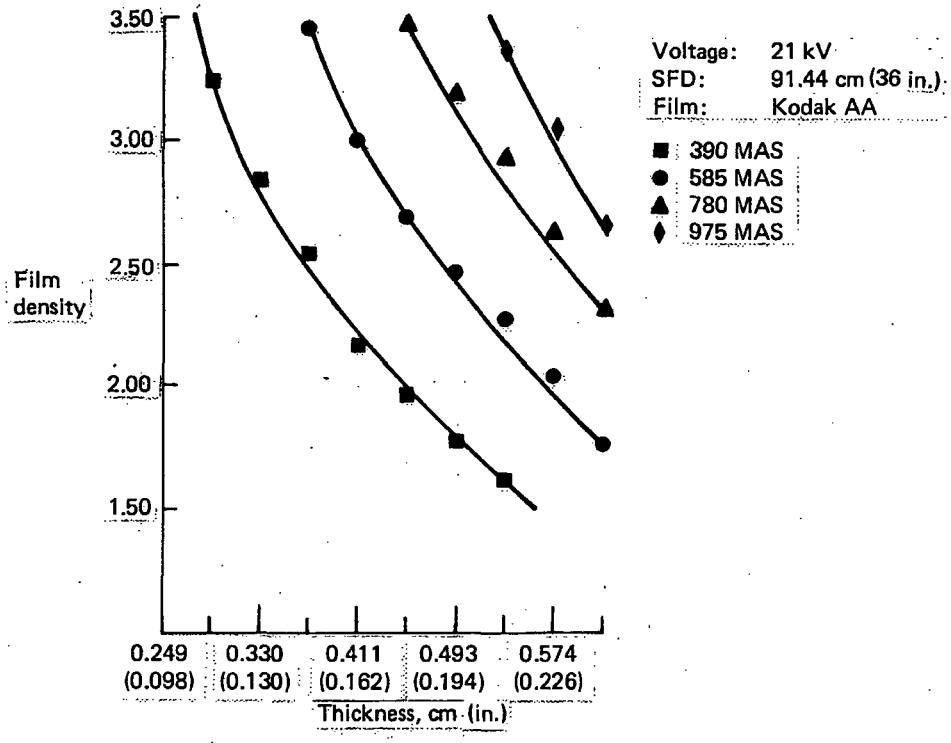

Figure B-4. — (Continued)

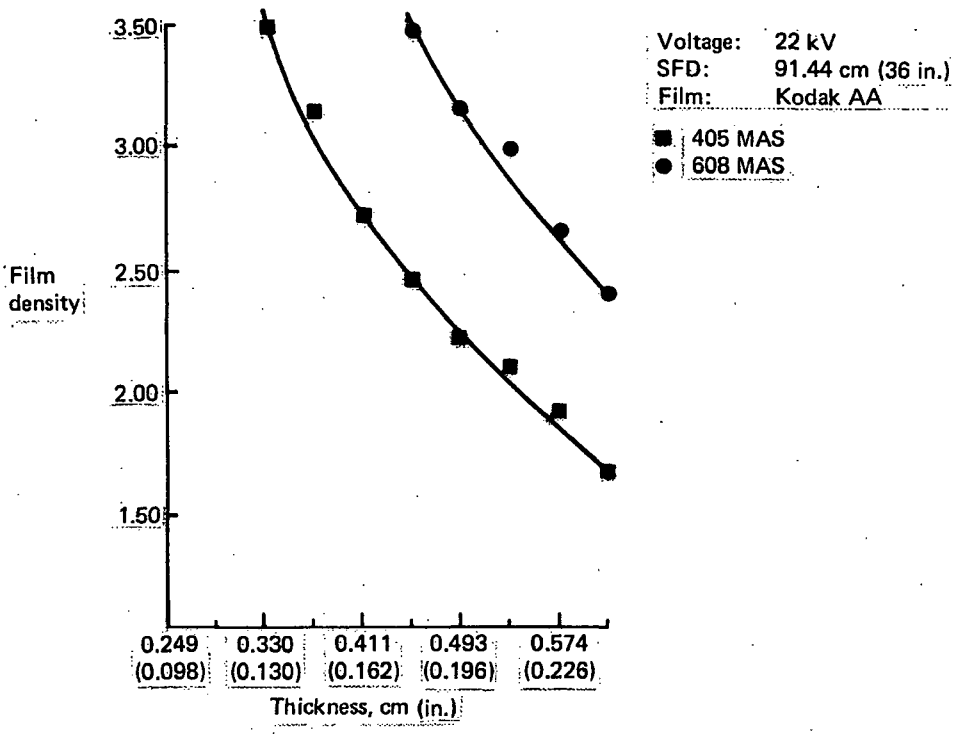

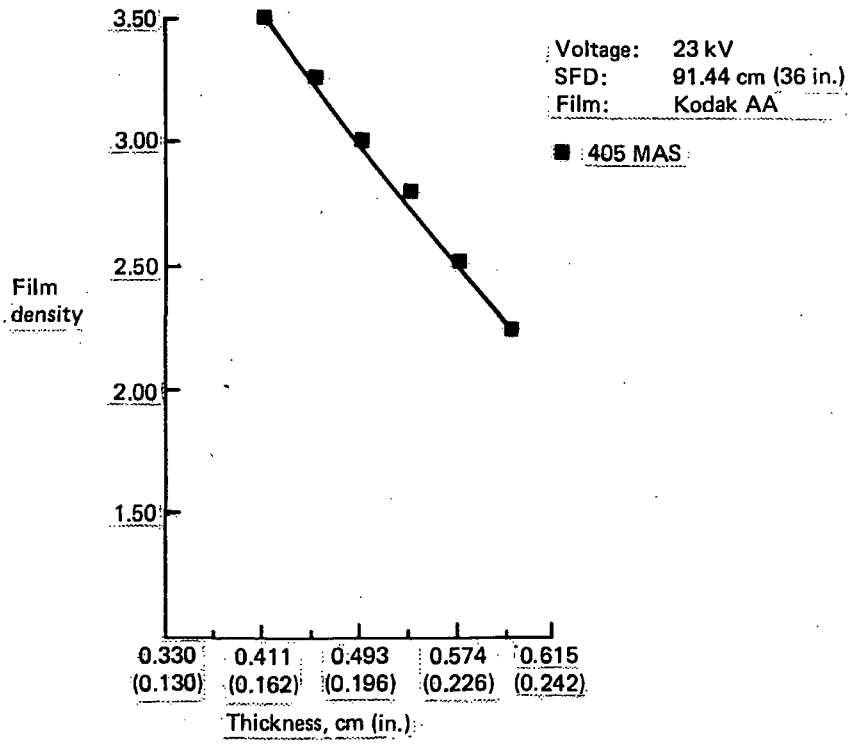

Figure B-4. — (Concluded)

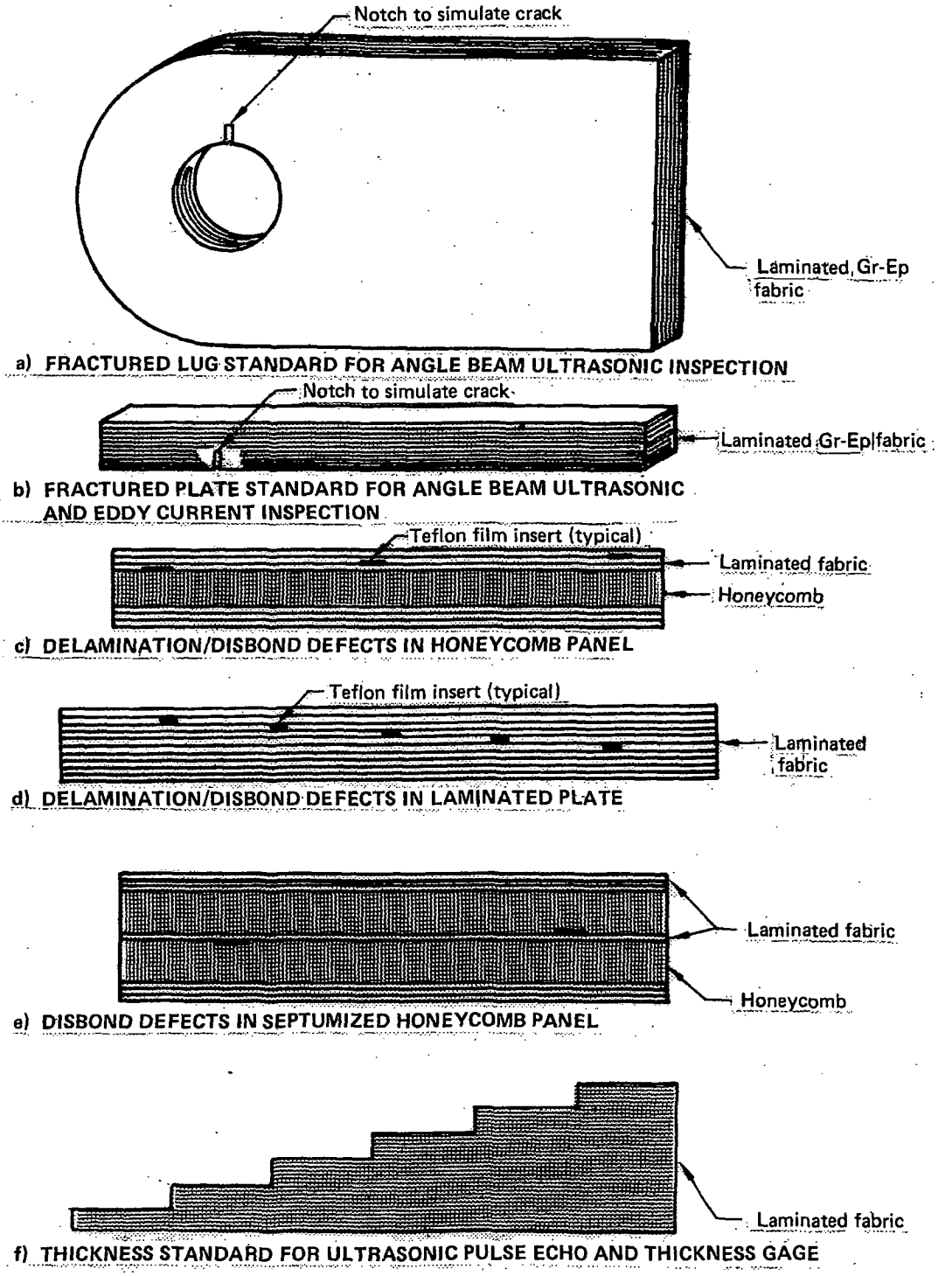

Figure B-5. — Recommended Reference Standard Configuration

1. Report No.	2. Government Accession No.	3. Recipient's Catalog No.
NASA CR-165746		

4. Title and Subtitle	5. Report Date
IN-SERVICE INSPECTION METHODS FOR GRAPHITE-EPOXY STRUCTURES ON COMMERCIAL TRANSPORT AIRCRAFT	November, 1981
	6. Performing Organization Code
7. Author(s)	8. Performing Organization Report No.
M. L. PHELPS	
9. Performing Organization Name and Address	10. Work Unit No.
The Boeing Commercial Airplane Company P.O. Box 3707 Seattle, Washington 98124	11. Contract or Grant No. NAS1-15304
	13. Type of Report and Period Covered
12. Sponsoring Agency Name and Address	Contractor Report
National Aeronautics and Space Administration Washington, DC 20546	14. Sponsoring Agency Code

15. Supplementary Notes

Final Report
Langley Technical Monitor: J. W. Deaton

16. Abstract

A program was conducted to determine in-service inspection methods for graphite-epoxy composite structures on commercial transport aircraft. Graphite/epoxy structures, service incurred defects, current inspection practices and concerns of the airline and manufacturers, and other related information were determined by survey. Based on this information, applicable inspection/NDI methods were evaluated and inspection techniques determined. New technology was developed primarily in eddy current inspection.

Recommended inspection guidelines are included.

17. Key Words	18. Distribution Statement
Nondestructive Inspection, In-service Inspection, Graphite/Epoxy, Advanced Composites, Visual, Bond Test, Eddy Current, Tap Test, Ultraxonic, Radiography	Unclassified – Unlimited

19. Security Classif. (of this report)	20. Security Classif. (of this page)	21. No. of Pages	22. Price
Unclassified	Unclassified	101	